Statistical Mechanics of Static and Low-Velocity Kinetic Friction

Martin H. Müser[1], Michael Urbakh[2], and Mark O. Robbins[3]
[1] *Institut für Physik, Johannes Gutenberg-Universität, 55099 Mainz, Germany*
[2] *School of Chemistry, Tel Aviv University, Tel Aviv 69978, Israel*
[3] *Dept. of Physics & Astronomy, The Johns Hopkins University, Baltimore, MD 21218, USA*
(April 30, 2002)

Contents

I. PRELIMINARY REMARKS

A. Introduction

Since prehistoric times, major technological advances have gone hand-in-hand with fundamental advances in tribology, the science of friction, lubrication, and wear. In each era, new mechanical technology has enabled improved experiments that drive new theoretical understanding, and new understanding has led to further improvements in technology. D. Dowson's book on the *History of Tribology* [1] gives an impressive overlook from the invention of fire rods by the Neanderthals (friction induced chemical reactions are now called tribochemistry) to the attempts of eminent scientists such as Leonardo da Vinci, Coulomb, and Euler to formulate and to understand the basic laws of solid friction.

We are currently in the midst of a new revolution in tribology, driven by the advent of experimental techniques that allow controlled friction measurements at atomic scales, and computers that allow the complex dynamics in atomic scale contacts to be analyzed. This new line of study, dubbed nanotribology, is playing a central role in the quest to build robust machines with nanometer scale moving parts and is poised in turn to benefit from the resulting advances in nanotechnology.

The three major new atomic-scale experimental methods developed in the last decade are the quartz crystal microbalance (QCM) [2–4], atomic and friction force microscopes (AFM/FFM) [5,6], and the surface force apparatus (SFA) [7,8]. These new tools reveal complementary information about tribology at the nanometer scale. The QCM measures dissipation as an adsorbed film of submonolayer to several monolayer thickness slides over a substrate. AFM and FFM explore the interactions between a surface and a tip whose radius of curvature is 10 to 100nm [9]. The number of atoms in the contact ranges from a few to a few thousand. Larger radii of curvature and contacts have been examined by gluing spheres to an AFM cantilever [10,11]. SFA experiments measure shear forces in even larger diameter ($\sim 10\mu$m) contacts, but with Angström scale control of the thickness of lubricating films.

Pioneering experiments with these new techniques have reinvigorated theoretical studies of tribology, which had languished for the previous half century. The difficulty in testing hypotheses was a major factor in this theoretical hiatus. A tremendous number of parameters affect the lateral forces between two solids, yet the primary output of a typical set of macroscopic experiments is a single number – the dimensionless ratio of lateral and normal forces, or friction coefficient μ. Thus verification or falsification of theories was basically impossible. The advent of controlled atomic scale measurements changed this situation, and new computational techniques allowed theorists to study models that included more of the internal degrees of freedom of the contacting surfaces [12,13].

The goal of this article is to review statistical mechanical approaches to the molecular origins of friction. A brief outline of macroscopic experimental results and the fundamental theoretical issues they raise is provided in the remainder of this section. Then progressively more detailed models of the contacting solids are described. Our goal is to illustrate basic phenomena with the simplest model that captures them, and then to generalize the lessons learned to more complicated models. We begin by presenting results for completely rigid solids with no internal degrees of freedom (Sec. II). Then elastic and non-elastic deformations within the solids are considered in Sections III and IV. In most practical cases, the solids are separated by an intervening layer of lubricant, physisorbed contaminants, dust, etc.. The effect of such intervening material is described in Sec. V. The next section considers the origin of the complex oscillatory dynamics observed in some sliding systems. The interface between macroscopic objects generally contains many micron scale contacts, and we discuss the interplay between these contacts in Sec. VII. Sec. VIII presents brief concluding remarks.

B. Some Fundamental Definitions and Questions

Two types of friction are commonly measured and calculated. The static friction F_s is defined as the minimum lateral force needed to initiate sliding of one object over a second, while the kinetic friction $F_k(v)$ is the force needed to maintain sliding at a steady velocity v. Observation of static friction implies that the contacting solids have locked in a local free-energy minimum and F_s represents the force needed to lift them out of this minimum. It is a threshold rather than an actual force acting on the system, and limits lateral motion in any direction. No work is done by the static friction, since no motion occurs. The kinetic friction is intrinsically related to dissipation mechanisms, and equals the work done on the system by external forces divided by the distance moved.

One central issue in tribology is why static friction is so universally observed between solid objects. How does any pair of macroscopic objects, placed in contact at any position and orientation, manage to lock together in a local free energy minimum? A second is why experimental values of F_s and F_k tend to be closely correlated. The two reflect

fundamentally different processes and their behavior is qualitatively different in many of the simple models described below.

A third central issue concerns the relationship between friction and the normal force or load L that pushes the two objects together. The macroscopic laws of friction found in textbooks were first published by the French engineer Amontons about 300 years ago [14], albeit the first recorded studies go back even further to the Italian genius da Vinci. Both found that the friction F_s between two solid bodies is (i) independent of the (apparent) area of contact and (ii) proportional to L. These laws can be summarized in the equation

$$F = \mu L \ , \tag{1.1}$$

and different friction coefficients μ_s and μ_k are obtained for static and kinetic friction.

These simple laws apply fairly well to an abundance of materials, but also have many exceptions. For example, most materials exhibit friction at zero load, and many materials, such as tape, exhibit friction at negative loads. These forces tend to be small for the relatively rough surfaces that were available to Amontons and da Vinci, but researchers going back to Coulomb have accounted for them by adding a term proportional to area to Eq. (1.1). This is often motivated as an additional load coming from the adhesive interactions between the surfaces and is discussed further in Sec. I D.

Coulomb contributed what is often called the third law of friction, namely that μ_k is relatively independent of sliding velocity. The experiments discussed in Sec. I D show that the actual dependence is logarithmic in many experimental systems, and that μ_k often *increases* with decreasing velocity. Thus there is a fundamental difference between kinetic friction and viscous or drag forces that decrease to zero linearly with v. A nearly constant kinetic friction implies that motion does not become adiabatic even as the center of mass velocity decreases to zero, and the system is never in the linear response regime described by the fluctuation-dissipation theorem. Why and how this behavior occurs is closely related to the second issue raised above.

C. Basic Scenarios for Friction

The earliest attempts to explain Amontons's laws were based on the idea that macroscopic peaks or asperities on one surface interlocked with valleys on the opposing surface [1]. As illustrated in Fig. 1(a), the bottom surface then forms a ramp that the top surface must be lifted up over in order to slide. If the typical angle of the ramp is θ, and there is no microscopic friction between the surfaces, then the lateral force needed to produce motion is just $F_s = L \tan\theta$. Thus this simple model predicts a load independent coefficient of friction $\mu_s = \tan\theta$ that can be consistent with any experimental value between zero and infinity. However, there are both practical and fundamental difficulties with this picture for static friction.

One obvious difficulty is that it is hard to imagine how the roughness on two independent surfaces can always manage to interlock. Sec. II examines to what degree the corrugations of a rigid slider can interlock with those of a rigid substrate. A more subtle issue is that this picture can not explain a constant kinetic friction. Once the top surface climbs past a peak on the bottom surface, the lateral force changes sign as the surface slides to the next interlocked state. Since the energy of successive interlocked states is statistically equivalent, the net force and average work vanish. Adding damping terms to the model only produces a kinetic friction that vanishes linearly with velocity. Leslie [15] noted that the observation of a constant kinetic friction at low velocities suggests that, like Sisyphus, the top wall always climbs upwards without ever getting any higher.

To our knowledge, Brillouin was the first to recognize that a non-vanishing dissipation at low velocity can only occur if some *quasi-discontinuous* jumps from one state to another become unavoidable [16]. During these jumps some part of the system becomes linearly unstable and the instantaneous motion remains far from equilibrium even as the average velocity goes to zero. This requires that some part of the system be compliant enough to allow for different mechanically stable states at the same center of mass position. The simplest model illustrating such instabilities and their relation to hysteresis is generally attributed to Tomlinson [17], but had been introduced earlier by Prandtl [18]. In the Prandtl-Tomlinson model (Sec. III A), a simple mass point is pulled over a corrugated surface by a harmonic spring, which models the elastic coupling within the slider. If the spring is soft enough, the mass advances in a sequence of discontinuous pops and there is a constant kinetic friction at low velocity. Another type of rapid instability has been suggested recently [19,20]. In this model, the top surface advances by propagation of a small crack across the surface at a velocity that remains comparable to the speed of sound for any sliding velocity.

Elastic deformations within the solid can also produce static friction between surfaces that would not otherwise interlock. Figure 1(b) illustrates a system where the spacing between peaks on the top surface is stretched to conform to the bottom surface. This could occur either at the scale of macroscopic asperities [21] (Sec. VII) or individual surface atoms (Sec. III). The elastic energy required to displace each peak into an opposing valley must be compensated by the

gain in potential energy due to interactions between the surfaces. This requires that the interactions between surfaces be strong compared to the interactions within each surface, and theoretical studies indicate that this mechanism is unlikely to allow locking of each peak [22–25]. However, the elastic energy cost can be lowered by deforming the system more gradually. The energy required for interlocking at rare defects (Fig. 1(c)) vanishes as the separation between them grows [26,27,21], although the friction force also vanishes in this limit (Secs. III C 5 and VII A). While this mechanism is important for pinning of charge-density waves and flux lattices in superconductors [28,29], it is unlikely to be able to explain most friction measurements (Sec. VII).

One recently proposed scenario (Sec. V) is that unstable jumps and plastic deformation occur within a layer of weakly bound material between the two surfaces (Fig. 1(d)) [30]. This layer could consist of physisorbed molecules, dust, grit, wear debris, etc.. If interactions within the layer are weak, it is free to rearrange into a metatable state that conforms to any geometry of the bounding surfaces. Once in this state, it will resist any change in geometry due to translation, leading to static friction. When forced to slide, the constituent elements advance independently in a series of rapid pops, leading to a constant kinetic friction.

All of the above mechanisms can be characterized as wearless and therefore are consistent with steady state sliding. The classical explanation of the origin of static and small-velocity kinetic friction is based on irreversible plastic deformation within the two contacting solids (Sec. IV). If stresses are strong enough to permanently deform the solids their surfaces will naturally interlock to produce static friction and the work needed to deform material during sliding will produce a constant kinetic friction. Obvious examples where this mechanism is important include scratching or "plowing" of a substrate (Fig. 1(e)) and large-scale removal of material as in machining (Sec. IV D). The plastic deformation may result from large stresses in the contact, or be driven by thermodynamics as in cold welding or material mixing (Fig. 1 (f)). Plastic deformation and the concurrent generation of wear and debris make it impossible to define a steady state value for the kinetic friction force. However, one may not infer that time variation in F_k implies that plastic deformation is the main source of friction.

All the above mentioned scenarios may be relevant in specific systems, and more than one may be active at the same time in any real macrotribological system. Our goal below is to examine the implications and limits of each mechanism and identify the cases where they are most likely. Before embarking on this quest, we briefly review important experimental findings.

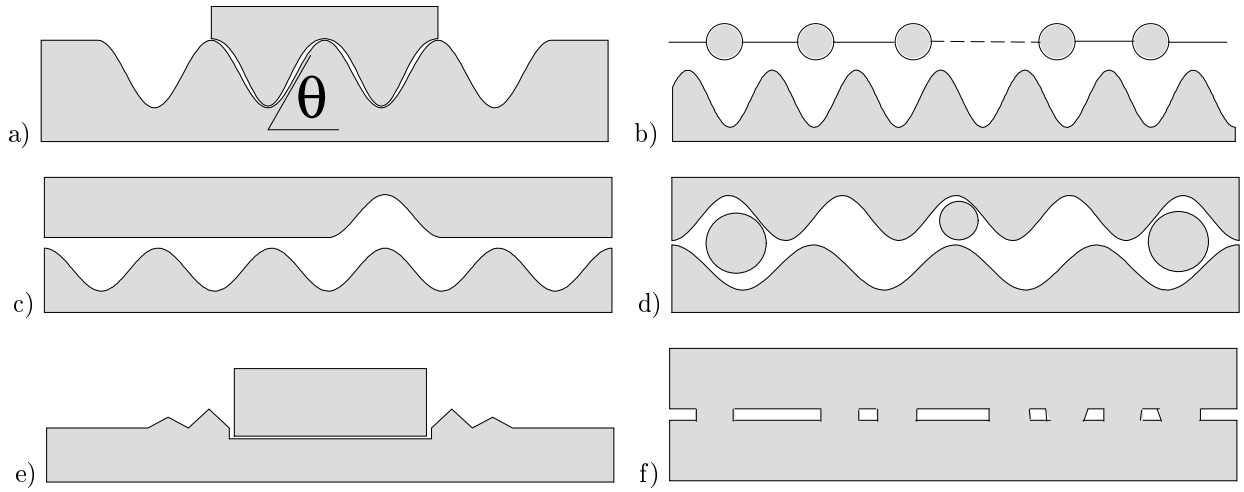

FIG. 1. Schematic representation of various possible friction mechanisms: a) Geometric interlocking of asperities with typical angle θ, b) elastic deformation to interlock atoms and/or macroscopic peaks, resulting in multiple metastable states, c) defect pinning by long wavelength elastic deformations, d) pinning by an intervening layer of weakly bound material, e) plastic deformation or plowing, and f) material mixing or cold welding.

D. Phenomenology of static and small-velocity kinetic friction

Experimental measurements show that rough surfaces do not interpenetrate as envisioned in Fig. 1(a), at least at the most macroscopic scales. Electrical [31], mechanical [32], and optical [33,34] measurements show that contact only occurs where the peaks of asperities on opposing surfaces coincide. As a result, the real area of molecular contact

$A_{\rm real}$ is much smaller than the apparent geometrical area of the sufaces $A_{\rm app}$. It was the latter that da Vinci and Amontons found did not affect the friction force in most cases.

Elastic and plastic deformations flatten the contact regions into micrometer-scale patches, many times larger than molecular scales. The static friction corresponds to an average yield stress within these contacts of $\tau_{\rm s} = F_{\rm s}/A_{\rm real}$, and a similar relation gives the local shear stress $\tau_{\rm k}$ corresponding to the kinetic friction. Experimental studies of a wide range of materials indicate that τ rises linearly with the local pressure P [35–40]:

$$\tau_{\rm s} = \tau_0 + \alpha\, P\,. \tag{1.2}$$

This provides a simple phenomenological explanation for Amontons's laws as well as some exceptions to them. Summing over $A_{\rm real}$ one finds

$$F_{\rm s} = \tau_0 A_{\rm real} + \alpha L \tag{1.3}$$

or:

$$\mu_{\rm s} = \alpha + \tau_0/p\,. \tag{1.4}$$

where $p = L/A_{\rm real}$ is the average pressure in the contact. Note that Amontons's laws that $\mu_{\rm s}$ is independent of load and macroscopic contact area are obeyed if p is constant or large compared to τ_0. The former holds if the surfaces deform completely plastically [31] so that the local pressure is pinned at the hardness of the material. The pressure can also be constant if the asperities have a random distribution of heights and deform elastically [41–43], however the constant is not a material property like the hardness. Since τ_0 is generally positive, Equation 1.3 gives a finite friction force at zero or even negative loads, thus avoiding the most glaring failure of Amontons' laws. A large number of experiments [35,31,44] show an apparent divergence of μ at small loads that is consistent with the second term in Equation 1.4.

Experiments also show that the friction is very sensitive to the last layer of atoms on the contacting surfaces [31,44]. For example, graphite is a good lubricant in ambient air because of water adsorbed on the surface. It is not a useful lubricant in space or vacuum applications. Another dramatic example is that a single molecular layer of lubricant can decrease the friction between two metallic surfaces by an order of magnitude [45]. This is clearly inconsistent with the mechanical interlocking picture (Fig. 1, since the macroscopic slope of the surfaces remains unaffected. Other evidence against macroscopic interlocking comes from the fact that the friction generally begins to rise when surfaces are made sufficiently smooth. This observation can be understood from the expressions in the previous paragraph and the fact that $A_{\rm real}$ increases as surfaces are made smoother. Note that the above observations do not imply that shear and dissipation are always confined to the interface. Plastic deformation can extend to a great depth beneath the surface, particularly when the hardnesses of the two materials in contact are very different [31].

Experiments clearly show that the frictional force is history dependent. The static friction generally increases with the time of contact. The kinetic friction fluctuates in magnitude and direction, and its average value depends on past sliding velocities. Rabinowicz has shown that the friction fluctuations in some systems result from the presence of a limited number of large asperities, and used the force autocorrelation function to extract the characteristic size of these asperities [44]. Memory of past sliding velocities indicates that sliding produces a gradual evolution in the area, structure or composition of the contacts between surfaces. Phenomenological "rate-state" models have been very successful in describing such memory effects in macroscopic friction measurements.

Rate-state models assume that the friction depends on the rate and a small number of "state variables" that describe the properties of the interface. Different physical interpretations of the microscopic properties that these state variables describe have been proposed, such as the amount of dilation at the interface [46] or the degree of crystallinity of an intervening film [47,48]. Most approaches leave the nature of the state variable unspecified and merely assume it depends on some average of recent velocities [49–51]. The coefficients of a simple dynamical equation are fit to experiment and can then be used to describe a wide range of dynamic sliding conditions, particularly stick-slip motion.

A simple rate-state model that describes dry sliding friction between rocks, plastics, wood and many other rough materials [33,52,53] was proposed by Dieterich [50] and developed by Ruina [51]. The instantaneous friction coefficient is written as:

$$\mu = \mu_0 + A\ln(v/v_0) + B\ln(\theta/\theta_0) \tag{1.5}$$

where v and θ are the current velocity and state, and μ_0 is the friction at some reference state where $v = v_0$ and $\theta = \theta_0$. The equation of motion for the state variable is:

$$\partial_t\theta = 1 - \left(\frac{\theta}{D_c}\right) v - \left(\frac{C\theta}{B\sigma}\right)\partial_t\sigma, \tag{1.6}$$

where θ has units of time and can be thought of as the age of the contact, σ is the applied normal stress, and D_c is a characteristic sliding distance over which the contact evolves. Experimental values of D_c vary from 2 to 100 μ, which is comparable to the contact diameters deterimined by Rabinowicz from force fluctuations [44]. There are also four positive dimensionless fit parameters in this theory: μ_0, A, B and C. For typical rocks, $\mu_0 \sim 0.6$, A and B are from 0.005 to 0.015, and C is between 0.25 and 0.5.

Under static conditions θ rises linearly with time and the static friction coefficient rises as $\ln t$. The steady state value of θ during sliding can be found by setting the time derivatives in Eq. (1.6) to zero: $\theta_{ss} = D_c/v$. Inserting this in Eq. (1.5) gives $\mu_{ss} = \mu_0 + (A - B)\ln(v/v_0)$. Thus the steady state kinetic friction may increase or decrease with increasing velocity depending on the relative size of A and B. However, an instantaneous change in velocity always increases μ because A is positive.

Fig. 2 shows the predicted and observed changes in friction after a jump in velocity for a variety of systems. In each case the friction jumps down after a sudden decrease in velocity and then rises after a sliding distance of order D_c. Increasing the velocity to its initial value causes a sharp rise in μ followed by a gradual decrease. It is important to note that the friction relaxes over the same sliding distance after the two changes, even though the sliding times are different by an order of magnitude. This is the motivation for expressing memory in terms of a characteristic distance in Eq. (1.6).

In a beautiful set of experiments, Dieterich and Kilgore were able to show that for many systems the state variable is directly related to the contact geometry [33,34]. Using transmitted light they could observe each asperity contact and its evolution with time. Changes in the state variable correlated directly with changes in the real area of contact obtained by summing over all asperities. Moreover, the change in friction over the length scale D_c could be quantitatively described by changes in the distribution of contacts. After a given sliding distance d, contacts that are smaller than d have disappeared and been replaced by new contacts whose area reflects the current sliding velocity. The distance to reach steady state is thus directly related to the distribution of contact sizes. Dieterich and Kilgore observed a wide range of contact areas, from their resolution of about 1μm up to $\sim 50\mu$m. The value of D_c lies in this range. Dieterich and Kilgore also found a logarithmic increase with time in the contact area between two static surfaces that could be correlated with the increase in static friction. They concluded that for the rough surfaces and high loads in their experiments the contacts are always near the plastic limit, and that $A_{\rm real}$ increases with time through a creep process.

Dieterich and Kilgore's observations suggest that for their systems the friction force can be written as the product of a real contact area A_{real} that depends on past history and a shear stress τ that depends on the instantaneous velocity. They find that $A_{real}(\theta) = A_{real}(\theta_0)(1 + (B/\mu_0)\ln(\theta/\theta_0)$. If the shear stress rises logarithmically with velocity as $\tau(v) = \tau_0(1 + A/\mu_0 \ln(v/v_0)$, one recovers Eq. (1.5) up to linear order in the small parameters A and B. Baumberger and collaborators have also observed increases in contact area with resting time or inverse velocity [54].

Logarithmic dependences of shear stress on shear rate are seen in many bulk materials such as amorphous polymers. The logarithm follows naturally from a simple model proposed by Eyring [55] that assumes shear is thermally activated and that the activation barrier decreases linearly with the applied stress. If the equilibrium barrier is much larger than k_BT, one can ignore backwards motion and write that the velocity $v = v_0 \exp(-(U - \tau V^*)/k_BT)$ where the coefficient V^* has units of volume and is called the activation volume. Solving for τ, one finds

$$\tau = \tau_0 + (k_BT/V^*)\ln(v/v_0) \tag{1.7}$$

where $\tau_0 = U/V^*$. If V^* is independent of T, then the coefficient of the $\ln(v)$ term is proportional to T. This behavior is observed in both the bulk shear stress of polymers and in their frictional force. Dieterich and Kilgore also find that A and B rise roughly linearly with temperature in the much harder materials that they study. The variation of B can be understood if the creep that causes A_{real} to increase is thermally activated, and recent work on polymers has shown that there is a correlation between the distance from the glass transition temperature and the rate of area growth [56]. However, the above work does not address the type of processes that control activation at the interface and thus A. Recent work on this topic is discussed in Section V D.

To summarize this subchapter, the total area of real contact between macroscopic surfaces is usually much smaller than the apparent area, and consists of many local contacts with a broad range of diameters from ~ 1 to 100μm. The friction can be expressed as a product of $A_{\rm real}$ and the average yield or shear stress τ within the contacts. The number of atoms within the contacts is large enough that statistical mechanical methods can be used to calculate τ. The stress depends on past history due to two types of creep process. Creep normal to the interface leads to an (almost) ever-increasing $A_{\rm real}$. As a result, τ_s increases with resting time and τ_k increases with decreasing velocity. Lateral creep leads to a reduction of friction as v is decreased. Ultimately, at *astronomically* small sliding velocities, $A_{\rm real}$ should saturate at $A_{\rm app}$. The effect of lateral creep would then dominate and one can even expect a linear relation between F_k and v as discussed by Estrin [57] from a material science point of view and by Chauve *et al.* [58,59] based on a finite-temperature renormalization group analysis. However, this limit is not generally reached in practical experiments.

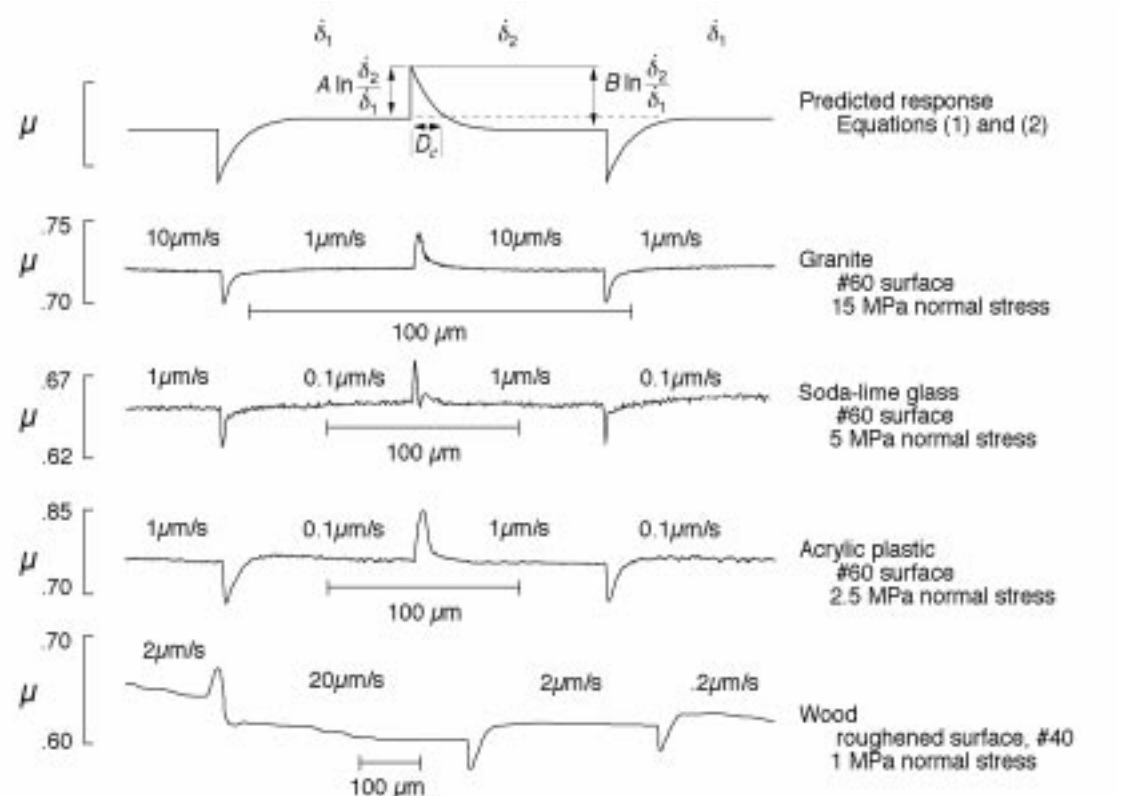

FIG. 2. Comparison of the change in friction with velocity predicted by Eq. (1.5 and observations on a number of materials.

II. RIGID WALLS

An important step in developing an understanding of friction is to start with as few explicitely treated degrees of freedom as possible and to add increasingly more complexity. It is thus quite natural to consider solids as completely rigid and impenentrable in a first approximation. Lubricant atoms - if present at all - are in complete thermal equilibrium so that the slider sees a well-defined (free) energy profile. The first historic attempts by Amontons, Coulomb, Euler, Bélidor, and others [1] to understand friction as a purely geometric interlocking of rough but essentially rigid surfaces may be referred to as a rigid wall model. The underlying assumptions of this model are often far from being realistic. Incorporating elastic or plastic deformations, cold welding, etc. will change the tribological behavior of the two solids in contact qualitatively. It is yet important to understand the properties of the rigid-wall model quantitatively, since most models are in one way or another generalizations of it, for example the Prandtl-Tomlinson and the Frenkel-Kontorova model correspond to a rigid-wall model in the limit of infinitely strong springs. It is moreover conceivable that the picture of rigid walls is rather accurate for nanoscale objects, in which case geometric interlocking is the predominant contribution to friction.

The most simple and most illustrative starting point is to consider an infinitely large, single-crystalline substrate and a rigid slider. For reasons of symmetry, the interactions V between the two rigid objects must then be periodic in the substrate's lattice constant b, thus

$$V = V_0 \cos(2\pi x/b) + V_1 \cos(4\pi x/b) + ..., \tag{2.1}$$

where x denotes the relative, lateral displacement between slider and substrate at given normal load L and where the V_n's are expansion coefficients.

There are two important issues addressed in the literature: What is the size of the prefactors V_n? These prefactors determine the maximum possible lateral force between the two objects, which provides a meaningful upper bound for the static friction force. The other issue is how the friction is altered through thermal fluctuations/activation that stem from the not explicitly treated internal degrees of freedom. These two questions will be discussed separately in Sec.'s II A and II B before some applications are presented in Sec. II C

We wish to make a final general comment on the properties of the rigid-wall model. Non-zero static friction does not imply non-zero kinetic friction due to energy recovery as pointed out by Leslie [15]. The energy required to lift up the slider on the top of the barrier can be regained in principle by moving it downhill in a controlled, adiabatic way. A compliant driving device, however, will not allow us to move the tip in a controlled way and new effects emerge best described by the Prandtl-Tomlinson model. Similarly, when the slider is moved via a constant field, the downhill sliding is uncontrolled, which leads to additional dissipation as compared to a quasi-static adiabatic motion.

A. Geometric interlocking

The reason why a rigid-wall model is appealing can be seen from Fig. 1a): In order to initiate sliding through the application of a lateral force F, the upper solid has to be lifted up a maximum slope θ. This slope is independent of the normal load L if we assume simple hard-disk interactions, that is to say, as soon as the two solids overlap the interaction energy increases from zero to infinity. The maximum lateral force F_s between the two solids would then simply be

$$F_s = L \tan\theta, \tag{2.2}$$

if we assume that friction is absent for perfectly flat surfaces. This equation is consistent with Amontons's law, Eq. (1.1). In 1737, Bélidor [1] modeled rough surfaces by means of such hard-disk asperities of spherical shape arranged to make commensurate crystalline walls (in these days, we call those asperities atoms!). Two surfaces are called commensurate if they share the same periodicities within the interface. Bélidor found $\mu_s \approx 0.35$, which is a 'typical' value for measured friction coefficients. An automatic consequence of commensurability is the proportionality between F_s or alternatively V_n in Eq. (2.1) with L irrespective of the area of contact provided adhesive interactions are negligible.

One problem of Bélidor's explanation is the assumption of commensurate walls. Surface corrugations usually do not match between two macroscopic bodies as well as sketched in Fig. 1a), unless they are specifically designed to interlock. Even in those SFA experiments in which two chemically identical surfaces are slid with respect to each other, special care has to be taken in order to orient the two surfaces perfectly such that commensurability is obtained.

In general, one may expect that the surface corrugation between two solid bodies do not match at any length scale or to be more precise they only match in a stochastic way. The effect of the correlation of surface roughness on the

shear force will be disussed in the following, for smooth surfaces with a roughness exponent $H = 0$. Extremely rough and self-affine surfaces for which $H > 0$ will be considered later in Sec. VII. For $H = 0$, it is relatively easy to make general quantitative predictions for lateral forces between the surfaces as a function of the symmetry of the surfaces. In order to calculate the lateral forces between two rigid solid bodies from an atomistic point of view, it is necessary to make assumptions about the interaction between the solids. However it turns out that the details of the interactions do not influence important, qualitative results. Two different models [60,61] yield similar properties for the scaling of the maximum shear forces F_s with increasing size of the interface (for instance contact area A or rod length L) at a fixed normal pressure $p_\perp$. Panyukov and Rabin [60] considered randomly, irreversibly charged rods and plates, where the net charge vanished on each object. Müser et al. [61] analyzed two rigid solids that experience forces that grow exponentially fast with the overlap between them. The latter model roughly mimics the exponential repulsion due to the Pauli principle as electronic orbitals belonging to different solids are starting to overlap.

For both models, it is possible to calculate the energy landscape generated by relative translation analytically. Both times it is found that (i) $\tau_s = F_s/A$ is independent of A if the two periods of the two surfaces match, (ii) τ_s decreases with $\sqrt{A}$ if the two surfaces are random, and (iii) τ_s is zero if the surfaces are incommensurate. Contributions from the circumference of finite contacts between incommensurate surfaces yield contributions to τ_s that vanish with a higher power law than $1/\sqrt(A)$, see also Fig. 5.

Further results of the overlap model are: (iv) the prefactor that determines the strength of the exponential repulsion has no effect on F_s at fixed normal load L, (v) the lateral force scales linearly with L for an any fixed lateral displacement between slider and substrate, (vi) allowing for moderate elastic interactions within the bulk does not necessarily increase F_s, because the roughness may decrease as the surfaces become more compliant, and (vii) the prefactor of F_s for non-identical commensurate surfaces decreases exponentially with the length of the common period $\mathcal{L}_c$. This last result had already been found by Lee and Rice [62] for a yet different model system. We note that the derivation of properties (iv) and (v) relied strongly on the assumption of exponential repulsion or hard disk interactions. Therefore one must expect charged objects to behave differently concerning these two points.

Assuming constant normal pressure in the contacts, which is equivalent to a linearity between L and A, the static friction coefficient obeys the following, general scaling laws for rigid object with roughness exponent $H = 0$ apply:

$$\mu_s \propto \begin{cases} \exp\left(-\mathcal{L}_c\right) & \text{commensurate surfaces} \\ 1/\sqrt{A} & \text{random surfaces} \\ 0 & \text{incommensurate surfaces,} \end{cases} \tag{2.3}$$

where in all cases finite-size corrections apply that fall faster than with $1/\sqrt{A}$. The experimental test of Eq. (2.3) and the above mentioned hypotheses is a challenging task, since it requires the use of flat and chemically inert surfaces. However, atomistic computer simulations, in which the necessary, idealized conditions can be more easily implemented confirm the conclusions, in particular those concerning commensurate and incommensurate interfaces [22,23,30,61,63,24]. The scaling predictions (i)-(vi) were tested systematically by Müser et al. [61] via molecular dynamics simulations, in which the two opposing walls contained discrete atoms. The intrabulk interactions consisted of an elastic coupling of atoms to their lattice site, while interbulk interactions consisted of Lennard Jones (LJ) interactions. Despite allowing the walls some degree of elasticity and despite the interactions being different from the simple exponential repulsion model, agreement with the theoretical arguments (i)-(vi) was found. Only (iv) and (v) had to be slightly modified in terms of an adhesive offset load, when the adhesive part of the LJ interactions was taken into account.

B. Thermal effects

Before considering the coupling of the wall to a driving device, it is instructive to study the motion of the slider under a constant force in the presence of thermal fluctuations. This constant force can be exerted by inclining the substrate or by putting a test charge on the slider in an electric field.

The substrate is still assumed to be crystalline and for the sake of simplicity the interaction V between the slider and the substrate is described by one single harmonic, thus

$$V = f_0 b' \cos(x/b'). \tag{2.4}$$

Here x is the position of the slider relative to the substrate, $b'/2\pi$ is the substrate's period, and f_0 is the (zero-temperature) static friction force, whose scaling with the area of contact and normal load we just discussed. In order to incorporate the effects of thermal fluctuations on the motion of the slider, one can exploit the isomorphism to

the motion of a Brownian particle moving on a substrate. A nice description of that problem is given by Risken in Chapter 11 of Ref. [64]. Here we will discuss some of the aspects that we believe to be important for friction.

Thermal effects can be incorporated into the model by adding a thermal random force $\Gamma(t)$ and a damping term $m\gamma v$ to the conservative force between slider and substrate:

$$m\ddot{x} + m\gamma\dot{x} = f_0 \sin(x/b') + \Gamma(t), \tag{2.5}$$

where m is the slider's mass. The random force should satisfy the fluctuation-dissipation theorem, i.e. for the simple damping term $-m\gamma v$ it must have zero mean $\langle\Gamma(t)\rangle = 0$ and be δ-correlated [65,66]

$$\langle\Gamma(t)\Gamma(t')\rangle = 2mk_BT\delta(t-t'), \tag{2.6}$$

where k_B denotes the Boltzmann constant and T the temperature. The random forces and the damping term $-m\gamma v$ arise from interactions with phonons and/or other excitations. Typically, the time scales associated with these excitations are short compared to the motion of a particle from one minimum to another. This justifies the assumption of δ correlation in the random forces.

In the small-velocity limit, one can usually neglect the inertial term $m\ddot{x}$ in Eq. (2.5) for the calculation of the friction force. For this limit, Risken and Vollmer [66] derived a matrix-continued-fraction method that allows one to calculate the nonlinear response to a constant external force F as an expansion in terms of inverse damping constants. The expansion also converges for very small (but finite) damping constants. It is worth discussing certain limits. The central quantity is the mobility $\mu_{\rm mob}$, which is defined as:

$$\langle v\rangle = \mu_{\rm mob} F, \tag{2.7}$$

where $\langle v\rangle$ is the average sliding velocity. From a phenomenological point of view, one may interprete $\mu_{\rm mob}^{-1}$ as an effective viscosity $\eta_{\rm eff}$.

In the limit of large damping and *small* F (linear response regime), Risken and Vollmer find for the mobility of a particle moving in a simple cosine potential:

$$\mu_{\rm mob} = \frac{\tilde{T}}{\gamma}\ \left\{I_0\left(\tilde{T}^{-1}\right)\right\}^{-2} + \mathcal{O}\left(\frac{1}{\gamma^3}\right) \tag{2.8}$$

$$\approx \frac{1}{\gamma} \times \begin{cases} \left(1 - \frac{1}{2}\tilde{T}^{-2}\right) & \text{for } \tilde{T} \gg 1 \\ \tilde{T}^{-1}\exp\left(-2\tilde{T}^{-1}\right) & \text{for } \tilde{T} \ll 1 \end{cases} \tag{2.9}$$

where I_0 is the modified Bessel function and $\tilde{T} = k_BT/f_0b'$ a reduced temperature. The two approximations given in Eq. (2.9) are valid at large and small thermal energies respectively. At large thermal energies, the corrugation of the substrate potential barely influences the motion and phononic dissipation dominates the friction. At small thermal energies, the motion of the slider becomes activated. The exponential decrease of the mobility, or the exponential increase of $\eta_{\rm eff}$, is prototypical for creep. Note that the mobilities (or $\eta_{\rm eff}^{-1}$) given in Eq. (2.8) is only valid for sufficiently small external forces F, i.e., the system is sufficiently close to thermal equilibrium.

When F increases, $\mu_{\rm mob}$ starts to deviate from its equilibrium values as shown in Fig. 3. At large F and/or at large temperatures, the distribution of the variable x becomes flat and the influence of the corrugation does not play an important role any longer. One must thus distinguish between three different concepts: (i) dissipation, which is reflected in the phenomenological damping constant γ, (ii) equilibrium mobility $\mu_{\rm mob}(F \to 0)$ or $\eta_{\rm eff}^{-1}$, which arises from an interplay of dissipation, surface corrugation, and thermal fluctuations, and (iii) non-equilibrium mobility $\mu_{\rm mob}$ at finite, suffficiently large values of F. In the present case, the increase of the mobility could be interpreted as an apparent shear thinning, despite the fact that the rigid wall has no internal degrees of freedom. On the other hand, one may interpret x as an internal degree of freedom of the combined system and say that due to the externally imposed shear, x spends different fractions of time at a given point of phase space at different forces. This argumentation would be consistent with the effect of shear thinning.

Another information conveyd by Fig. 3 is that at finite temperatures, the mobility remains finite, although it may become exponentially small as T tends to zero. Hence strictly speaking, the zero-velocity kinetic friction F_k is always zero as long as temperature T is finite, thus

$$\lim_{T\to 0^+}\lim_{v\to 0} F_k(v) = 0. \tag{2.10}$$

On the other hand, if we first send temperature to zero, then F_k will tend to the value f_0, thus

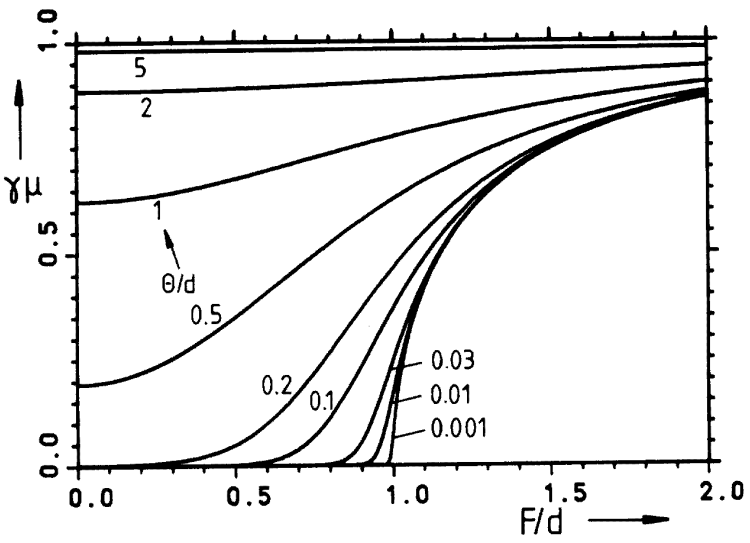

FIG. 3. Effective mobility as a function of reduced forces for varios reduced temperatures θ/d. Adapted from Ref. [64]

$$\lim_{v\to 0}\lim_{T\to 0^+} F_k(v) = f_0. \tag{2.11}$$

The fact that two limits cannot be exchanged as shown in Eqs. (2.10) and (2.11) for the limits $v \to 0$ and $T \to 0^+$ is frequently encountered in tribological contexts. This concerns for example the determination of static friction F_s as a function of the speed $\dot{\sigma}_{\rm ext}$ with which the externally applied shear force is ramped up and the time we are willing to wait to see the slider move by one lattice constant. It also concerns the way with which the thermodynamic limit is realized as discussed by Müser and Robbins [24]: For a finite system, static friction will always tend to zero in the limit $\dot{\sigma}_{\rm ext} \to 0$, even if the walls are commensurate. Thus, the meaningful determination of a static friction forces requires a sufficiently large time scale separation between the creep motion of the junction and the vibronic degrees of freedom.

C. Applications

1. Nanotubes

AFM manipulation of carbon nanotubes (CNT) on highly oriented graphite substrate [67,68] and of concentric multiwalled CNT's [69] presents a unique ability to study friction between rigid objects. The CNT systems allows one to tune the commensurability between two contacting atomically smooth crystalline surfaces in a controlled way and to investigate the effect of commensurability on friction.

When a CNT lying in an incommensurate state is manipulated, it slides smoothly and rotates in-plane [67,68]. However, this motion is interrupted at discrete in-plane orientations in which the CNT "locks" into a low-energy state [68,70] indicated by an increase in the force required to move the CNT. Fig. 4 shows a lateral force trace illustrating the pronounced change in the force in going from the commensurate to incommensurate state and visa versa [68]. As the nanotube is rotated in-plane, several of these discrete commensurate orientations are observed, each separated by 60 ± 1 degrees (Fig. 4, upper inset). The contrast of the friction in the commensurate and incommensurate states is dramatic (order of magnitude) and abrupt (a discrete change within experimental uncertainty). It was also found [67,68] that for this system, the transition from the incommensurate to commensurate state is accompanied by a transition from sliding motion in which the CNT rotates in-plane, to gearlike rolling motion.

Molecular statics calculations by Buldum and Ciraci [71] support the hypothesis that the observed lockin orientations are directly related to commensurate registry, and the particular set of commensurate orientations is determined by the CNT chirality (the wrapping orientation of the outer graphene sheet of the CNT). Thus the friction experiments provide a novel method for measuring the nanotube chirality. Large multiwall CNT's of different diameters are expected to have different chiralities and should show different commensurate orientations [71].

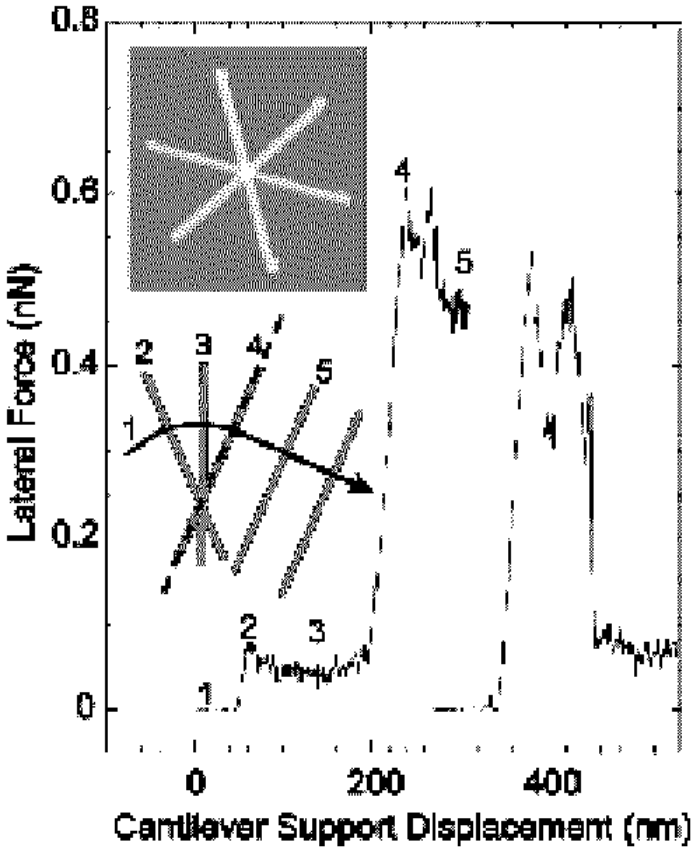

FIG. 4. Lateral force trace as a CNT is rotated into (left trace) and out of (right trace) commensurate contact [68]. The lower inset shows a top-view schematicly, the process for the left trace. The AFM tip is moving along in contact with the graphite substrate (1), the CNT is contacted (2) and begins rotating in-plane (3), the commensurate state is reached (indicated by the dashed line) and the lateral force rises dramatically (4) before rolling motion begins (5). The right trace begins with the tip on the substrate, the tip then contacts the CNT in the commensurate state, begins rolling and then pops out of commensurate contact and begins rotating in plane with a corresponding drop in lateral force. The upper inset is a composite of three AFM images of a CNT in its three commensurate orientations. Note that the nanotube was not rotated about its center as the compositite implies. The images were translated in order to emphasize the 60 degree intervals

Concentric multiwalled carbon nanotubes present a simple geometry, which restricts interlayer motion to a single (axial) direction with a fixed interlayer orientation of stiff, smooth layers. Each layer in a concentric multiwalled carbon nanotube is indexed by two integers (n,m) which give the circumference in graphitic lattice coordinates. The difference in radii between successive layers frustrates the circumferential interlayer registry. The axial period of a single layer is $3\sqrt{n^2+nm+m^2}/GCF(2n+m, n+2m)$ bond lengths (GCF is greatest common factor). Two layers with $n_1/m_1 \neq n_2/m_2$ are typically axially incommensurate [72].

Potential energy calculations by Kolmogorov and Crespi [73] demonstrated that the (7,7)/(12,12) commensurate system shows a relatively large barrier to sliding which is defined as as the maximal variation in total energy as the outer layer slides through the full unit cell of the inner layer. The barrier increases linearly with system size. In contrast, the incommensurate (14,0)/(16,10) nanotube has a potential corrugation from 0.0-0.3 eV which, excepting fluctuations, is independent of system size. The energetic barrier to interlayer sliding in defect-free nanotubes containing thousands of atoms is comparable to that for a single unit cell of crystalline graphite. Efficient cancellation of registration-dependent interactions in incommensurate tubes can induce extremely small and nonextensive shear strengths. For finite (and therefore imperfectly) incommensurate systems, a barrier to sliding arises from fluctuations in the finite-sampled registry-averaged interlayer binding energy. The size of the fluctuations depends on the number and distribution of the sample points for the different local registries. The unusual nonextensive behavior observed here is in fact a generic behavior of (unlubricated) incommensurate sysems.

Structural defects can play a very important role in the response under interlayer sliding. The commensurate nanotubes with uniform-wrapping angle have the expected behavior under shear: disruptions in translational symmetry due to, e.g., on-wall defects should typically lower the corrugation below that expected for a perfect crystal. However, for incommensurate layers, the defects play the opposite role: the perfect system has an extremely low corrugation, and the introduction of a small concentration of defects increases the shear strength, through a contribution that scales linearly with length at constant defect density.

2. Curved, nanoscale contacts

Wenning and Müser [74] extended the considerations made above for athermal, flat walls to the interaction between a curved tip and a flat substrate by including Hertzian contact mechanics. Since the contact area A increases proportionally to $L^{2/3}$, they concluded that for a dry, non-adhesive, *commensurate* tip-substrate system F_s should scale linearly with L, since μ_s is independent of A. For a dry, non-adhesive, *disordered* tip pressed on a crystalline substrate, they obtained $F_s \propto L^{2/3}$, which was obtained by inserting $A \propto L^{2/3}$ into $F_s \propto L/\sqrt{A}$. The predictions were confirmed by explicit molecular dynamics simulations, in which special care was taken to obtain the proper contact mechanics. The results of the friction-force curve are shown in Fig. 5.

The power laws found in their simulations for the interaction of an amorphous tip with a crystalline substrate is similar to that observed in AFM experiments in argon atmosphere [75,76]. Also AFM studies of friction on layered materials [77] showed striking similiraty with Fig. 5 in the wearless regime, although the experiments were conducted in atmosphere. In the latter case, even the order of magnitude between exerimentally measured friction and the simulated friction are found. The experimental prefactors observed in other experiments [75,76] are distinctly larger than those in the simulations. Moreover the experimental results by Schwarz *et al.* [76] obtained with tips of different radii of curvature seem consistent with a picture in which the friction force is proportional to the area of contact and independent of the normal pressure. It thus remains an open question what friction mechanism is predominant in thoese experiments.

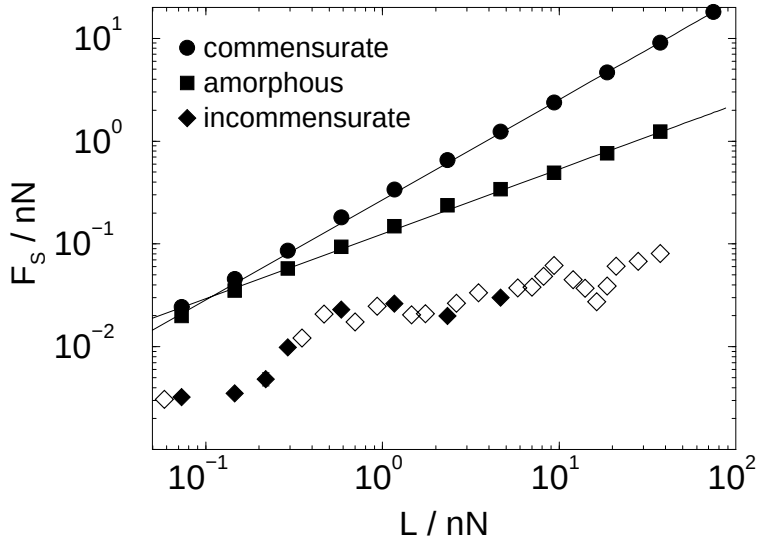

FIG. 5. Static friction force F_s vs. normal load L for different tip geometries. In all cases, the radius of curvature was $R_c = 70\,\mathring{A}$ and contacts were non-adhesive. Straight lines are fits according to $F_s \propto L^\beta$ with the results $\beta = 0.97 \pm 0.005$ (commensurate) and $\beta = 0.63 \pm 0.01$ (amorphous). ¿From Ref. [74] plus additional data provided by L. Wenning (open diamonds).

III. DRY, ELASTIC FRICTION

A. Properties of the Prandtl-Tomlinson model

1. Definition of the model and the low velocity limit

The Prandtl-Tomlinson (PT) model [17] (usually only referred to as the Tomlinson model) is the simplest model to allow for elastic instability and hence for pinning between two incommensurate solids. In its original version, see Fig. 6, atoms in the upper wall are coupled harmonically to their ideal lattice sites. The substrate is assumed to be rigid with a fixed center of mass. Thus the surface atoms from the upper wall experience a force periodic in the substrate's lattice constant b. Dissipation due to phononic or electronic damping is considered to be linear in the sliding velocity. The equation of motion for individual atoms then reads:

$$m\ddot{x}_n + m\gamma\dot{x}_n = -k(x_n - x_{0,n}) + f_0 \sin(x_n/b'). \tag{3.1}$$

with $b' = b/2\pi$. Here, x_n and $x_{0,n}$ denote respectively the current position and the ideal lattice site of atom n with mass m; γ is a damping term, k the coupling strength to the ideal lattice site and f_0 the subsrate's corrugation strength. Neighbored lattice points are assumed to be separated by a distance a, hence $x_{0,n+1} - x_{0,n} = a$. Despite its seeming simplicity, the analytical treatment of the PT model or simple generalizations thereof can be rather complex. It is still used widely in order to interprete tribological properties of systems in relative lateral motion [13,78–82].

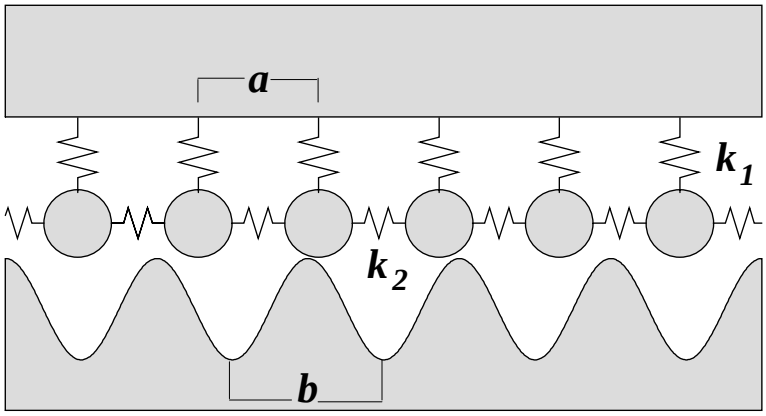

FIG. 6. Schematic representation of the one-dimensional Frenkel-Kontorova-Tomlinson model. a and b denote the lattice constant of the upper solid and the substrate respectively. The substrate is considered rigid and its center of mass is kept fixed. In the slider, each atom is coupled with a spring of stiffness k_1 to its ideal lattice site and with a spring of stiffness k_2 to its neighbor. The PT model is obtained for $k_2 = 0$, while the Frenkel-Kontorova model corresponds to $k_1 = 0$.

A paper by Prandtl [18] on the kinetic theory of solid bodies, which was published in 1928 one year prior to Tomlinson's paper [17], never achieved the recognition in the tribology community that it deserves. Prandtl's model is similar to the Tomlinson model and was likewise focused on elastic hysteresis effects within the bulk. Nevertheless Prandtl did not miss to emphasise the relevance of his work to dry friction between solid bodies. In particular, he formulated the condition that can be considered the holy grale of dry, elastic friction: *If the elastic coupling of the mass points is chosen such that at every instance of time a fraction of the mass points posseses several stable equilibrium positions, then the system shows hysteresis....* In the context of friction, hysteresis translates to finite static friction or to a finite kinetic friction that does not vanish in the limit of small sliding velocities. Note that the dissipative term that is introduced *ad hoc* in Eq. (3.1) does vanish linearly with small velocities.

Prandtl's condition is satisfied (see Fig. 6) if the elastic coupling to a lattice site is sufficiently small, namely $k < k^*$ with

$$k^* = f_0/b. \tag{3.2}$$

Suppose for a moment that $k \geq k^*$, in which case there is a unique static solution for every x_n in Eq. (3.1) irrespective of the value of $x_{0,n}$. When the upper solid is moved at a constant (small) velocity v_0 relative to the substrate, each atom is always close to its unique equilibrium position. This equilibrium position moves with a velocity that is in the

order of v_0. Hence the friction force is of the order of $m\gamma v_0$ and consequently F_k vanishes linearly with v_0 as v_0 tends to zero. The situation becomes different for $k < k^*$. Atoms with more than one stable equilibrium position will now pop from one stable position to another one when the slider is moved laterally. For small pulling velocities v_0, such a process occurs when an atom does not have a mechanically stable position at time $t + \delta t$ in the vicinity of the old stable mechanical position near which it was located at time t. Such a situation is discussed in Fig. 7 in terms of the time-dependent potential energy $V(x)$ associated with the conservative forces, namely

$$V(x) = f_0 b' \cos(x/b') + \frac{1}{2}k(x - x_0)^2 \tag{3.3}$$

with $\dot{x}_0 = v_0 > 0$. In the "popping" processes (indicated by the thick solid line in Fig. 7), the velocities $\dot{x}_n$ will exceed v_0 by orders of magnitudes for $v_0 \to 0$. At small v_0, the dynamics along most of the sinusoidal line is rather independent of the precise value of v_0 and the dissipated energy $\int dx\gamma mv$ has a well-defined positive limit $F_k(v_0 = 0)$. Hence in the absence of thermal fluctuations that have been disregarded so far, F_k remains finite even in the limit of infinitely small v_0. We refer to Fig. 9 in Ref. [82] for a discussion in similar terms. We note in passing that a detailed analysis of the motion along the sinusoidal line, which is emphasized in Fig. 7, lasts a time $t \propto v_0^{-1/3}$ resulting in $F_k(v_0) - F_k(0) \propto v_0^{2/3}$ [83,29].

The number of free parameters that define the athermal Prandtl-Tomlinson model can be reduced to three by a convenient choice of units. b' can be used to define the unit of the length scale, $f_0 b'$ the unit of the energy scale, and $\sqrt{f_0/mb'}$ the unit of the frequency. Eq. (3.1) then reads in reduced units indicated by the tilde:

$$\ddot{\tilde{x}}_n + \tilde{\gamma}\dot{\tilde{x}}_n = -\tilde{k}(\tilde{x}_n - \tilde{x}_{0,n}) + \sin(\tilde{x}), \tag{3.4}$$

with $\tilde{x}_{0,n+1} - \tilde{x}_{0,n} = \tilde{a}$. Hence, the free parameters are $\tilde{k}$, $\tilde{\gamma}$, and $\tilde{a}$. It is usually assumed that the size or the length of the interface is infinitely large. Depending on the values of the reduced parameters one distinguishes the following regimes: The (strongly) pinned regime refers to $\tilde{k} < \tilde{k}^* = 1$ in which $\tilde{F}_k$ remains finite even at infinitesimally small $\tilde{v}_0$ and the unpinned (or weakly pinned) regime ($\tilde{k} \geq \tilde{k}^*$) for which $\tilde{F}_k(0) = 0$. One also distinguishes between underdamped motion $\tilde{\gamma} << 1$ and overdamped motion $\tilde{\gamma} >> 1$. In the case of overdamped motion inertial effects attributed to the atomic motion can be neglected. If $\tilde{a} = 1$ the two solids are called perfectly commensurate. In this case one finds $\tilde{F}_s = 1$ independent of the values for $\tilde{k}$ and $\tilde{\gamma}$. If $\tilde{a}$ corresponds to a rational number, the two solids are called commensurate and $\tilde{F}_s$ is finite even in the weakly pinned regime. However the values for $\tilde{F}_s$ are typically rather small unless $\tilde{a} = 1$. The consideration of higher harmonics in Eq. (3.1) can result in larger F_s for other rational values of $\tilde{a}$, however, for most practical purposes, higher order contributions are typically small and may be neglected [13].

Concerning the low-velocity kinetic friction in the pinned, overdamped regime, we want to stress that the kinetic friction $\tilde{F}_k(v_0)$ barely depends on the precise value of $\tilde{\gamma}$ in the limit $\tilde{v}_0 \to 0$ since the dissipated energy is proportional to $\int dxm\tilde{\gamma}\tilde{v}$ and the product of $\tilde{\gamma}$ and $\tilde{v}$ is relatively independent of $\tilde{\gamma}$ during most of the pop, i.e., small values of $\tilde{\gamma}$ invoke large $\tilde{v}$ and vice versa. As argued by Fisher [29], the precise value of m in Eq. 3.1 remains irrelevant below a certain threshold value for the energy dissipation during sliding. The low-velocity limit of the friction force is shown in Fig. 8. One can see that $\tilde{F}_k(v_0 \to 0)$ changes qualitatively when $\tilde{\gamma}$ is sufficiently small in order to render the motion underdamped. This is due to the fact that for small $\tilde{\gamma}$ atoms can pick up momentum as they slide downhill. This assists the atoms to overcome the barriers.

2. The static friction force

So far we have only investigated the average value of $\tilde{F}_k$ in the PT model for small $\tilde{v}_0$ under the assumption that the slider's center-of-mass moves smoothly with velocity $\tilde{v}_0$. Smooth sliding can be achieved by driving the system in an appropriate way, which will be discussed later. For the calculation of the smooth sliding $\langle F_k \rangle$, it is indeed sufficient to investigate the coupling of a *single* atom to its ideal lattice site and to the substrate, since the motion of all atoms relative to their preferred positions is identical up to temporal shifts. $\langle \tilde{F}_k(\tilde{v}_0 \to 0) \rangle$ therefore only depends on $\tilde{k}$ and $\tilde{\gamma}$ but not on $\tilde{a}$. The discussion of the Prandtl-Tomlinson model [82,84] is often reduced to this particular calculation of $\tilde{F}_k$ which is as argued above a one-particle property. For the *instantaneous* values of $\tilde{F}_k$ and also for $\tilde{F}_s$, however, it does matter, how the contributions from different atoms add up (interfere) to yield a net force. This in turn depends on the spacing between neighbored atoms. The summation to the net force is relatively straightforward for the two limiting cases of perfectly commensurate walls and for incommensurate walls.

If $\tilde{a} = 1$, every atom in the slider has the same velocity at every instance of time, once steady state (not necessarily smooth sliding) has been reached. Hence the problem is reduced to the motion of a single particle, for which one obtains $\tilde{F}_s = 1$. This provides an upper bound of $\tilde{F}_s$ for arbitrary $\tilde{a}$. If the walls are incommensurate or disordered,

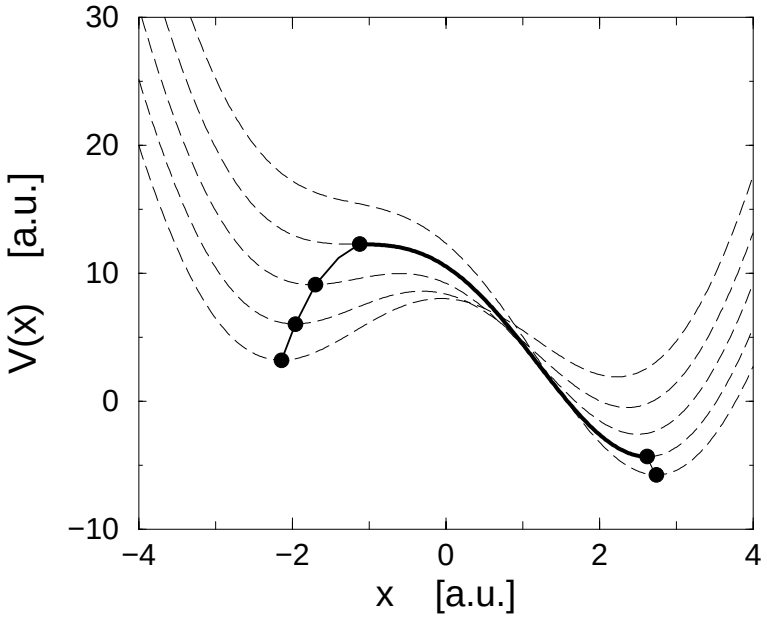

FIG. 7. Schematic representation of the time evolution of the potential energy in the Prandtl-Tomlinson model (dashed lines), see Eq. (3.3). All curves are equidistant in time, separated by a time interval Δt. The circles denote mechanically stable positions and the solid line connects mechanically stable points, indicating the motion of an overdamped point particle.

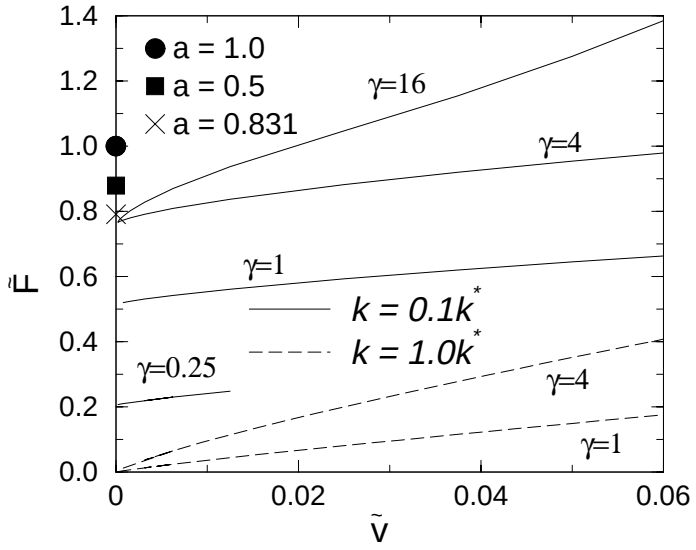

FIG. 8. Average kinetic friction $\tilde{F}$ in the athermal Prandtl-Tomlinson model at low velocities $\tilde{v}$ for two different spring strengths k and various damping coefficients γ. The symbols at $\tilde{v} = 0$ indicate the static friction force for $k = 0.1k^*$. All units are reduced units.

one can again make use of the argument that the motion of all atoms relative to their preferred positions is the same up to temporal shifts once steady state has been reached. Owing to the incommensurability, the distribution of these temporal shifts with respect to a reference trajectory cannot change with time in the thermodynamic limit and the instantaneous value of F_k is identical with $\langle \tilde{F}_k \rangle$ at all times. This gives a lower bound for $\tilde{F}_s$ for arbitrary $\tilde{a}$. The static friction for arbitrary commensurability or finite systems lies in between the upper and the lower bound.

As argued by Fisher, pinned and sliding solutions can only coexist in some range of the externally applied force, if the inertial term exceeds a certain threshold value [29]. For sufficiently small intertial terms, Middleton [85] has shown for a wide class of models, which includes the PT model as a special case, that the transition between pinned and sliding states is nonhysteretic and that there is a unique average value of F_k which does depend on v_0 but not on the initial microstate. The instantaneous value of F_k can nevertheless fluctuate and the maximum of F_k can be used as a lower bound for the static friction force F_s. The measurement of F_s can yet fluctuate, because unlike F_k, it may depend on the initial microstate of the system [85].

3. Thermal effects

Temperature can be incorporated into the PT model by including similar random forces to the equation of motion, Eq. (3.4), as those introduced in the rigid-wall model, Eqs. (2.5) and (2.6). The additional complication in the PT model is the elastic coupling of the central particle to a (moving) equilibrium site, which makes it difficult to apply the rigorous concepts developed for the Brownian motion of a particle in a periodic potential to the PT model.

The first discussion of the effect of thermal fluctuations on friction forces in the Prandtl-Tomlinson model was given by Prandtl in 1928 [18]. He considered a mass point attached to a single spring in a situation where the spring k_1 in Fig. 6 was compliant enough to exhibit elastic instabilities, but yet sufficiently strong in order to allow only for maximaly two mechanically stable positions, see also Fig. 7, in which this scenario is shown. Prandtl argued that at finite temperatures, the atom would not follow the thick line shown in Fig. 7, but thermal fluctuations would assist the atom to convert from one minimum to another one. He then wrote wrote down what we now call a master equation or a transition state theory for the convertion between the mechanically stable states and concluded that the low-temperature, low-velocity *kinetic* friciton force should have a logarithmic dependence on sliding velocity:

$$F(v) = F(v_{\rm ref}) - \chi \ln v/v_{\rm ref}, \tag{3.5}$$

where $v_{\rm ref}$ is a reference velocity and χ a constant. This equation is applicable for velocities small enough such that the (average) kinetic energy is distinctly smaller than the energy barriers, but still large enough in order for the system to be out of thermodynamic equilibrium.

The same equation can be derived within a simple Kramers picture [80,86] for the escape from a well (locked state) assuming that the pulling force produces a small constant potential bias which reduces a height of a potential barrier. The progressive increase of the force results in a corresponding increase of the escape rate that leads to a creep motion of the atom. However, this behavior is different from what occurs when the atom (or an AFM tip) is driven across the surface and the potential bias is continuously ramped up as the support is moved [87,88]. The consequences of this effect will be discussed in more detail in Section III B 2.

Corrections similar to those in Eq. (3.5) apply for the static friction which depends on the rate of loading $\dot{F}'$:

$$F_s = F_s(\dot{F}'_{\rm ref}) - \chi \ln(\dot{F}'/\dot{F}'_{\rm ref}). \tag{3.6}$$

This has been discussed extensively by Evans and Ritchie in the context of the dynamic strength of molecular adhesion bonds [89], who also consider regimes in which F' is extremely large and extremely small (approach to thermal equilibrium).

B. Applications of the Prandtl-Tomlinson model

1. General remarks

The PT model is frequently used as a minimalistic approximation for more complex models. For instance, it is the mean-field version of the Frenkel-Kontorova (FK) model as stressed by D. S. Fisher [83,29] in the context of the motion of charge-density waves. The (mean-field) description of driven, coupled Josephson junctions is also mathematically equivalent to the PT model. This equivalence has been exploited by Baumberger and Caroli for a model that however

was termed the lumped junction model [84] and that attempts to relate the parameters of the PT model to properties of the system embedded between two sliding surfaces. This analogy will be discussed in further detail in Sec. VI B.

The PT model [90] and a generalized PT model [91] were also used to interpret molecular dynamics (MD) simulations [90] of a sliding, commensurate interface between ordered, organic monolayers. Glosli and McClelland [90] identified instabilities ("plucking motion") that lead to typical low-velocity kinetic friction between the two walls. The commensurability in these simulations certainly facilitated the description in terms of a model that is as simple as the PT model, because the relevant degrees of freedom all acted in a rather coherent way. However, in order to understand the experimentally relevant instabilities, it would be necessary to also consider incommensurate alignments of the two surfaces, which has not yet been reported to the best of our knowledge.

Concerning the application of the PT model to dry friction, we want to focus our following discussion mainly on the interpretation of AFM experiments.

2. Interpretation of friction on the nanometer scale

Experimentally, the static friction force is determined as a maximal force needed to initiate sliding motion. The question arises, whether the static friction obtained in this way is a unique (inherent) property of the system, or whether it depends also on the conditions of the measurement. Sec. II C 2 only discussed the maximum possible shear force between a tip and a substrate, but the effect of thermal fluctuations and the effect of the driving device, for instance the stiffness of the driving device or the tip itself, was not included.

Recent experimental studies on atomic force microscopy [92,80] rederived the logarithmic velocity dependence of kinetic friction argued that, due to thermal fluctuations the maximal values of friction force (static friction) has a logarithmic dependence on driving velocity v as described in Eq. (3.5). That equation has been also suggested for interpretation of single molecular mechanical probe experiments [86,93–96] in which the molecule under study is connected to a driven 'spring', an AFM cantilever or a laser trap. Investigated processes include specific binding of ligand-receptor [93], protein unfolding [94,95], and mechanical properties of single polymer molecules such as DNA [96]. In all these experiments one probes forces along a reaction coordinate and their maximal values are ascribed to rupture or unfolding forces.

In the following, we focus on the application of the Prandtl-Tomlinson model to the intepretation of AFM experiments. As mentioned in Chapter III A 3, the potential bias is continuously ramped up as the support of an AFM tip is moved. This results in a different friction-velocity relationship that can be analyzed in terms of the Langevin equation, Eq. (3.5). Thermal fluctuations contribute to the response of the tip in two opposite directions: (a) they help in getting out of locked states at the minima of the total potential $V(x,t)$

$$V(x,t) = V_0 \cos\left(\frac{2\pi}{b}x\right) + \frac{k}{2}(x - vt)^2, \tag{3.7}$$

see also dashed lines in Fig. 7, and (b) they can make a sliding tip return back to a locked state. Therefore the fluctuation assisted motion is expected to cause a decrease in the frictional force at low velocities (stick-slip regime), when the activation dominates over the potential. At high velocities the second effect becomes relevant and causes the observed enhancement of the friction in the sliding regime.

An analytical expression for a velocity dependence of the static friction has been derived considering the thermal activation of the tip out of the locked state has been given recently by Sang et al. [87] and Dudko et al. [88]. In the absence of noise the driven tip leaves a locked state (a minimum of the total potential (x,t)) only when the potential barrier vanishes, i.e. at the instability point where $d^2V/dx^2 = 0$. At this point the spring force reaches the maximum value of $2\pi U_0/b$. In the presence of noise the transition to sliding occurs earlier, and the probability $P_0(t)$ to find the tip in the locked state is given by the following kinetic equation,

$$\frac{dP_o(t)}{dt} = -\omega_0 P_0(t) \exp(-E(t)/k_B T) \tag{3.8}$$

where $E(t)$ is the energy distance between neighboring minimum and maximum of the potential $V(x,t)$ and ω_0 is the characteristic frequency of the order of $(2\pi/b)\sqrt{V_0/m}$. In a locked state, the time dependence of the tip position is given by the equilibrium condition $dV(x,t)/dx = 0$. The value of the activation energy $E(t)$ changes between $2V_0$, at zero driving force, and zero at the instability point. For a weak spring near the instability point, $E(t)$ can be written in the form

$$E(t) = V_0\left(2V_0 - \frac{kvtb}{\pi V_0}\right)^{3/2}. \tag{3.9}$$

This leads to the following equation for the observed maximal force

$$F_{\max} = \text{const} - \frac{\pi}{b} V_0^{1/3} \left[k_B T \ln \left(v \frac{Kb}{2\pi V_0 \omega_0} \right) \right]^{2/3} \tag{3.10}$$

This result describes well the numerical calculations according to the modified Tomlinson model [88] and moreover is in a very good agreement with experiment [87]. This is shown in Fig. 9, where the predicted velocity and temperature dependence agrees in an impressive way with high-precision experimental results by Gnecco at al. [80].

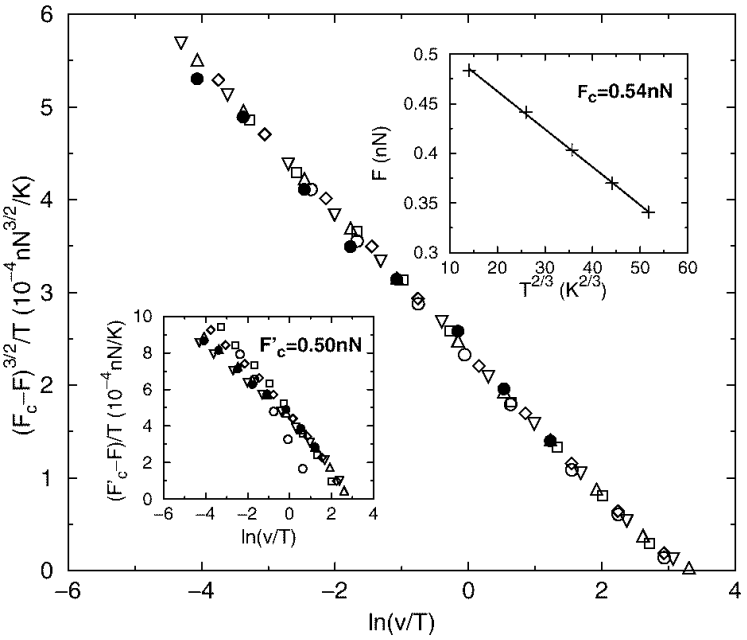

FIG. 9. Test of scaling prediction made implicitly in Eq. (3.10). Experimental data for different temperatures between 53 and 373 K were is taken from Ref. [80]. The upper inset shows the maximim friction force as a function of temperature. The lower inset shows significantly worse scaling for linear creep, using $\ln(v/T)$. The units of velocity v are nm/sec, temperature is in degrees kelvin. Adapted from Ref. [87]

Eq. (3.10) includes explicitly the dependence of the force on the parameters of the microscopic underlying potential and the macroscopic spring constant k. Thus the measured static friction depends not only on the properties of the system under study but also on the driving velocity and mechanical setup (K). For weak spring constants the $(\ln v)^{3/2}$ behavior holds over a wider range of temperatures and driving velocities. Eq. (3.10) differs essentially from the phenomenological estimations [18,80,86,53] that predict a logarithmic variation of $F(v)$ as suggested in Eq. (3.5).

The leading correction to zero-velocity, zero-temperature kinetic friction of the form $(T \ln v)^{2/3}$ as described in Eq. (3.10) apparently also applies to more complicated elastic manifolds. Charitat and Joanny [97] investigated a polymer that was dragged over a surface containing sparsely distributed, trapping sites. They analyzed the competition between the soft elastic, intramolecular interactions, thermal noise, and the tendency of some monomers in the chain to remain pinned to a trapping site. Charitat and Joanny found Coulomb friction with a leading correction term equivalent to that described above.

C. Properties of the Frenkel-Kontorova model

1. Definition of the model and concepts

A generalization of the PT model is the Frenkel-Kontorova [98] (FK), which plays an important role in varios aspects of solid friction. The simplest form of the FK model [98] consists of a one-dimensional chain of N harmonically coupled atoms that interact with a periodic substrate potential, see Fig. 6. The potential energy is:

$$V = \sum_{n=1}^{N} \frac{1}{2} k(x_{n+1} - x_n - a)^2 + V_0 \cos(x_n/b'), \tag{3.11}$$

where a is the separation between two neighbored atoms in the free chain, k the strength of the harmonic coupling between two atoms, $b = 2\pi b'$ is the substrate's periodicity and V_0 the interaction strength between atoms in the chain and the substrate.

Frenkel and Kontorova were not the first ones to use the model which is now associated with their names. However, unlike Dehlinger who suggested the model [99], they succeeded in solving some aspects of the continuum approximation. Like the PT model, the FK model was first used as a description of dislocations in crystals. Many of the recent applications are concerned with the motion of an elastically treated object over (or in) ordered [100] and disordered [101] structures. The FK model and generalizations thereof are also increasingly used to understand the friction between two solid bodies.

Unlike the PT model, the FK model allows for long-range elastic deformations (LRED), which is believed to play an important role in various aspects of solid friction. Also new types of static and dynamic excitatitions such as kinks and solitons are possible in the FK model. As a consequence of the LRED, the lattice constant of the slider is allowed to relax in response to the slider's interaction with the substrate. The resulting average distance $\tilde{a}$ (sometimes imposed through periodic boundary conditions) may differ from the free chain's period a. The ratio $\tilde{\Omega} = \tilde{a}/b$ is sometimes refered to as the winding number. Similar to the PT model, the crucial parameters of the FK model are the ratios $\Omega = a/b$ ($\tilde{\Omega} = \tilde{a}/b$) and $\tilde{k} = kb'^2/V_0$. One novelty of the FK model with respect to the PT model is that the low-velocity limit of the (average) kinetic friction depends sensitively on the ratio $\Omega = a/b$. Also the static friction dependency on the precise value of Ω is much stronger in the FK model than in the PT model.

For any given irrational value of Ω there is an Ω-dependent (dimensionless) threshold spring constant $\tilde{k}_c$. Static friction vanishes for sufficiently strong springs $\tilde{k} > \tilde{k}_c$. Below the critical value $\tilde{k}_c$, metastability occurs and static friction is finite. The transition from finite F_s to zero F_s is accompanied by a phase transition from a commensurate structure to an incommensurate structure [102,103]. For most values of Ω and fixed, non-zero k and V_0, the winding number $\tilde{\Omega}$ is a rational number near Ω. Two neighbored intervals for which $\tilde{\Omega}(\Omega)$ is a rational constant are separated by a point for which $\tilde{\Omega}$ and Ω are both irrational. The transition from commensurate to incommensurate is classified as a second-order transition [102,103], and consequently many properties are powerlaws as a function of $\kappa = \tilde{k} - \tilde{k}'$, i.e. for small κ

$$F_s \propto F_0 \kappa^{\psi'}. \tag{3.12}$$

Critical exponents can also be introduced for other quantities such as phonon gap and elastic coherence length. The varios exponents can be explained in terms of renormalisation theories, see for instance Ref. [104]. We will summarize some properties of the (one-dimensional) FK model qualitatively before focusing on more quantitative studies. Ref. [105] gives a pedagogical introduction into the FK model and Ref. [100] provides an excellent overview over the rich dynamics of the FK model.

2. Continuum approximation and beyond

If the winding number is close to unity and k' is large, then the displacement of an atom with respect to an ideal substrate site will be a slowly varying function with the index n. This implies that if one writes the position of atom n as:

$$x_n/b = 2\pi n + \phi_n, \tag{3.13}$$

one may treat the index n in ϕ_n as a continuous variable [106].

This allows one to transform the discrete equation of motion:

$$m\ddot{x}_n = k(x_{n+1} + x_{n-1} - 2x_n) + \frac{V_0}{b'} \sin(x_n/b') \tag{3.14}$$

into the sine-Gordon equation (SGE)

$$m'\phi_{tt} = k'\phi_{nn} + \sin\phi \tag{3.15}$$

with $m' = mb'^2/V_0$ and $k' = kb'^2/V_0$. For many purpuses one also considers damped dynamics, in which case the inertial term on the left-hand side of Eq. (3.15) is replaced with the first derivative of time, namely with $\gamma\phi_t$ where γ is a damping coefficient.

In the present discussion, we assume periodic boundary conditions and moreover a situation where there is one more (or one less) atom in the chain than minima in the substrate potential. In the SGE, this translates into a boundary condition where ϕ makes a phase shift of $\pm 2\pi$ as one moves through the periodically repeated sequence. For the energetically most stable solutions, atoms will mostly try to sit at the bottom of the potential, but in a relatively narrow region, the required phase shift of $\pm 2\pi$ will occur. Such phase shifts are called walls, discommensurations, or kinks. A representation of a kink is given in Fig. 10. The motion of isolated (and also interactiong) kinks under an externally applied force or field is of course crucial to understand friction in the FK model.

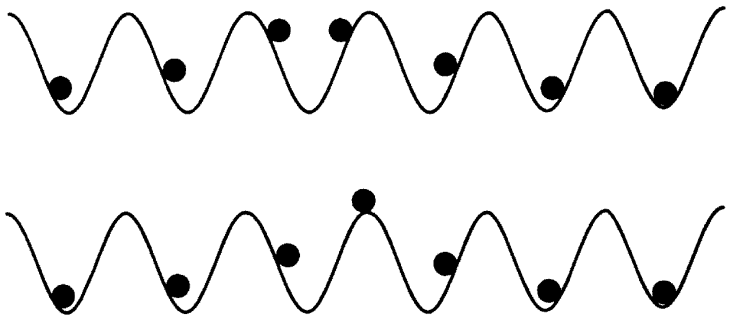

FIG. 10. Stationary configurations of particles in the FK model representing a single kink; top: groundstate and bottom: unstable configuration, corresponding to a saddle point. Adapted from Ref. [100]

In the continuum model, the motion of a kink occurs without energy barriers if $\tilde{\Omega}$ is irrational. For rational $\tilde{\Omega}$ the distribution of ϕ_n in the groundstate must be discrete, which makes it impossible to transform the phases continuously without extra energy. The dynamic solutions of Eqs. (3.15) exploit the isomorphism with nonlinear relativistic wave equations [107,108] and a moving kink (soliton) can be interpreted as an elementary excitation with energy $E_{\rm k}(v)$

$$E_{\rm k} = m_{\rm k}c^2 + \frac{1}{2}m_{\rm k}v^2 + \mathcal{O}(m_{\rm k}v^4/c^2), \tag{3.16}$$

where $c = b\sqrt{k/m}$ is the sound velocity in the free chain. Furthermore, the effective kink mass $m_{\rm k}$ is given by

$$m_{\rm k} = 8m\sqrt{V_0/kb^2}, \tag{3.17}$$

where we have expressed all quantities within the dimensions of the discrete description.

While the system is invariant to any translation of the kink along the chain in the continuum limit (hence the gap-free solitons), discrete models only need to be invariant with respect to a translation by a lattice constant b. If the chain is commensurate with the substrate and/or k' sufficiently small, then a suitably defined kink coordinate X [109] will experience a potential periodic in b, thus

$$V_{\rm PN} = \frac{1}{2}E_{\rm PN}\cos(2\pi X/b). \tag{3.18}$$

$E_{\rm PN}$ is the so-called Peierls-Nabarro barrier [110,111], which can be estimated analytically from extentions of the continuum approximation, see Ref. [100] for an overview. It is important to point out that in the thermodynamic limit of such a quasi-continuum treatment, there is a *finite* energy barrier for the initiation of kink motion (and ultimately sliding). This is different from what one finds in the PT model in the strong pinning limit, namely a well-defined shear pressure and consequently an energy barrier that increases linearly with system size.

3. Thermal and quantum effects

Owing to the discreteness of the FK chain, even the small-velocity motion of a kink does not obey Newtonian dynamics in the sense that the equation of motion $m_{\rm k}\ddot{X} = E_{\rm PN}\sin(X/b')/2b'$ is satisfied. The kink can exchange energy with other internal degrees of freedom of the chain, which can effectively be described as a coupling of the kink to an external heat bath [112]. This suggests that on long time scales in thermal equilibrium, the motion of a kink (which is necessary for mass transport) is equivalent to the thermal motion of an isolated particle on a substrate, see

Sec. III A 3. Stressing this analogy implies that a kink in the 1-d FK model has finite mobility at finite temperature, provided kinks are present. Hence the true static friction can be zero even if slider and substrate are perfectly commensurate. Only if the dimensionality of the interface is sufficiently large, can the energy barrier for the creation of a kink diverge in the thermodynamic limit, as can be the case in two-dimensional FK models [113]. For divergeing activation barriers, a zero mobility of the kink would follow even at finite T.

The discussion above anticipates the presence of kinks. For an open, one-dimensional chain that is not subject to periodic boundary conditions, kinks will always be present even for a slider commensurate with the substrate. The kinks can be thermally induced, because the energy to create a kink is finite. Although their number becomes exponentially small with decreasing temperature T, it remains finite at any finite value of T. Thus the concept of broken analycity (no atom sits on top of an energy barrier) is striclty applicable only at absolute zero temperature. Bak and Fukuyama [114] found that quantum fluctuations also automatically destroy broken analycity even at absolute zero. This finding has been challenged recently by Hu *et al.* [115], but it remains an issue to be settled. For instance, a semiclassical treatment of charge density waves by Miyake and Matsukawa [116] suggests that quantum creep should be present at small temperatures, although it may be very small.

Another interesting quantum effect was suggested by Popov [117] and concerns the phononic friction between two incommensurate, weakly interacting solids rather than the friction due to elastic instabilities. He argues that an efficient energy transfer between the solids ceases to exist at small T, owing to the quantum mechanical nature of phonons, namely the umklapp processes are frozen out at small T. The phononic drag force between the solids would then decrease with a power T^4 for temperatures small compared to the Debye temperature. Popov, however, did not include damping due to energy transfer between internal vibration.

4. Generalized Frenkel-Kontorova models

Various generalizations of the Frenkel-Kontorova model have been proposed in the literature. An important generalization of the FK model with dramatic consequences for the resulting physical properties (critical exponents, scaling of friction force with system size, etc.) is to change the dimensionality of the interface and/or the dimensionality of the sliding elastic medium. Increasing the dimensionality of the sliding object makes the interactions between deformations near the interface effectively more long ranged, and above a critical dimension, the critical behavior of the FK model and that of the PT model become identical. While many studies focus on the tribology of 1-d bodies and 1-d interfaces, the most relevant case for friction between solid bodies is of course a 2-d interface between two 3-d objects.

In many cases, however, only the interactions are altered with respect to Eq. (3.11). One may classify those interaction alterations into three rubrics and combinations of those. (i) Changing the interactions of the atoms within the sliding chain: One possibility is to allow for anhamornicity in the next-neighbor interactions [118], another one to include direct elastic long-range coupling [119]. These alterations can affect the universal behavior of the FK model. One special case of combining local elasticity of the slider as reflected in the FK model and mean-field elasticity such as in the PT model, will be discussed in more detail in Sec. III C 6. (ii) Changing the substrate slider potential: As long as the substrate is still crystalline, this can be done by allowing higher harmonics in the interaction potential. Another possibility, which facilitates analytical calculations is to assume pairwise interactions modeled via Gaussians between slider and substrate atoms. Another possibility is the inclusion of disorder, which is important enough to be discussed further below in Sec. III C 5. New type of behavior is also observed if the substrate is quasiperiodic as discussed by Vanossi et al. [120]. (iii) Allowing for elastic deformations within the substrate [121].

5. Role of dimensionality and disorder

Most real solids and hence surfaces are not perfectly periodic but contain a certain degree of disorder. This can change the tribological properties of a system qualitatively. There are many ways to introduce the effects of disorder into the FK model. One possibility is to assume that the subsrate potential contains random elements, another possibility is to assume that the bond lengths or the spring stiffnisses fluctuate around a mean value.

To discuss the effects of disorder and dimensionality qualitatively, let us consider an $d_{\rm int}$ dimensional substrate surface in interaction with a $d_{\rm obj}$-dimensional elastic solid, which we can envision as a generalization of the FK chain to higher dimensions. In such a situation, there will be a competition between the random substrate-slider interactions and the elastic coupling within the solids. An important question to ask is how the interactions change when we change the scale of the system, for example, how strong are the random and the elastic interactions on a scale $2L$ if we know their respective strengths on a scale L? Here L gives the linear dimension of the solids parallel and normal to the

interface. As discussed above, the random forces between substrate and slider will scale with the square root of the interface's size, hence the random forces scale with $L^{d_{\rm int}/2}$. The elastic forces on the other hand scale[1] with $L^{d_{\rm obj}-2}$. In the thermodynamic limit $L \to \infty$, the effect of disorder will always dominate the elastic interactions or vice-versa, *unless*

$$L^{d_{\rm int}/2} \propto L^{d_{\rm obj}-2}. \tag{3.19}$$

For $\lim_{L\to\infty} L^{d_{\rm int}/2}/L^{d_{\rm obj}-2} >> 1$, the random interactions will dominate and hence pinning via elastic instabilities cannot be avoided. This disorder-induced elastic pinning is then similar to that of compliant, ordered systems as discussed above within the Prandtl-Tomlinson and the Frenkel-Kontorova model. For $\lim_{L\to\infty} L^{d_{\rm int}/2}/L^{d_{\rm obj}-2} << 1$, the long-range elastic forces dominate the long-range random forces. The slider's motion can only be opposed by elastic instabilities if the elastic coupling is sufficiently weak at finite L in order to make local pinning possible, again akin of the case $\lambda > 1$ in the Prandtl-Tomlinson model.

The so-called *marginal* situation, in which both contributions scale with the same exponent, $d_{\rm int}/2 = d_{\rm obj} - 2$, occurs in the important case of 3-d solid bodies with 2-d surfaces. This case will be discussed further below in the context of multiasperity contacts in Sec. VII A. In the marginal situation, the friction force can stay finite, however, one may expect the friction force per unit area and hence the friction coefficient to be exponentially small. For surfaces with roughness exponent zero and typical spacing of a few μm between individual microcontacts, Sokoloff predicted static friction coefficients in the order of 10^{-5} provided that no additional, local instabilities occured in individual microcontacts [122]. The *marginal* dimension in the case of $d_{\rm obj} = d_{\rm int}$ (adsorbed monoatomic layers, charge density waves, etc.) is $d_{\rm mar} = 4$ [29].

Above the critical dimension, the system will be pinned if the systems are sufficiently compliant or "superlubric" if the system are sufficiently stiff. Below the critical dimension the disorder always wins over elasticity and a finite threshold force per unit area is obtained provided that the force acts homogeneously on the particles. We note in passing that there is surprisingly little discussion of systems that are driven via a "hook", which might reflect some tribological situations better than constant field driving.

6. Frenkel-Kontorova-Tomlinson model

As discussed above, there are many generalization of the PT model and the FK model. One particularly interesting case is where the interactions between the atoms within the slider are altered, because one may interpret this change as an attempt is to include both the possibility of long-range elastic deformations (LRED) and the counteracting long-range elastic interactions (LREI). In the PT model, LRED are suppressed and LREI are overestimated. In the FK model, LREI are neglected and LRED are overestimated if the slider is a three-dimensional solid. The Frenkel-Kontorova-Tomlinson (FKT) model [78,123] introduced by Weiss and Elmer is a one-dimensional model that includes both LREI and LRED. It mimics the motion of soft solid on a hard plate and is shown in Fig. 6. Interactions between slider atom and substrate are described by the leading term of the potential in Eq. (2.1) The frictional properties predicted by this model strongly depend on the strength of the interaction between the sliding surfaces (amplitude of the periodic potential V_0) and the commensurability of the surface lattices. There are three threshold values of V_0 at which the behavior changes qualitatively.

Below the first threshold, $V_0^{(1)}$, the static friction is zero whereas above $V_0^{(1)}$ it increases like a power law and approaches the value $F_s^{\rm max} = 2\pi V_0 N/b$ in the asymptotic limit. In the commensurate case, where the ratio a/b of the lattice constants of both sliding surfaces is rational, $V_0^{(1)}$ is zero, because then the two surfaces automatically interlock geometrically. The exponent of the power law is given by the denominator of the fraction a/b. In the incommensurate case, $V_0^{(1)}$ is finite and increases with the ratio κ of the stiffnesses of the particle-upper plate and particle-particle springs. For the golden mean the exponent is roughly 2. This behavior of F_s is similar to what is found for the depinning force of the ground state of the FK model [103], except that in the latter case the value of the exponent for FK model is close to 3.

For V_0 below the second threshold denoted by $V_0^{(2)}$, the kinetic friction FK is zero in the limit of quasistatic sliding, i.e. for sliding velocity $V \to 0$. That is, for $V_0 < V_0^{(2)}$ the kinetic friction behaves similarly to a viscous friction. For

---

[1] A linear chain can be more easily compressed if we replace one spring by two springs coupled in series. In two dimensions, springs are not only coupled in series but also in parallel, so that the elastic coupling remains invariant to a "block transformation". Each additional dimension strengthens the effect of "parallel" coupling.

$V_0 > V_0^{(2)}$ the dynamics is determined by the Prandtl-Tomlinson-like mechanism of elastic instability which leads to a finite kinetic friction. The threshold amplitude $V_0^{(2)}$ increases with κ and is always larger than zero. Therefore, in the commensurate case vanishing kinetic friction does not imply vanishing static friction just like in the PT model. The FKT model for $V_0 > V_0^{(2)}$ is an example of a dry-friction system that dynamically behaves like a viscous fluid under shear even though the static friction is not zero.

The third threshold amplitude, $V_0^{(3)}$, is important for the precise meaning of the static friction F_s. Below this threshold the ground state of the undriven FKT model is the only mechanically stable state. For $V_0 > V_0^{(3)}$ additional metastable states appear. The first metastable state is not very different from the ground state. It can be described as a ground state plus a defect, and it is characterized by equally sized domains. In the commensurate case the gap in the energy between the first metastable state and the ground state is an extensive quantity, i.e., it is proportional to the number of particles. This is a consequence of the nonlocal character of the FKT model.

Since the static friction is the force that is necessary to start sliding, it depends on the state of the system. Therefore static friction is not uniquely defined for $V_0 > V_0^{(3)}$. However, one can introduce the force which gives an upper limit of the actual static friction. It is defined as the smallest force above which there exists no stable state.

The relation between the thresholds introduced above depends on the commensurability of the surface lattices of the upper and lower bodies. In the incommensurate case all three thresholds are identical, $0 < V_0^{(1)} = V_0^{(2)} = V_0^{(3)}$, while for the commensurate case there is the following relation between them, $0 = V_0^{(1)} < V_0^{(2)} < V_0^{(3)}$. Although the FKT model is a very simplified model even for atomically flat surfaces, it is often believed to mimic some of the qualitative behavior of dry friction.

D. Applications of the Frenkel-Kontorova model

1. Incommensurate Crystals

Hirano and Shinjo [22] calculated the condition for static friction between high symmetry surfaces of fcc and bcc metals. Many of their results are consistent with the conclusion that the elastic interactions within the bulk dominate the interactions between the crystals in contact. This would correspond to $k > k^*$ in the PT model, see Eq. (3.2), or to $V_0 < V_0^{(1)}$ in the FKT model, discussed in Sec. III C 6. Hirano and Shinjo [22] tested contacts between various surface orientations of the same metal (i.e. (111) and (100) or (110) and (111)). In all cases the interactions were too weak to produce static friction.

Lancon et al. [124] came to similar conclusions for grain boundaries in gold. Their simulations suggested zero static friction along the incommensurate direction, whereas finite barriers resisted sliding parallel to the commensurate axis. In later work, Lancon [125] varied the normal pressure $p_\perp$ and hence the relative strength between interfacial and intrabulk interactions. At $p_\perp \approx 4$ GPa, he found an elastic instability and finite resistance to sliding also parallel to the incommensurate direction. While this is certainly an exciting result that shows that elastic instabilities are possible, it would nevertheless be difficult to prevent plastic flow or other non-elastic instabilities at the circumference of the contact if no periodic boundary conditions were present.

There have been relatively few experimental tests of the Frenkel-Kontorova model because of the difficulty in making sufficiently flat surfaces and of removing chemical contamination from surfaces. In one of the earliest experiments, Hirano and coworkers examined the orientational dependence of the friction between atomically flat mica surfaces [126]. They found as much as an order of magnitude decrease in friction when the mica was rotated to become incommensurate. Although this experiment was done in vacuum, the residual friction in the incommensurate case may have been due to surface contamination. When the surfaces were contaminated by exposure to air, there was no significant variation in friction with the orientation of the surfaces.

Similar results were obtained in studies of surfaces lubricated with MoS_2 [127]. The MoS_2 forms plate-like crystals that slide over each other within the contact. They appear to be randomly oriented and thus incommensurate. In ultrahigh vacuum the measured friction coefficient was always lower than 0.002 and in many cases dropped below the experimental noise. The authors infer that this low friction is due to sliding between incommensurate plates. When the films are exposed to air the friction coefficient rises to 0.01 to 0.05. This suggests, as in the mica experiments, that a thin film between incommensurate surfaces produces a nonzero static friction. However, the rise in friction may also be related to chemical changes in the MoS_2 on exposure to oxygen [128].

In later work, Hirano and coworkers [129] studied friction as a function of the angle between a flat crystalline AFM tip and a crystalline substrate. Static friction was observed when the crystals were aligned, and decreased below the threshold of detection when the crystals were rotated out of alignment. Unfortunately the crystals were orders

of magnitude smaller than typical contacts. As discussed below IV A, edges can lead to significant friction in small contacts.

2. Adsorbed layers

The most extensive studies of incommensurate systems have used a quartz-crystal microbalance (QCM) to measure the friction between adsorbed layers and crystalline substrates. The QCM is usually used to determine the mass of an adsorbed layer from the decrease in resonance frequency of the quartz crystal. Krim and collaborators [2,4,130] have shown that the increase in the width of the resonance can be used to determine the amount of dissipation due to sliding. The crystal is cut so that the applied voltage drives a shear mode, and the dissipation is studied as a function of drive amplitude.

Measurements have been made on a wide variety of molecules adsorbed on Au, Ag or Pb surfaces [3,4,131,132]. The phase of the adsorbed layer changes from fluid to crystal as the density is increased. As expected, motion of fluid layers produces viscous dissipation, i.e. the friction vanishes linearly with the sliding velocity. The only surprise is that the ratio between friction and velocity, called the drag coefficient, is orders of magnitude smaller than would be implied by the conventional no-slip boundary condition. When the layer enters an incommensurate phase the friction retains the viscous form. Not only does the incommensurate crystal slide without measurable static friction, the drag coefficient is as much as an order of magnitude smaller than for the liquid phase!

The viscous drag observed for these adsorbed layers represents a linear response and can thus be described by the fluctuation-dissipation theorem. This has been used to measure the drag coefficient in MD simulations of Xe on Ag [133]. A simple analytic expression for the drag coefficient can be derived in terms of the phonon damping rate and static response of the film, and agrees well with MD simulations of fluid and incommensurate layers [134,135] The decrease in drag on going from liquid to incommensurate states is found to reflect the decreased deformability of the solid film, and simulations quantitatively reproduce the changes observed in experiments on Kr on Au [134,135] and Xe on Ag [133] (Fig. 11).

Persson has noted that energy can also be dissipated through coupling to low lying electronic excitations of the metallic substrate [48,136]. The relative importance of this mechanism is expected to increase with decreasing temperature (since the phonon life-time increases [132]) and should be larger for molecules with a quadrupole moment like N_2 [137]. Studies of N_2 on Pb [131,138] show a sharp drop in dissipation at the onset of superconductivity which could be attributed to vanishing of the electronic loss mechanism [139,140]. Another group saw neither a drop or any evidence of sliding [141], perhaps due to increased disorder on the surface [142,138]. Indeed one might expect from the arguments of the preceding section that sufficiently large islands of adsorbate will always be pinned by disorder and exhibit a static friction. Simulations suggest that a common form of defect should pin films [143], however the measured friction sometimes *decreases* with increasing disorder [144]. The most recent studies [138] indicate that films may be thermally depinned at high enough temperatures. Another possibility is that the layer deforms plastically rather than elastically and flows around disorder. This type of motion has been directly observed in type-II superconductors where elastic pinning only occurs in finite systems [145].

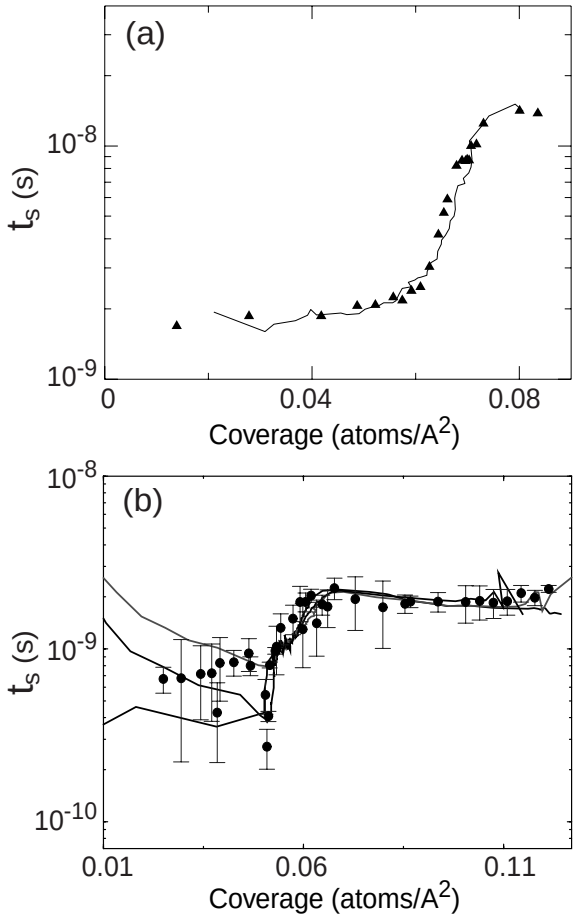

FIG. 11. Slip times vs. coverage for (a) Kr on Au [4], [134] and (b) Xe on Ag [133]. Calculated values are indicated by symbols, and experimental results by solid lines. Experimental data for three different runs are shown in (b).

IV. DRY, NON-ELASTIC CONTACTS

A. Commensurate interfaces

Sufficiently large normal or lateral stresses can lead to plastic deformation and wear. Both processes contribute to the friction force. The simple geometry illustrated in Figure 12 has been the subject of many studies [12]. Here a single crystalline asperity with a clean flat tip is slid over a flat substrate. If the surfaces are commensurate there will be a finite energy barrier for lateral motion. While thermal activation will allow exponentially slow sliding to occur at any finite stress [24], more rapid motion requires lateral stresses large enough to overcome these energy barriers. If this stress is large enough, it may lead to plastic deformation within the tip rather than interfacial sliding.

Sørensen et al. [63] simulated contacts between clean tips and surfaces using a potential for copper atoms. In the case of commensurate (111) surfaces, sliding occurred without wear. The tip followed a zig-zag trajectory, jumping between close-packed configurations. Detailed analysis of the jumps showed that they occurred via a dislocation mechanism. Dislocations were nucleated at the corner of the tip, and then moved rapidly along the interface through the contact region. Analysis of the local stress tensor, showed the stress in these nucleating regions was much larger than the mean values in the contact. When two infinite periodic surfaces were used, there was no region of stress concentration that could nucleate dislocations, and the static friction increased substantially.

The stress concentration near corners follows naturally from the equations of continuum elasticity, which predict diverging stresses at corners between sufficiently dissimilar materials like a tip and the surrounding vacuum. [146–148] The best known example is the case of a crack tip, where the stress at a distance r from the tip grows as $r^{-1/2}$. In the general case the stress diverges as r^{-x} with $x < 1/2$. Vafek and Robbins [149] have recently compared continuum predictions to molecular simulations of the stress near sharp corners. The microscopic stress follows the divergence predicted by continuum theory until it is cut off at some small scale l by the discreteness of the lattice, by anharmonicity, or by plastic yield. Of particular relevance is that the maximum stress diverges as $(L/l)^x$ where L is the system size. This implies that the ratio between the stress at the edge of a finite contact and the mean stress will grow as a power of contact size. Nucleation of dislocations will be possible at lower and lower stresses, leading to decreased static friction. Only in the artificial case of periodic boundary conditions can the edge be removed and nucleation supressed.

This conclusion is closely related to work by Hurtado and Kim [150,151] who used continuum theories of plastic flow to analyze the variation in friction with contact area. They identify three different regimes of behavior. When the contact diameter is less than or comparable to the core size of a dislocation, the entire contact will slip together. In this regime the lateral stress is close to the large values obtained for periodic boundary conditions. As the contact becomes bigger than the core size, nucleation of dislocations at the edges leads to a steady decrease in frictional stress with contact size. At the largest sizes there are many dislocations in the contact that move smoothly along the interface. The lateral stress approaches a lower constant value in this regime. Hurtado and Kim argue that AFM tips and SFA experiments are in the small and large scale limits, respectively, leading to different frictional forces. However, there are many other differences between these two types of experiments, including the chemical constituents of the surfaces.

The above mechanism for sliding involves dislocations, but no wear. Sørensen et al. found no wear between (111) tips and surfaces up to the largest loads studied. Adhesion led to a large static friction at zero load ($\tau_0 \sim 3$GPa) and the friction increased very slowly with load. The slope $\alpha = 0.03$ is comparable to the values found for adsorbed layers as described in the next section. Because of this small slope, friction was observed down to very large *negative* loads corresponding to tensile stresses of ~ 6GPa. Friction at negative loads is not uncommon for experiments between flat, adhesive surfaces. Although it contradicts Amontons's laws (Eq. 1.1), it is consistent with the more general relation based on a local shear stress (Eq. 1.2). One can think of τ_0/α as an adhesive stress that acts like an extra external pressure.

The (111) plane is the easy slip plane for fcc crystals and Sørensen et al. observed very different behavior for (100) tips and surfaces. Sliding in the (011) direction led to inter-plane sliding between (111) planes inside the tip rather than at the contact. As shown in Fig. 12, this plastic deformation led to wear of the tip, which left a trail of atoms in its wake. This adhesive wear led to a steady rise in the contact area, total energy, and friction with sliding distance. The friction showed cyclical fluctuations as stress built up and was then released by nucleation of slip at internal (111) planes.

Nieminen et al. [152] observed a different mechanism of plastic deformation in essentially the same geometry, but at higher velocities (100m/s vs. 5m/s) and with a different model for the potential between Cu atoms. Sliding took place place between (100) layers inside the tip. This led to a reduction of the tip by two layers that was described as the climb of two successive edge dislocations, under the action of the compressive load. Although wear covered more of the surface with material from the tip, the friction remained constant at constant normal load. The reason was

that the portion of the surface where the tip advanced had a constant area. As in Sørensen et al.'s work, dislocations nucleated at the corners of the contact and then propagated through it.

The above simulations both considered identical tips and substrates. Failure moved away from the interface for geometric reasons, and the orientation of the interface relative to easy slip planes was important. In the more general case of two different materials, the interfacial interactions may be stronger than those within one of the materials. If the tip is the weaker material, it will be likely to yield internally regardless of the crystallographic orientation. This behavior has been observed in experiments [31] between clean metal surfaces where a thin tip is scraped across a flat substrate. When the thin tip is softer than the substrate, failure is localized in the tip and it leaves material behind as it advances. However, the simulations considered in this section treated the artificial case of a commensurate interface. It is not obvious that the shear strength of an interface between two incommensurate surfaces should be sufficient to cause such yield or even how the dislocation model of Hurtado and Kim applies to such surfaces.

B. Incommensurate Interfaces

Sørensen et al. [63] also examined the effect of incommensurability. The tip was made incommensurate by rotating it about the axis perpendicular to the substrate by an angle θ. The amount of friction and wear dependend sensitively on the size of the contact, the load and θ. The friction between large slabs exhibited the behavior expected for incommensurate surfaces: There was no wear and the kinetic friction was zero within computational accuracy. The fricion on small tips was also zero until a threshold load was exceeded. Then elastic instabilities were observed leading to a finite friction. Even larger loads lead to wear like that found for commensurate surfaces

The transition from zero to finite friction with increasing load found for small tips can be understood from the Prandtl-Tomlinson model. The control parameter $\tilde{k}$ decreases with load because the interaction between surfaces is increased and the internal stiffness of the solid and tip is relatively unchanged. The pinning potential is an edge effect that grows more slowly than the area. Thus the transition to finite friction occurs at larger loads as the area increases. Tips that were only 5 atoms in diameter could exhibit friction at very small loads. However, when the tip was started at a different position on the surface no friction was observed even at 7.3GPa. When the diameter was increased to 19 atoms, no friction was observed for any position or load considered.

The above studies indicate that while finite contacts are never truly incommensurate, contact areas as small as a few hundred atoms are large enough to exhibit incommensurate behavior. The also confirm Hirano and Shinjo's conclusion that even bare metal surfaces of the same material will not exhibit static friction if the surfaces are incommensurate. Other studies indicate that the interactions between the two surfaces must be many times larger than the internal interactions before elastic multistability leads to pinning. Müser and Robbins considered a simple Prandtl-Tomlinson like model [24] and concluded the inter-surface interactions ϵ_1 needed to be about 6 times large than the intra-surface interactions ϵ_0. Müser [25] later studied contact between 2 to 6 layers of incommensurate surfaces and found no elastic metastability. Instead, spontaneous interdiffusion welded the surfaces together at ϵ_1/ϵ_0 between 6 and 8. Thus elastic metastability is very unlikely to be the origin of static friction between incommensurate surfaces.

Many experiments between clean metals do exhibit static friction even though there is no effort to make them commensurate, so some other mechanism must operate. One possibility is that diffusion allows rearrangements of atoms in the contact into locally commensurate regions on experimental time scales. For example, a high angle grain boundary could roughen to produce a greater surface area, but with lower surface energy. This would naturally lock the surfaces together, leading to static friction. Large-scale rearrangements are too slow to access directly with simulations of bulk surfaces using realistic interactions. However, diffusion and plastic deformation can be accelerated by magnifying the driving energy [25]. Note that in Müser's study [25], interdiffusion was thermodynamically favored as soon as ϵ_1/ϵ_0 exceeded unity. However, it was not observed on simulation time scales until the driving force became strong enough to overcome thermal barriers for diffusion. Barriers to diffusion are also minimized by considering very small tips, as we now discuss.

C. Indentation

A large number of simulations have considered plastic deformation caused by applying a large normal load to a small tip. An extensive review has been given by Harrison et al. [12]. Typically the tip is only 2 or 3 atoms across, in order to mimic AFM tips used for imaging. This small radius of curvature maximizes the interfacial energy driving atomic rearrangements. The barriers for diffusion, and the distances atoms must diffuse are also minimized.

Among the indentation studies of metals are simulations of a Ni tip indenting Au(100) [153], a Ni tip coated with an epitaxial gold monolayer indenting Au(100) [154], an Au tip indenting Ni(001) [155,156], an Ir tip indenting a soft

Pb substrate [157], an Au tip indenting Pb(110) [158], and Cu indenting Cu [63]. In general, plastic deformation occurs mainly in the softer of the two materials, typically Au or Pb in the cases above. The force between the tip and solid remains nearly zero until a separation of order 1 Å. Then there is a rapid jump to contact that produces a large contact area and significant plastic deformation. In the case of Au indenting Ni [156], the Au atoms in the tip displace by 2 Å within ~ 1 ps. The strong adhesive stresses produce reconstruction of the Au layers through the fifth layer of the tip. There is additional reconstruction as the load increases, allowing the contact area to grow much more rapidly than in a purely elastic contact.

Further plastic deformation is generally observed when the tip is withdrawn [159,63,12]. In many cases a crystalline neck of the softer material forms between the tip and substrate. The pulling force oscillates as stress gradually builds and then is suddenly released. During each drop in stress, slip along planes within the neck leads to an increase in the number of atomic layers along its length. The neck gradually thins and may expand many times in length before it ultimately breaks. Sorensen et al. [63] examined the friction due to such necks. The lateral force also shows a cyclical building and release of stress, with a large average friction force. The drops in stress result from slip along (111) planes within the tip. The tip gradually thins and then breaks when the top is displaced by about the contact diameter.

Similar cold-welding and yield may occur in the contacts between asperities on two clean metal surfaces, and many textbooks, following Bowden and Tabor, advance this as the molecular-scale origin of friction. However, any metal exposed to air will acquire a layer of oxide and other contamination. Contact between the underlying metal will only occur at high stresses. Moreover, this mechanism implies extraordinarily high wear: Damage occurs over a depth of several atomic layers during sliding by a similar lateral distance. Many experimental systems slide meters before an atomic layer is worn away. Thus this mechanism is likely to be applicable to a relatively restricted set of circumstances. An important example is the case of machining discussed in the next subsection.

Harrison et al. have considered indentation of non-metallic systems including hydrogen terminated diamond [160,12]. Unlike the metal/metal systems, diamond/diamond systems did not show a pronounced jump to contact. This is because the adhesion between diamond (111) surfaces is quite small if at least one is hydrogen-terminated [161]. For effective normal loads up to 200 nN,(i.e. small indentations), the diamond tip and surface deformed elastically and the force distance curve was reversible. A slight increase to 250nN, led to plastic deformation that produced hysteresis. If the tip was removed after plastic deformation occurred, there was some transfer of material between tip and substrate. However, because diamond is not ductile, pronounced necking was not observed.

Müser [25] examined yield of much larger tips modeled as incommensurate Lennard-Jones solids. The tips deformed elastically until the normal stress became comparable to the ideal stress and then deformed plastically. No static friction was observed between elastically deformed surfaces, while plastic deformation always led to pinning. Sliding led to mixing of the two materials like that found in larger 2D simulations of copper discussed below IV E.

D. Plowing and Machining

One of the commonly described mechanisms for producing friction is plowing [31]. In this case a hard tip is indented into a softer material and "plows" a permanent groove into the material as it slides. The work needed to produce this plastic deformation of the substrate has to be provided by the frictional force. This mechanism clearly occurs whenever a substrate is scratched during sliding. This naturally leads to rapid wear, which may be desirable in the context of machining.

Large scale, two and three-dimensional molecular dynamics simulations of the indentation and scraping of metal surfaces were carried out by Belak and Stowers [162]. A blunted carbon tip was first indented into a copper surface and then pulled over the surface. In the two-dimensional simulation, the contact followed Hertzian behavior up to a load $L \approx 2.7$ nN and an indentation of about 3.5 Cu layers. The surface then yielded through creation of a series of single dislocation edges along the easy slip planes. After indentating by about 6 Cu layers, the carbon tip was slid parallel to the original Cu surface. The work per unit volume of removed material was found to scale as $(D)^{-0.6}$, where D is the depth of cut. The same power law was observed in machining of Cu with a 25nm tip [163], but macroscopic experiments typically give an exponent of -0.2. Belak and Stowers note that the change in exponent occurs in experiments when the depth of cut is comparable to the grain size, leading to new deformation mechanism.

In the three-dimensional (3D) simulations, the substrate contained as many as 36 layers or 72,576 atoms. Hence long-range elastic deformations were included. The surface yielded plastically after an indentation of only 1.5 layers, through the creation of a small dislocation loop. The accompanying release of load was much bigger than in 2D. Further indentation to about 6.5 layers produced several of these loading-unloading events. When the tip was pulled out of the substrate, both elastic and plastic recovery was observed. Surprisingly, the plastic deformation in the 3D studies was confined to a region within a few lattice spacings of the tip, while dislocations spread several hundred lattice

spacings in the 2D simulations. Belak and Stowers concluded that dislocations were not a very efficient mechanism for accommodating strain at the nanometer length scale in 3D.

When the tip was slid laterally at $v = 100$m/s during indentation, the friction or "cutting" force fluctuated around zero as long as the substrate did not yield (Fig. 13). This nearly frictionless sliding can be attributed to the fact that the surfaces were incommensurate, and the adhesive force was too small to induce locking. Once plastic deformation occurred, the cutting force increased dramatically. Fig. 13 shows that the lateral and normal forces are comparable, implying a friction coefficient of about one. This large value was expected for cutting by a conical asperity with small adhesive forces [164].

More recently Zhang and Tanaka have performed similar simulations of 2D [165] and 3D [166] machining. The latter work considered both a spherical tip translating rigidly over a silicon surface and a spherical "wear" particle that rotated as it advanced. At low loads the substrate deforms elastically and there is no friction or wear. At higher loads the top layer of silicon is plastically deformed into an amorphous state, and some atoms may adhere to the tip. Still higher loads lead to the plowing of a permanent groove in the material, and finally to cutting, where a chip forms ahead of the tip and then flakes off. Cutting is very unlikely to occur when the tip is replaced by a wear particle that is free to rotate.

E. Plastic Deformation and Material Mixing

All of the above simulations were done in relatively small systems where there are no pre-existing dislocations and the yield stress is near its theoretical maximum. At the larger scales relevant to many experiments, the yield stresses and the oscillations in stress during yield events may be much smaller. On these scales and in ductile materials, plastic deformation is likely to occur throughout a region of some characteristic width about the nominal sliding interface [167]. Sliding induced mixing of material from the two surfaces and sliding induced grain boundaries are two of processes that have been observed in experiments and in recent simulations of large systems.

Hammerberg et al. [168] performed large-scale simulations of a two-dimensional model for copper. The simulation cell contained 256×256 Cu atoms that were subject to a constant normal pressure $P_\perp$. Two reservoir regions at the upper and lower boundaries of the cell were constrained to move at opposite lateral velocities $\pm u_{\rm p}$. The initial interface was midway between the two reservoirs.

The friction was measured at $P_\perp = 30$GPa as a function of the relative sliding velocity v. Different behavior was seen at velocities above and below about 10% of the speed of transverse sound. At low velocities, the interface welded together and the system formed a single workhardened object. Sliding took place at the artificial boundary with one of the reservoirs. At higher velocities the friction was smaller, and decreased steadily with increasing velocity. In this regime, intense plastic deformation occurred at the interface. Hammerberg et al. (1998) found that the early time-dynamics of the interfacial structure could be reproduced with a Frenkel-Kontorova model. As time increased, the interface was unstable to the formation of a fine-grained polycrystalline microstructure, which coarsened with distance away from the interface as a function of time. Associated with this microstructure was the mixing of material across the interface.

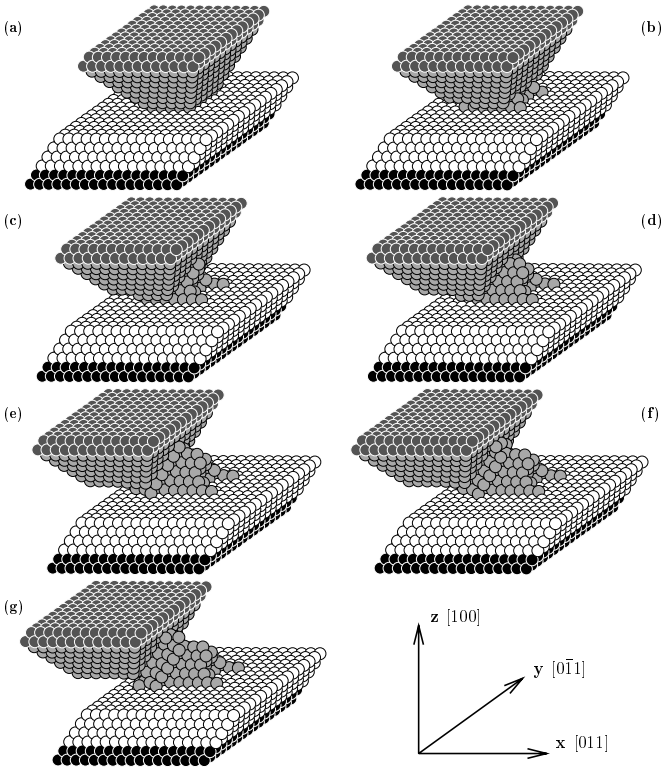

FIG. 12. Snapshots showing the evolution of a Cu(100) tip on a Cu(100) substrate during sliding to the left. (From Sørensen et al., 1996.)

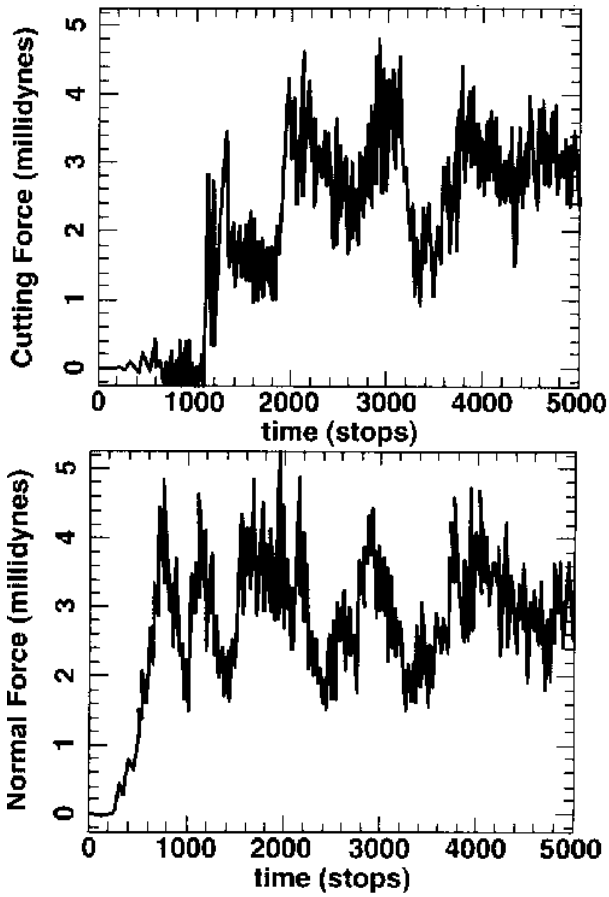

FIG. 13. Normal (bottom) and lateral (top) force on a three dimensional, pyramidal Si tip on a copper surface as a function of time. No plastic flow was reported up to 1,000 time steps. The indentation stopped at about 5 layers after 2,000 time steps. (From Belak and Stowers, 1992.)

V. EMBEDDED SYSTEMS AND LUBRICANTS

A. Structural changes at a solid/fluid interface

There have been many analytic and numerical studies of the structure that solids induce in an adjacent fluid. Early studies focussed on layering in planes parallel to a flat solid surface. The sharp cutoff in fluid density at the wall induces density modulations with a period set by oscillations in the pair correlation function for the bulk fluid [169–173]. An initial fluid layer forms at the preferred wall-fluid spacing. Additional fluid molecules tend to lie in a second layer, at the preferred fluid-fluid spacing. This layer induces a third, and so on. The pair correlation function usually decays over a few molecular diameters, except near a critical point or in other special cases. Simulations of simple spherical fluids show of order 5 clear layers [174–176], while the number is typically reduced to 3 or less for chain or branched molecules that have several competing length scales [177–180].

Crystalline walls also induce commensurate density modulations within the plane of the fluid layers [174,181,182,176,183,184]. In extreme cases, one or more layers may actually crystallize, forming a solid wetting layer [155,174,176]. These changes in structure near the wall modify the local viscosity. Somewhat surprisingly, the strength of layering has almost no direct effect on viscosity [174]. Indeed, layering is strongest for ideal flat surfaces that can not exert any lateral stress. In contrast, there is a one-to-one correspondence between the degree of commensurate in-plane order and the viscous coupling between the first layer and the substrate [174]. This can be understood from simple perturbation arguments [185] that are directly related to the analytic theory for friction between an adsorbed monolayer and a substrate described above [134,135].

The viscosity change near a solid interface can be quantified by a slip length S that represents the change in the effective hydrodynamic width of the film. If v is the lateral velocity, then the shear rate in the center of a film confined by two identical walls separated by distance h is changed from v/h to $v/(h+2S)$. Positive values of S imply a decrease in viscosity or "slip" at the wall, so that the effective width of the channel is larger. Negative values imply that fluid within a distance $|S|$ is "stuck" and moves with the same velocity as the wall. Simulations show that S can be of either sign, and its magnitude is usually comparable to a molecular diameter [175,181,186]. It can grow to much larger scales if the coupling between the wall and fluid is weak or the lateral density modulations are frustrated by incompatible spatial periods [187,181]. The slip length can also increase when the stress exceeds the maximum value the interface can support [188].

B. Phase transitions in thin films

When the thickness of a fluid film is reduced below of order 10 molecular diameters, the ordering influences of the two confining walls begin to interfere. As a result, the normal pressure P, viscosity and other properties of the film show periodic oscillations as a function of the thickness h. One dramatic result is that the system becomes linearly unstable in regions where $dP/dh > 0$, leading to discontinuous changes in the number of layers of atoms between the two surfaces [189].

Pioneering grand canonical Monte Carlo simulations by Schoen et al. [176,183,184] examined the equilibrium behavior of a film of spherical molecules between two commensurate walls. As h and the lateral translation $\vec{x}$ of the top wall were varied, the film underwent transitions between fluid and crystalline states. The crystal was stable when the thickness was near an integral multiple of the spacing between crystalline layers, and when the lateral translation was also consistent with the crystalline repeat. In this case, the ordering influences of the two walls interfered constructively and provided a strong ordering influence. Other values of h and $\vec{x}$ led to destructive interference and stabilized the fluid phase.

The resulting variations in free energy with $\vec{x}$ imply a strong static friction mediated by the film. Müser and Robbins later argued that the in-plane order induced by commensurate walls should always lead to a finite static friction – even if the film is in the fluid state [24]. The reason is that the linear response to one wall produces a commensurate modulation in the density of the fluid that propagates to the second wall. The energy of the second wall must depend on its phase with respect to this commensurate disturbance. Although the perturbation may be exponentially weak at large thicknesses, it is proportional to the contact area and will eventually pin the walls. Müser and Robbins verified this conclusion using simulation studies of the lateral diffusion of the walls in the absence of any lateral force [24]. The walls remained pinned by a periodic potential even when the intervening fluid layers were in a gaseous state! Curry et al. [190] also observed pinning by a film with rapid diffusion. As for bulk crystals, diffusion is not incompatible with the long-range structural order that separates a fluid and solid state.

Thompson et al. [191,178] studied phase transitions of spherical and chain molecules between commensurate walls. As the film thickness h decreased or pressure P increased, films of spherical molecules underwent a first-order transition

to a commensurate crystalline state. However, short chain molecules underwent a continuous glass transition. The divergence of the characteristic relaxation time, viscosity, and inverse of the diffusion constant could be fit to a free volume theory [178] like that used to describe the glass transition in many bulk systems [192]. The amount of commensurate structure induced in solid glassy films [178] was too small to explain the large static friction. The transition is analogous instead to "jamming" transitions in many other equilibrium and non-equilibrium systems, such as glass forming materials, granular media, and foams [193]. Jamming of spherical and chain molecules has also observed between amorphous [181,61] and incommensurate walls [30,61,194,195] where the effect of any induced lateral modulations averages to zero. A finite yield stress that corresponds to a static friction is required to unjam the system and produce shear.

Gao et al. [179,180] have examined changes in the equilibrium structure of films with film thickness. Their work uses more realistic potentials and allows molecules to be exchanged between the film and a surrounding reservoir. However, both these simulations and experiments may have difficulties in achieving equilibrium due to the sluggish dynamics of films as they approach a glassy state. Gao et al. contrast the behavior of simple linear and more complex branched molecules. Simple linear alkanes show much more pronounced layering. There is also more in-plane order within the layers, although at the intrinsic spacing of an alkane crystal rather than at the period of the wall. Branched molecules show less order in both directions. Gao et al. also calculate the normal load, or solvation force, needed to maintain a given film thickness. This force oscillates as the layering influences from the two walls change from constructive to destructive interference. The oscillations are more pronounced for the linear molecules that show sharper layers. The more ordered layers also take more time to squeeze out, indicating that they are more solid-like, however the viscosity of the films was not studied. Gao et al. [196] also investigated the effects of (sub)nanoscale roughness and found that even a small amount can strongly reduce the solvation force and lead to better stick condition of the confined fluid.

C. Connection to experimental studies

The above studies have benefited from a fertile exchange with experimental groups using the Surface Force Apparatus (SFA). The SFA allows the mechanical properties of fluid films to be studied as a function of thickness over a range from hundreds of nanometers down to contact. The fluid is confined between two atomically flat surfaces. The most commonly used surfaces are mica, but silica, polymers, and mica coated with amorphous carbon, sapphire, or aluminum oxide have also been used. The surfaces are pressed together with a constant normal load and the separation between them is measured using optical interferometry. The fluid can then be sheared by translating one surface at a constant tangential velocity [39,7] or by oscillating it at a controlled amplitude and frequency in a tangential [197–200] or normal [201,202] direction. The steady sliding mode mimics a typical macroscopic friction measurement, while the oscillatory mode is more typical of bulk rheological measurements (see Sec. VI C). Both modes reveal the same sequence of transitions in the behavior of thin films.

When the film thickness h is sufficiently large, one observes the rheological behavior typical of bulk fluids [201,202]. Flow can be described by the bulk viscosity μ_B and a slip length S at each wall. As in simulations, typical values of S are comparable to molecular dimensions and would be irrelevant at the macroscopic scale. However, a few systems show extremely large slip lengths, particularly at high shear rates [203,204].

When the film thickness decreases below of order ten molecular diameters, the deviations from bulk behavior become more dramatic [39,199,205]. There are pronounced oscillations in the solvation force. As in simulations [179,180], these oscillations are most pronounced for simple spherical molecules, less pronounced for short chain molecules, and smallest for branched molecules. There is also a dramatic increase in the stress needed to shear the films as h decreases. The shear stress is far too large to interpret in terms of a bulk viscosity and slip length, because the width of the fluid region $h + 2S$ would have to be much smaller than an Angström. Experimental results are often expressed in terms of an effective viscosity $\mu_{eff} \equiv \tau h/v$ and effective shear rate $\dot{\gamma}_{eff} \equiv v/h$. For almost all fluids studied, the low frequency limit of μ_{eff} rises by many orders of magnitude as the film thickness drops to a few molecular diameters [39,197,205]. At the same time, the shear rate at which the low frequency limit is reached decreases by more than 10 to 12 orders of magnitude. Both observations imply a divergence in the relaxation time for structural rearrangements in the film. By the time h reaches two or three molecular diameters, most films behave like solids over the accessible range of time scales. The main exception is water which seems to retain its fluid character [206–208].

In some cases the transition looks like a continuous glass transition, but at temperatures and pressures that are far from the glass region in the bulk phase diagram. In fact, the molecules may not readily form glasses in the bulk. In other cases the transition from liquid to solid behavior of the film appears to occur discontinuously, as if the film underwent a first-order freezing transition [200,205]. Simulations suggest that this is most likely to happen when the crystalline phase of the film is commensurate with the solid walls, and when the molecules have a relatively simple structure that facilitates order [39,178–180,209]. Unfortunately, no direct experimental determination of the structure

of confined films has been made to determine whether they are crystalline or amorphous and different behavior has been reported for the same fluid. Part of the variation in experimental results is attributable to different mechanical properties and modes of operation (Sec. VI C) of the experimental setups and perhaps to variations in the purity of the fluids, however there are also differences in definition. The discontinuous jumps in shear response reported by Klein and Kumacheva [200,205] occurred during a discontinuous decrease in the number of layers confined between the surfaces [200,205]. A mechanical instability leading to a change in the number of layers will always produce discontinuous changes in mechanical properties. One can only expect a continuous glass transition if the density, or free volume, is varied continuously. Because the thickness is not a unique function of load, the density can be varied by decrease the load with a fixed number of layers. Klein and Kumacheva do report a fairly continuous decrease of the yield stress when the load was decreased in this way. If the fluid were crystalline, one would expect a discontinuous transition during this decrease in load. Another observation that suggests that films form glassy states is that a crystal would in general be incommensurate with at least one of the two unaligned surfaces, leading to much smaller friction forces than observed.

Clearly the film thickness, fluid density, and perhaps the orientation of the surfaces [207], are additional thermodynamic variables that may shift or alter phase boundaries. Cases where a single interface stabilizes a different phase than the bulk are central to the field of wetting. The presence of two interfaces separated by only a few nanometers leads to more pervasive phase changes.

The rheological response of bulk materials frequently obeys time-temperature scaling near the glass transition [210,211]. The real and imaginary parts of the elastic moduli, describe the stiffness and viscosity as a function of frequency. Results from different temperatures can be collapsed onto a universal curve if the frequency is multiplied by a temperature dependent relaxation time, and the viscosity is normalized by its low frequency limit. Demirel and Granick [197] achieved a similar collapse by scaling their data by a relaxation time that depended on film thickness rather than temperature. This suggested that their film underwent a glass transition much like that of a bulk material.

Figure 14 shows that simulation results for the viscosity of thin films can also be collapsed using Demirel and Granick's approach [212]. Data for different thicknesses, normal pressures, and interaction parameters [178,191] were scaled by the low shear rate viscosity μ_0. The shear rate was then scaled by the rate $\dot{\gamma}_c$ at which the viscosity dropped to $\mu_0/2$. Also shown on the plot (circles) are data for different temperatures that were obtained for longer chains in films that are thick enough to exhibit bulk behavior [213,212,214]. The data fit well on to the same curve, providing a strong indication that a similar glass transition occurs whether thickness, normal pressure, or temperature is varied.

As in the case of bulk glasses, the issue of whether there is a true glass transition at finite temperature is controversial because observation times are limited, particularly for simulations. However thin films of most molecules act like solids over experimentally accessible times. No motion occurs until a yield stress is exceeded, and the calculated yield stress is comparable to values for bulk solid phases of the molecules at higher pressure or lower temperature. The response of the walls to a lateral force becomes typical of static friction, and Gee et al. analyze their results in terms of equation 1.2 using S_c and C in place of τ_0 and α, respectively. The values of τ_0 are of order a few to 20MPa, and values of α range from 0.3 to 1.5. However, the latter are influenced by the change in film thickness at the relatively low pressures used (< 40 MPa) and would probably not be representative of the behavior in a typical mechanical device.

D. Jammed monolayers and Amontons' laws

Physisorbed molecules, such as the short hydrocarbons in the SFA experiments described above, can be expected to sit on any surface exposed to atmospheric conditions. Even in ultra-high-vacuum, special surface treatments are needed to remove strongly physisorbed species from surfaces. Since such films jam between randomly oriented mica surfaces, Robbins and Smith suggested they could be responsible for the finite static friction between many macroscopic objects [215]. Recent simulations [30,194,61,24,25] and analytic work [61] have supported this speculation.

The static friction between bare incommensurate or amorphous surfaces vanishes in the thermodynamic limit because the density modulations on two bare surfaces can not lock into phase with each other unless the surfaces are unrealistically compliant [61]. However, a sub-monolayer of molecules that form no strong covalent bonds with the walls can simultaneously lock to the density modulations of both walls. Once they adapt to the existing configuration of the walls, they will resist any translation that would change their energy minima. This gives rise to a finite static friction for all surface symmetries: commensurate, incommensurate, and amorphous [61]. In essense, the layer plays the role of weak springs in the Prandtl-Tomlinson model (Sec. III A), although the detailed picture may be different for kinetic friction [216]. In order to also induce finite F_k, sudden jumps of the confined atoms must occur between symmetrically inequivalent positions when one wall is slid with respect to the other. Such jumps are frequently absent for commensurate surfaces, which implies zero kinetic but finite static friction.

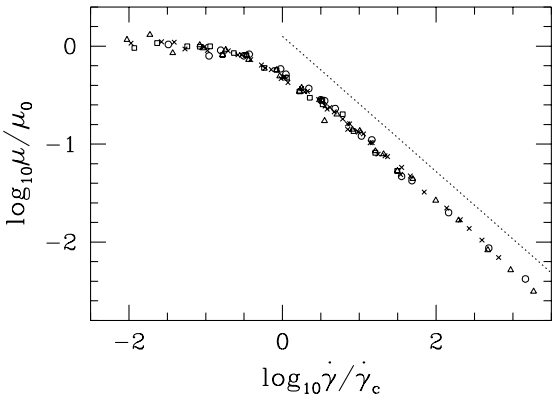

FIG. 14. Collapse of simulation data for the effective viscosity vs. shear rate as a glass transition is approached by decreasing temperature (circles), increasing normal pressure at fixed number of fluid layers (triangles) or decreasing film thickness at fixed pressure with two different sets of interaction potentials (squares and crosses). The dashed line has a slope of -0.69.

The variation of the friction with wall geometry, interaction potentials, temperature, velocity and other parameters has been determined with simulations using simple spherical or short-chain molecules to model the monolayer [30,194,61,24,25]. In all cases, the shear stress shows a linear dependence on pressure consistent with Equation 1.2 up to the gigapascal pressures expected in real contacts. Moreover, the friction is relatively insensitive to parameters that are not controlled in typical experiments, such as the orientation of crystalline walls, the direction of sliding, the density of the layer, the length of the hydrocarbon chains, etc.. Variations are of order 20% which is comparable to variations in results from different laboratories [44,217]. Larger variations are only seen for commensurate walls, which may also exhibit a nonlinear pressure dependence [218].

The linear variation of τ with P (Eq. 1.2) can be understood from a simple hard sphere picture. Once the molecules have conformed to the surface, they produce an interlocking configuration like that envisioned by early researchers Fig. 1(a), but at an atomic scale. The value of α is the effective slope that the surface must be lifted up over this interlocking layer. The main factor that changed τ_s in the above simulations was the ratio of the characteristic length for wall-adsorbate interactions $\sigma_{\rm wa}$ to the nearest-neighbor spacing on the walls, d. As the ratio $\sigma_{\rm wa}/d$ decreased, adsorbed atoms could penetrate more deeply into the corrugation on the wall and both the effective slope and α increased.

Physisorbed molecules also provide a natural explanation for the logarithmic increase in kinetic friction with sliding velocity that is observed for many materials, and represented by the coefficient A in the rate-state model of Equation 1.5. Figure 15 shows calculated values of τ_0 and α as a function of $\log v$ for a submonolayer of chain molecules between incommensurate surfaces [194]. The value of τ_0 becomes independent of v at low velocities. The value of α, which dominates the friction at large loads, rises linearly with $\log_1 0v$ over more than two decades in velocity. He and Robbins were able to correlate this scaling with thermally activated hops of the chain molecules. At low velocities, almost all the molecules are stuck in a local potential minimum at any instant [61,194]. At zero temperature, they can only move when the applied stress makes their local minimum become mechanically unstable. At finite temperature, thermal activation allows motion at a lower stress. As the velocity decreases, there is more time for activated hops, and the friction decreases. If the shift in barrier height drops linearly with stress, τ varies as $A \log v$ with A proportional to temperature. He and Robbins found that A did rise roughly linearly with temperature. Calculated values of A/μ_0 at the relatively large temperatures they used were between 0.025 and 0.05. Experimental values for rocks are in roughly the same range, about 0.008 to 0.025.

The above results suggest that adsorbed molecules and other "third-bodies" may prove key to understanding macroscopic friction measurements. It will be interesting to extend these studies to more realistic molecular potentials and to rough surfaces. Similar arguments apply to other so-called "third-bodies" that are trapped between two surfaces, such as wear debris, grit, dust, etc.. These particles are too large to lock in the valleys between individual atoms, but can lock in places where the two opposing rough surfaces both have larger valleys.

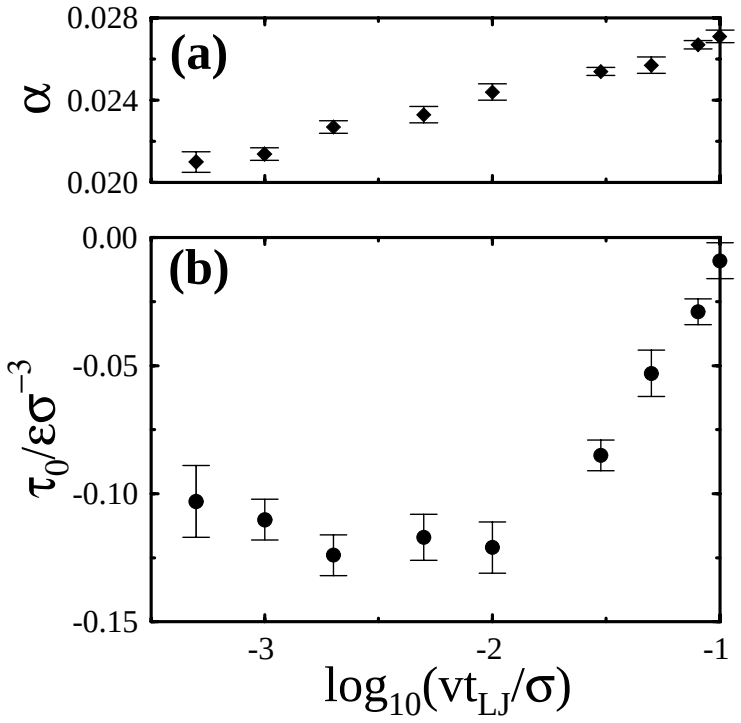

FIG. 15. Plot of (a) α and (b) τ_0 against the logarithm of the velocity for incommensurate walls separated by a monolayer of chain molecules containing six monomers each. Velocities are in Lennard-Jones units of σ/t_{LJ} that corresponds to roughly 100m/s.

VI. UNSTEADY SLIDING

A. Stick-Slip Dynamics

The dynamics of sliding systems can be very complex and depend on many factors, including the types of metastable states in the system, the times needed to transform between states, and the mechanical properties of the device that imposes the stress. At high rates or stresses, systems usually slide smoothly. At low rates the motion often becomes intermittent, with the system alternately sticking and slipping forward. [44,31] Everyday examples of such stick-slip motion include the squeak of hinges and the music of violins.

The alternation between stuck and sliding states of the system reflects changes in the way energy is stored. While the system is stuck, elastic energy is pumped into the system by the driving device. When the system slips, this elastic energy is released into kinetic energy, and eventually dissipated as heat. The system then sticks once more, begins to store elastic energy, and the process continues. Both elastic and kinetic energy can be stored in all the mechanical elements that drive the system. The whole coupled assembly must be included in any analysis of the dynamics.

The simplest type of intermittent motion is the atomic-scale stick-slip that occurs in the multistable regime ($\tilde{k} < 1$) of the Prandtl-Tomlinson model. Energy is stored in the springs while atoms are trapped in a metastable state, and converted to kinetic energy as they pop to the next metastable state. This phenomenon is quite general and has been observed in many simulations of wearless friction [12,13] as well as in the motion of atomic force microscope tips. [6,9] In these cases, motion involves a simple ratcheting over the surface potential through a regular series of hops between neighboring metastable states. The slip distance is determined entirely by the periodicity of the surface potential. Confined films, adsorbed layers, and other non-elastic systems have a much richer potential energy landscape due to their many internal degrees of freedom. One consequence is that stick-slip motion between neighboring metastable states can involve microslips by distances much less than a lattice constant. [181,213,212] An example is seen at $t/t_{\rm LJ} = 620$ in Fig. 16(b). Such microslips involve atomic-scale rearrangements within a small fraction of the system. Closely related microslips have been studied in granular media and foams. [219–221]

Many examples of stick-slip involve a rather different type of motion that can lead to intermittency and chaos. [53,51] Instead of jumping between neighboring metastable states, the system slips for very long distances before sticking. For example, Gee et al. [39] and Yoshizawa et al. [222] observed slip distances of many microns in their studies of confined films. This distance is much larger than any characteristic periodicity in the potential, and varied with velocity, load, and the mass and stiffness of the SFA. The fact that the SFA does not stick after moving by a lattice constant indicates that sliding has changed the state of the system in some manner, so that it can continue sliding even at forces less than the yield stress.

One simple property that depends on past history is the amount of stored kinetic energy. This can provide enough inertia to carry a system over potential energy barriers even when the stress is below the yield stress. This simplest example is the underdamped Prandtl-Tomlinson model which has been thoroughly studied in the mathematically equivalent case of an underdamped Josephson junction. [223] One finds a hysteretic response function where static and moving steady-states coexist over a range of forces between $F_{\rm min}$ and the static friction F_s. There is a minimum stable steady-state velocity $v_{\rm min}$ corresponding to $F_{\rm min}$. At lower velocities, the only steady state is linearly unstable because $\partial v/\partial F < 0$ – pulling harder slows the system. It is well-established that this type of instability can lead to stick-slip motion. [31,44] If the top wall of the Tomlinson model is pulled at an average velocity less than $v_{\rm min}$ by a sufficiently compliant system, it will exhibit large-scale stick-slip motion.

Experimental systems typically have many other internal degrees of freedom that may depend on past history. Most descriptions of stick-slip motion have assumed that a single unspecified state variable is relevant and used the phenomenonological rate-state models described in Sec. I D. This approach has captured experimental behavior from a wide range of systems including surface force apparatus experiments, [224,48] sliding paper, [53] and earthquakes. [52] However, in most cases there is no microscopic model for the state variable and its time dependence. This makes it difficult to understand how small changes in materials, such as the percentage of used aluminum cans, can effect stick-slip in a process such as aluminum extrusion.

One set of systems where microscopic pictures for the state variable have been considered are confined films in SFA experiments. Confined films have structural degrees of freedom that can change during sliding, and this provides an alternative mechanism for stick-slip motion. [181] Some of these structural changes are illustrated in Fig. 16 which shows stick-slip motion of a two layer film of simple spherical molecules. The bounding walls were held together by a constant normal load. A lateral force was applied to the top wall through a spring k attached to a stage that moved with fixed velocity v in the x direction. The equilibrium configuration of the film at $v = 0$ is a commensurate crystal that resists shear. Thus at small times, the top wall remains pinned at $x_W = 0$. The force grows linearly with time, $F = kv$, as the stage advances ahead of the wall. When F exceeds F_s, the wall slips forward. The force drops rapidly

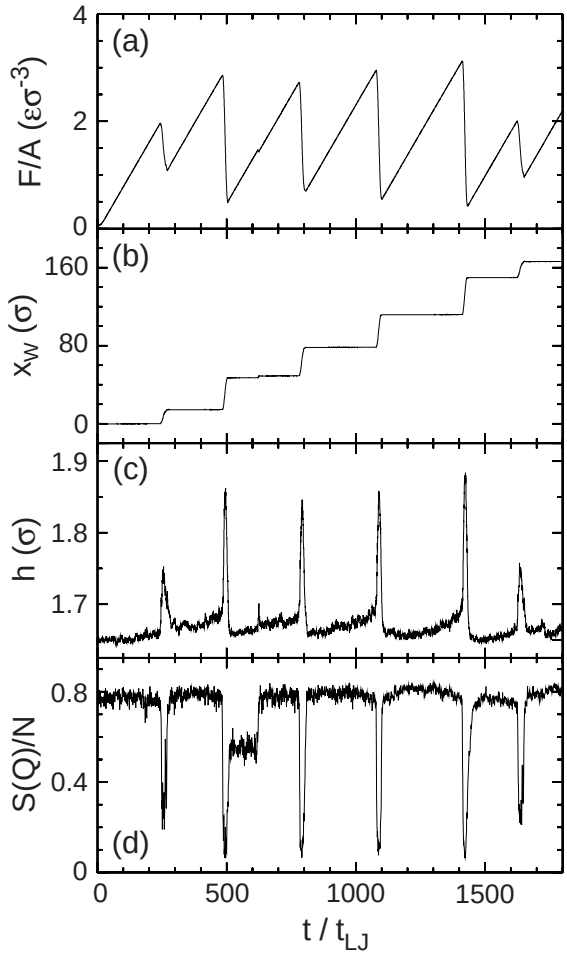

FIG. 16. Time profiles of the (a) frictional force per unit area F/A, (b) displacement of the top wall x_W, (c) wall spacing h, and (d) Debye-Waller factor $S(Q)/N$ during stick-slip motion of spherical molecules that form two crystalline layers in the static state. Note that the system dilates (c) during each slip event. The coinciding drop in Debye-Waller factor shows a dramatic decrease from a typical crystalline value to a characteristic value for a fluid.

because the slip velocity $\dot{x}_W$ is much greater than v. When the force drops sufficiently, the film recrystallizes, the wall stops, and the force begins to rise once more.

One structural change that occurs during each slip event is dilation by about 10% (Fig. 16(c)). Dhinojwala and Granick [225] have recently confirmed that dilation occurs during slip in SFA experiments. The increased volume makes it easier for atoms to slide past each other and is part of the reason that the sliding friction is lower than F_s. The system may be able to keep sliding in this dilated state as long as it takes more time for the volume to contract than for the wall to advance by a lattice constant. Dilation of this type plays a crucial role in the yield, flow and stick-slip dynamics of granular media. [226,227,219]

The degree of crystallinity also changes during sliding. Deviations from an ideal crystalline structure can be quantified by the Debye-Waller factor $S(Q)/N$ (Fig. 16d), where Q is one of the shortest reciprocal lattice vectors and N is the total number of atoms in the film. When the system is stuck, $S(Q)/N$ has a large value that is characteristic of a 3D crystal. During each slip event, $S(Q)/N$ drops dramatically. The minimum values are characteristic of simple fluids that would show a no-slip boundary condition (Sec. V A). The atoms also exhibit rapid diffusion that is characteristic of a fluid. The periodic melting and freezing transitions that occur during stick-slip are induced by shear and not by the negligible changes in temperature. Shear-melting transitions at constant temperature have been observed in both theoretical and experimental studies of bulk colloidal systems. [228,229]. While the above simulations of confined films used a fixed number of particles, [230] found equivalent results at fixed chemical potential.

Very similar behavior has been observed in simulations of sand, [226] chain molecules, [212] and incommensurate or amorphous walls. [181] These systems transform between glassy and fluid states during stick-slip motion. As in

equilibrium, the structural differences between glass and fluid states are small. However, there are strong changes in the self-diffusion and other dynamic properties when the film goes from the static glassy to sliding fluid state.

In the cases just described, the entire film transforms to a new state, and shear occurs throughout the film. Another type of behavior is also observed. In some systems shear is confined to a single plane - either a wall/film interface, or a plane within the film. [213,212]. There is always some dilation at the shear plane to facilitate sliding. In some cases there is also in-plane ordering of the film to enable it to slide more easily over the wall. This ordering remains after sliding stops, and provides a mechanism for the long-term memory seen in some experiments. [39,222,231] Buldum and Ciraci [232] found stick-slip motion due to periodic structural transformations in the bottom layers of a pyramidal Ni(111) tip sliding on an incommensurate Cu(110) surface.

The dynamics of the transitions between stuck and sliding states are crucial in determining the range of velocities where stick-slip motion is observed, the shape of the stick-slip events, and whether stick-slip disappears in a continuous or discontinuous manner. Current models are limited to energy balance arguments [233,234] or phenomenological models of the nucleation and growth of "frozen" regions. [48,222,224,53] Microscopic models and detailed experimental data on the sticking and unsticking process are still lacking. However, two simple models with reduced degrees of freedom provide useful insight into the origins of the complex dynamics seen in experiments.

B. Relation to Prandtl-Tomlinson model

It has been a continuing effort to model macroscopic motion of two sliding solids in terms of simple descriptions incorporating only one degree of freedom such as in the Prandtl-Tomlinson (PT) model. This does not only concern dry friction but also lubricated friction. Baumberger and Caroli [84] proposed a phenomenological model of boundary lubricated junctions in terms of the PT model. Their contact consists of two planeparallel walls of area a^2 which are separated by a distance h. The gap between the plates is filled with a fluid of viscosity η. The equation of motion for the top plate is identical with Eq. (3.1), however, the damping is related to the internal viscous response, suggesting the following substitution of the damping coefficient:

$$m\gamma \to \eta a^2/h. \tag{6.1}$$

Caroli and Baumberger argue that such a description is legitimate if there is a time-scale separation between the motion of the top plate and that of the lubricant atoms. However, if there is such a separation, one can object that in almost all cases there should be no significant, periodic corrugation potential: For symmetry reasons the corrugation potential must be periodic in the upper wall's lattice constant b_u and that of the lower wall b_l. Unless identical and perfectly aligned crystals are employed, b_u and b_l can be assumed to be effectively incommensurate, in which case the common periodic becomes extremely large and the corrugation potential arbitrarily small.

Baumberger's and Caroli's comparison of the PT model to boundary lubrication remains yet appealing. The PT model is known to show two stable modes of motion under certain circumstances: If the externally applied force is in between static friction force and kinetic friction force, then the running solution and the pinned solution are both stable against a small perturbation. This mimics the behavior of shear melting of confined lubricants. The shear pressures p_m necessary to induce shear melting are larger than the shear pressures p_f where a liquified lubricant freezes back into a glassy or a crystalline state.

C. Rheological versus tribological response

Two approaches are usually used to investigate shear forces in confined liquids the tribological one, where a constant driving velocity is applied and the rheological one, which applies an oscillatory drive. In the latter case the coordinate of the laterally driven stage changes as $X_d = X_0 \sin(t)$, X_0 and ω are the amplitude and the frequency of the drive. One of the goals of rheological measurements is to obtain information on the energy loss in the system. This is usually done in terms of the response theory. Practically, linear response is assumed in the analysis of rheological results, leading to a description of the properties of the system in terms of the complex dynamic modulus $G(\omega) = G'(\omega) + \mathrm{i}G'(\omega)$. The shear modulus is defined as a linear coefficient in the relationship between Fourier components of a force acting on the embedded system and the displacement, Y, of the driven plate [210,235]. The storage modulus G' and loss modulus G" are obtained from measurements and determine the elastic and dissipative properties of the confined system.

Since in rheological measurements the drive is oscillatory, one can fix the driving amplitude/frequency and vary the frequency/amplitude. For small driving amplitudes X_0 the displacement of the plate is smaller than a characteristic microscopic length and the response of the system is linear. After exceeding a critical driving amplitude $X_0{}^c$, the

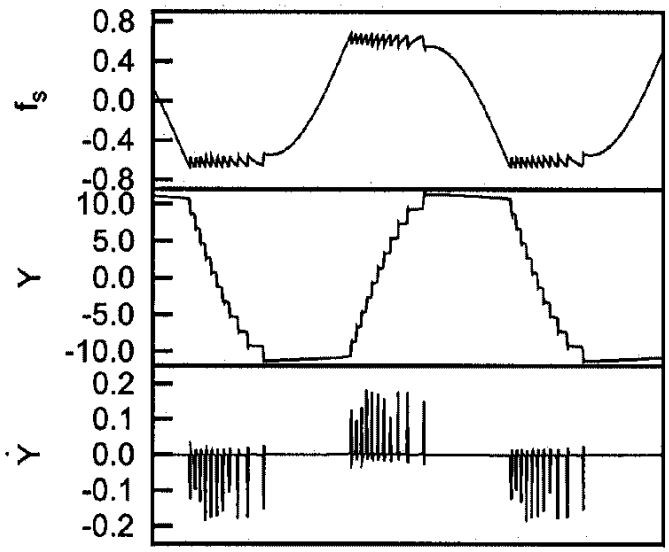

FIG. 17. Time dependence of spring force f_s, top plate displacement Y, and velocity $dotY$ as a function of time. From Ref. [237].

top plate executes oscillations with amplitude larger than the characteristic distance. If the rheological behavior of a confined fluid is mimicked in terms of simple model such as the Prandtl-Tomlinson (PT) model, then this characteristic length can be estimated to be ${X_0}^c F_s/K$, where F_s is the static friction force obtained from tribological experiments and K is the external spring constant [236].

For values of the driving amplitude above ${X_0}^c$, the PT model exhibits stick-slip motion before it crosses over to smooth sliding at amplitudes larger than a second threshold V_c/ω [236]. The stick-slip motion in this regime ${X_0}^c < X_0 < V_c/\omega$ is similar to stick-slip motion in tribological experiments, however, there are intermittent regimes during rheological driving, where the top wall remains pinned for a certain amount of time. Such rheological dynamics is shown in Fig. 17. Similar behavior is found for a small chain embedded between two corrugated, one-dimensional plates [237] and the calculations are also consistent with available experimental data of confined fluids under rheological shear [238–243].

For very high driving amplitudes, $X_0 > V_c/\omega$, the PT model and also the embedded model apparently follows linear response again. In this latter regime, the corrugation barriers are small compared to the (average) kinetic energy of the involved atoms and friction is dominated by the damping coefficient γ, see Eqs. (2.5) and (3.1) and the discussion of Fig. 3. Thus $X_0 > V_c/\omega$ roughly correspond to the smooth sliding regime in tribological experiments.

One feature of the rheological response is that the microscopic degrees of freedom can be in three different regimes for a given combination of X_0 and ω. (i) At times where $|\dot{Y}|$ is small, the atoms can oscillate around their potential energy minima and the observed loss will be small. (ii) At intermediate $|\dot{Y}|$, the microscopic degrees of freedom exhibit instabilities, akin of the elastic instabilities in the PT model or the phase transition instabilities of shear molten/frozen lubricants. (iii) Only if $|\dot{Y}|$ is sufficiently large does the system go into the smooth sliding or shear molten regime. The precise choice of X_0 and ω will thus determine how much time the system spends in what regime. However, it is not possible to associate the friction force measured in a rheological experiment with amplitude X_0 and frequency ω with a tribological experiment done at sliding velocity $v = X_0\omega$. This is shown in Fig. 18. If the driving amplitude is large, the system is more likely to be forced to exhibit instabilities and thus it can be expected to show larger friction. This is confirmed by a detailed analysis of the two above mentioned model systems [236,237].

From the above analysis follows that the increase in $\eta_{\rm eff}$ at small v cannot be interpreted as shear thinning. Tribological driving (at positive temperatures) would result in a curve similar to that shown in Fig. 14, in which the linear-response viscosity is obtained at the smallest shear rates. In the two model systems mentioned above, where zero temperature was employed, $\eta_{\rm eff}$ would tend to infinity with proportional to the inverse shear rate

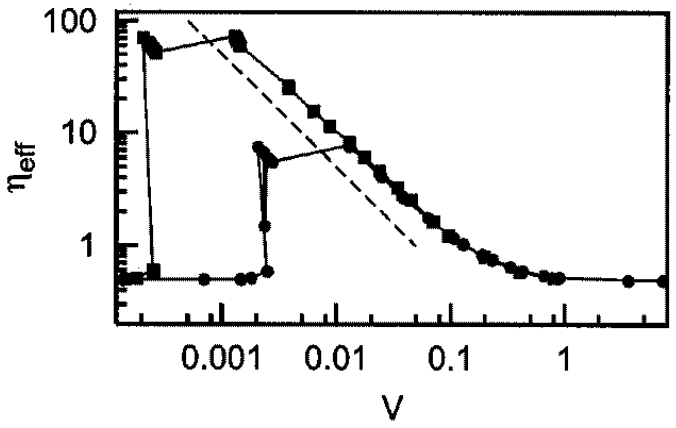

FIG. 18. Effective viscosity as a function of the product $v = X_0\omega$ at fixed driving frequencies ω. Circles represent a frequency ten times larger than squares. Consequently, the driving amplitude X_0 is ten times larger for the squares than for the circles at a given v. From Ref. [236].

D. Lateral normal coupling: Reducing static friction spikes

While most studies of frictional forces have focused on the lateral response to a lateral driving force, there have been a few theoretical [81,226,244,245] and experimental [238,241,246,247] observations of response in the normal direction. A feature characteristic of the response in the normal direction is the dilatancy during slippage and sliding, observed in experiments and molecular dynamics calculations. The interest in coupling between lateral and normal motions has recently gained additional attention due to the prediction that one should be able to modify the lateral response by imposing a controlling normal drive [244,245,81,248–251]. Main features of the lateral-normal coupling can be demonstrated considering a generalization of the one-dimensional Prandtl-Tomlinson model to include also the normal direction [245]. Introducing lateral-normal coupling leads to the following coupled equations of motion which describe the motion of the top plate of mass M

$$M\ddot{X} = -\eta_{\parallel}\dot{X} - \frac{\partial U(X,Z)}{\partial X} + K_d(Vt - X) \tag{6.2}$$

$$M\ddot{Z} = -\eta_{\perp}\dot{Z} - \frac{\partial U(X,Z)}{\partial Z} + K_n\left[Z_p(t) - Z\right] \tag{6.3}$$

where

$$\eta_{\parallel,\perp} = \eta^0_{\parallel,\perp}\exp(1 - Z/\Lambda) \tag{6.4}$$

and

$$U(X,Z) = U_0\exp(1 - Z/\Lambda)\left[1 - \sigma^2\cos(2\pi X/b)\right]. \tag{6.5}$$

The top plate is connected to a laterally driving spring, of spring constant K_d and to a spring K_n which is used to control the motion in the normal direction. $U(X,Z)$ is the effective potential experienced by the plate due to the presence of the embedded system, b is its periodicity, and σ characterizes the corrugation of the potential in the lateral direction. The parameters $\eta_{\parallel}$ and $\eta_{\perp}$ are responsible for the dissipation of the plate kinetic energy due to the motion in the lateral and normal directions. In contrast to the traditional Prandtl-Tomlinson model, here the dependence of U and $\eta_{\parallel,\perp}$ on the distance Z between plates is taken into account. The detailed distance dependence is determined by the nature of the interaction between the plate and embedded system. As an example, we assume an exponential decrease of U and $\eta_{\parallel,\perp}$, with a rate Λ^{-1} as Z increases. The possibility of an external modulation of the normal load $L_n(t) = K_n\left[Z_p(t) - Z\right]$ is taken into account by introducing a time dependence into the position of the normal stage, $Z_p(t)$.

A relevant property of the coupled equations is the existence of two stable surface separations Z_0 and Z_s, which correspond to the plate being either at rest or in fast motion. At rest the plate feels the lateral corrugation of the potential, $U(X,Z)$, and sits at the minima of the potential, while during fast motion there is a decoupling from this potential corrugation. From Eqs. (6.2) and (6.3), one obtains the following self-consistent equation for the maximal dilatancy:

$$\Delta Z_D = Z_s - Z_0 = \frac{L_n}{K_n}\left[(1-\sigma^2)^{-1}\exp(-\Delta Z_D/\Lambda) - 1\right], \tag{6.6}$$

where

$$L_n = (1-\sigma^2)(U_0/\Lambda)\exp(1 - Z_0/\Lambda) \tag{6.7}$$

is the normal load at rest. Eq. (6.6) demonstrates that the dilatancy ΔZ_D explicitly depends on the potential corrugation and on the normal spring constant. It is quite evident that measuring the dilatancy helps in determining the amplitude of the potential corrugation.

Fig. 16 (b) and (c) shows the response in the lateral and normal directions to a lateral constant velocity drive for stick-slip regime that occurs at low driving velocities. This behavior is similar for the presently discussed model. The separation between the plates, which is initially Z_0 at equilibrium, starts growing before slippage occurs and stabilizes at a larger interplate distance as long as the motion continues. Since the static friction is determined by the amplitude of the potential corrugation $\sigma^2 U_0\exp(1 - Z/\Lambda)$, it is obvious that the dilatancy leads to a decrease of the static friction compared to the case of a constant distance between plates.

In a wide range of system parameters the dilatancy is smaller than the characteristic length Λ. Under this condition the generalized Prandtl-Tomlinson model predicts a linear increase of the static friction with the normal load, which is in agreement with Amontons's law. It should be noted that in contrast to the multi-asperity surfaces here the

contact area is independent of the load. The fulfillment of the Amontons's law in the present model results from the enhancement of the potential corrugation, $\sigma^2 U_0 \exp(1 - Z/\Lambda)$, experienced by the driven plate with an increase of the normal load.

While the present discussion is concerned with the interaction of two commensurate walls only, similar dilatancy effects occur under more general circumstances as well. Indeed, dilatancy is expected in a broad range of systems where coupling between lateral and normal directions exists. Recently this phenomenon has been intensively studied in the context of sheared granular media [226,246,252] and seismic faults [253,254]. The observation of dilatancy is limited by the choice of the normal spring which should be weaker than the potential elasticity, $K_n \Lambda^2 \ll U_0$. From the dependence of the dilatancy ΔZ_D on the normal spring constant K_n it is clear that the weaker K_n is the larger is ΔZ_D and therefore the frictional force tends to decrease.

From Eq. (6.6) one can see that as the spring constant K_n decreases the dilatancy grows. This leads to smoothing of the stick-slip motion present for stiffer springs. Weakening the normal spring constant results in lowering the critical velocity at which stick-slip turns to sliding. The dependence of the critical velocity on K_n becomes most pronounced for underdamped conditions, when $\eta_{\parallel,\perp} \ll M K_d$. This consideration emphasizes again that the experimental observations in SFA strongly depend on the choice of the mechanical parameters.

Dilatancy has been shown above to occur naturally during slippage events. It has also been demonstrated that the measured frictional forces are sensitive to the interplate distance. One can therefore expect to be able to control frictional behavior by monitoring the motion in the normal direction. From a practical point of view one wishes to be able to control frictional forces so that the overall friction is reduced or enhanced, the stick-slip regime is eliminated, and instead, smooth sliding is achieved. Such control can be of high technological importance for micromechanical devices, for instance in computer disk drives, where the early stages of motion and the stopping processes, which exhibit chaotic stick-slip, pose a real problem [255].

Controlling frictional forces has been traditionally approached by chemical means, namely, using lubricating liquids. A different approach, which has attracted considerable interest recently [81,245,244,248–251], is by controlling the system mechanically. The idea is not to change physical properties of interfaces but to stabilize desirable modes of motion which are unstable in the absence of the control. The goal of this approach is twofold: (a) to achieve smooth sliding at low driving velocities, which otherwise correspond to the stick-slip regime; (b) to decrease the frictional forces. Two different methods of control have been discussed: The first one uses a feedback control, and the second one relies on a "brute-force" modification of the system dynamics without a feedback.

We start from the feedback mechanism of control. The analysis of the mechanism has been done with a one-dimensional model, which includes two rigid plates and non-interacting particles embedded between them [244]. In order to mimic the effect of normal load, the dependence of the amplitude of the periodic potential on the load has been introduced

$$U_0(L_n) = U_0[1 + \chi(L_n - L_n^0)]. \tag{6.8}$$

Here, U_0 is the value of the potential for some nominal value of the normal load L_n^0, and χ is a dimensional constant. The normal load has been used as the control parameter to modify friction. Eq. (6.8) assumes small load variations around L_n^0, which, as shown in Ref. [244], are sufficient to achieve control. The control method is characterized by two independent steps: (a) reaching the vicinity of an unstable sliding modes of motion, and (b) stabilizing it. The control has been realized by small variations of the normal load, which has been externally adjusted employing a proportional feedback mechanism [244]. A delayed-feedback mechanism has been also used for stabilizing the sliding states [248].

The aim of this approach is to stabilize a sliding state for driving velocities $V < V_c$, where one would expect chaotic stick-slip motion. Within the model discussed here sliding states correspond to periodic orbits of the system with two periods: (a) period $T = b/V$, which corresponds to a motion of the particles being trapped by one of the plate; and (b) period $T = 2b/V$, which corresponds to the particles moving with the drift velocity $V/2$. In the chaotic stick-slip region both orbits still exist, but are unstable. The approach is therefore to drive the system into a sliding state by controlling these unstable periodic orbits. This makes it possible to extend the smooth sliding to lower velocities. The control of such orbits in dynamical systems have been proposed [256] and experimentally applied to a wide variety of physical systems including mechanical systems, lasers, semiconductor circuits, chemical reactions, biological systems etc. (see Ref. [257] for references).

Fig. 19 demonstrates the effect of the mechanical control on the time dependene of the spring force. The results correspond to the control of the trapped-sliding state [244], in which the particles cling to one of the plates and move either with velocity zero (sticking at the bottom plate) or velocity V (sticking at the top plate). The control is switched on at time t_1 and is shut down at time t_2. We clearly see that as a result of the control the chaotic motion of the top plate is replaced by smooth sliding which corresponds to a trapped state with the frictional force.

In Refs. [244,248] the possibility to control friction has been discussed in model systems described by differential equations. Usually in realistic systems time series of dynamical variables, rather than governing equations, are

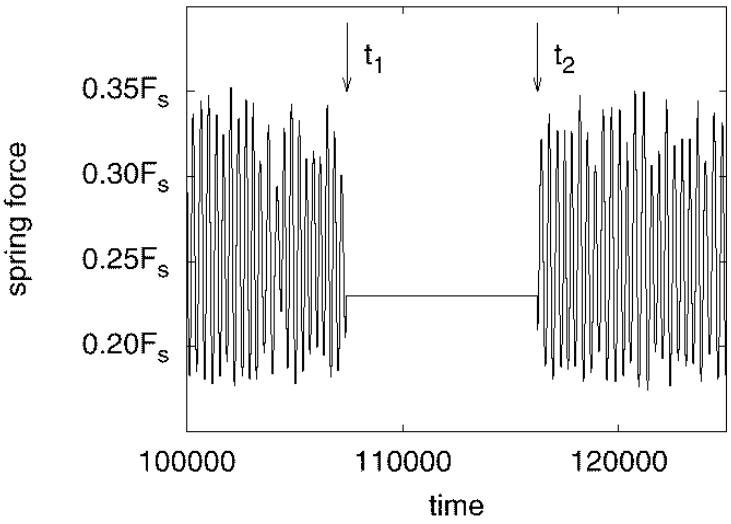

FIG. 19. Friction force F as a function of time. Stick-slip motion and static friction spikes are suppressed through small variation in the normal load at times $t_1 < t < t_2$.

experimentally available. In this case the time-delay embedding method [258] can be applied in order to transform a scalar time series into a trajectory in phase space. This procedure allows one to find the desired unstable periodic orbits and to calculate variations of parameters required to control friction.

The brute-force method of control based on a harmonic modulation of the normal load $L_n(t)$, has been studied within various approaches which include the generalized Tomlinson model [245], one-dimensional rate-state models [247,249,251] and grand-canonical MD simulations [247]. All calculations demonstrated that oscillations of the normal load could lead to a transition from a high-friction stick-slip dynamics to a low-friction sliding state. This effect can be controlled through the selection of the oscillation frequency. Mechanism of this phenomenon in lubricated junctions has been clarified by MD simulations [247] which show that oscillations of the normal load frustrate ordering in the lubricated film, maintaining it in a nonequilibrium sliding state with low friction. Theoretical predictions have been supported by recent experiments [250,251] which indicate that normal vibrations generally stabilize the system against stick-slip oscillations, at least for a modulation frequency much larger than the stick-slip one.

VII. MULTI ASPERITY CONTACTS

Most mechanical junctions discussed in the previous sections are single nanoscale or microscale contacts where the two opposing solids are in intimate, atomic contact and where the geometry of the walls can be approximated as either flat or curved. On larger lengthscales, however, surfaces are almost always rough or self-affine. A measure for the roughness is the so-called roughness exponent H, which states how fast the mean corrugation σ_z increases with the area $A = \pi R^2$, in which σ_z is determined, namely

$$\sigma_z(R) = \langle z^2 \rangle_R - \langle z \rangle_R^2 \propto R^H, \tag{7.1}$$

where $\langle z^n \rangle_R$ denotes the average n'th moment of the surface height z measured in an area of radius R. In practical applications, H is frequently assessed in a range 1 nm $\leq R \leq$ 1mm. The observed roughness depends strongly on the instruments used to determine σ_z and we refer to Ref. [259] for further details. Since for most surfaces $H > 0$, the actual area of molecular contact between two surfaces, $A_{\rm real}$, is generally a small fraction of the apparent macroscopic area [31,33].

The motion of the individual contacts is neither strictly correlated nor strictly uncorrelated, because different microjunctions interact with each other through elastic deformations within the bulk. The interplay of local shear forces in individual contacts and/or surface roughness and long-range elasticity will be discussed in this section. One of the pioneering studies of this competition has been done by Burridge and Knopoff [260]. They suggested a model similar to the FKT model shown in Fig. 6 and discussed in Sec. III C 6. The main difference is that one atom in the FK model represents a whole mechanical block in the Burridge-Knopoff (BK) model. The underlying assumption is that within one BK block all microcontacts move completely correlated, while neighbored blocks are much less correlated. One non-moving junction can counterbalance an intrabulk elastic force up to a static friction F_s. Once a junction slides, its lateral motion is counteracted by a kinetic friction force $F_k < F_s$. The BK model is mainly employed in the context of seismology and we refer to a review by Carlson et al [261] for more details.

In the remainder of this section, we will first analyze the competition between local shear and long-range elastic interaction in the case of hard solids. One of the central questions is how one can determine the size of one BK block. Finally, in Sec. VII B, the sliding motion of a soft elastic body with large internal friction on a corrugated substrate will be discussed. In the latter case, friction does not only arise as a consequence of finite shear forces in the individual microcontacts but rather due to the internal friction of the elastic medium.

A. Elastic coherence length

Consider a corrugated solid placed on a smooth substrate as a simplified model for a mechanical contact. The macroscopic contact will then consist of individual junctions where asperities from the corrugated solid touch the substrate. A microscopic point of contact p then carries a normal load l_p and a shear force $\vec{f}_p$ will be exerted from the substrate to the asperity and vice versa. These random forces $\vec{f}_p$ will try to deform both solids. For the sake of simplicity, let us only consider elastic deformations in the top solid. Asperities in intimate contact with the substrate will be subject to a competition between the (elastic) coupling to the top solid and the interaction with the substrate. If the elastic stress $\sigma_{e,p}$ exceeds the local critical shear stress $\sigma_{c,p}$ of junction p, the contact will break and asperity p will find a new mechanical equilibrium position. In order for $\sigma_{e,p}$ to exceed $\sigma_{c,p}$, the area $A = \pi L^2$ over which the random forces accumulate must be sufficiently large. The value of L where this condition is satisfied is called the elastic coherence length $\mathcal{L}$. It is believed to play an important role in various aspects of friction.

The concept of an elastic coherence length was first introduced in the context of charge density waves [28,62] and flux line lattices in superconducters [262]. The relevance of this concept for friction was suggested by Baumberger and Caroli [54]: The contact can be decomposed into pinning centers, also called Larkin domains, with a typical linear size $\mathcal{L}$, which constitute the BK blocks introduced in the beginning of this section.

We are now concerned with the calculation of $\mathcal{L}$. We roughly follow the derivation given by Persson and Tosatti [27]. The condition for the elastic coherence length can be formulated as follows. Over what area $A_{\mathcal{L}} = \pi \mathcal{L}^2$ does one need to accumulate the elastic displacement field $u(\mathbf{x})$ in order to exceed the critical value a_c at which an individual asperity breaks. Up to that point, linear response theory applies, beyond it fails. Hence $\mathcal{L}$ can be obtained from the condition:

$$a_c^2 = \frac{2}{A_{\mathcal{L}}} \int_0^{\mathcal{L}} d^2x' \left[\langle u(\mathbf{x})^2 \rangle \; - \; \langle u(\mathbf{x}) u(\mathbf{x}+\mathbf{x}') \rangle \right]. \tag{7.2}$$

The displacement field $u(\mathbf{x})$ is related to the externally imposed stress $\sigma(\mathbf{x})$ through

$$u(\mathbf{x}) = \int dx''\, G(\mathbf{x}-\mathbf{x}'')\sigma(\mathbf{x}''), \tag{7.3}$$

where $G(\mathbf{x})$ is a Green's function. Although, $u(\mathbf{x})$, $G(\mathbf{x})$, and $\sigma(\mathbf{x})$ correspond to vectors and matrices in principle, indices are skipped for the sake of simplicity. $G(\mathbf{x})$ can be related to Young's modulus E through a relation of the form $G(\mathbf{x}) = 1/E \mid \mathbf{x} \mid$, modulo geometric factors incorporating Poisson's ratio. One can now write the last term in the integrant of Eq. (7.3) as

$$\int d^2x'' \int d^2x''' G(\mathbf{x}-\mathbf{x}'')G(\mathbf{x}+\mathbf{x}'-\mathbf{x}''')\langle\sigma(\mathbf{x}'')\sigma(\mathbf{x}''')\rangle. \tag{7.4}$$

It is commonly assumed [26,27] that the shear is highly correlated within one contact and completely uncorrelated between different microjunctions. This introduces a lower cutoff at the (average) radius R_c of a microcontact in the integrals above and it allows one to replace $\langle\sigma(\mathbf{x}'')\sigma(\mathbf{x}''')\rangle$ with δ-correlated terms of the form $\pi R_c^2\langle\sigma_c^2\rangle\delta(\mathbf{x}''-\mathbf{x}''')$. Thus the expression in Eq. (7.4) can be reformulated to:

$$\pi R_c^2\langle\sigma_c^2\rangle \int_{R_c}^{\mathcal{L}} d^2x'' G(\mathbf{x}-\mathbf{x}'')G(\mathbf{x}+\mathbf{x}'-\mathbf{x}''). \tag{7.5}$$

The condition for the breakdown of linear response theory, Eq. (7.2), now reads

$$a_c^2 = \frac{2}{A_{\mathcal{L}}}\,\pi R_c^2\,\langle\sigma_c^2\rangle \int_{R_c}^{\mathcal{L}} d^2x'\,d^2x''\,\left[G(\mathbf{x}-\mathbf{x}'')^2 - G(\mathbf{x}-\mathbf{x}'')G(\mathbf{x}+\mathbf{x}'-\mathbf{x}'')\right] \tag{7.6}$$

$$\approx 4\pi^2 R_c^2 \frac{\langle\sigma_c^2\rangle}{E^2}\,\ln\frac{\mathcal{L}}{R_c} \quad \text{for } \mathcal{L} \gg R_c. \tag{7.7}$$

The elastic coherence length $\mathcal{L}$ thus depends exponentially on the square of the contact radius R_c and the square of the elastic displacement a_c of a junction before failure. Both, R_c and a_c will depend on material properties, surface geometry, and also on the properties of the interface. Thus R_c and a_c are both statistical quantities whose average value is extremely hard to assess and any calculation of $\mathcal{L}$ can only be interpreted as an attempt to estimate its order of magnitude. This can be seen in the large discrepancies in the values obtained for $\mathcal{L}$. Persson and Tosatti obtain astronomically large value for steel on steel, namely, $\mathcal{O}(\mathcal{L}) \approx 10^{100\,000}$ m, while Sokoloff [26] concludes that $\mathcal{O}(\mathcal{L}) \approx 1\,\mu$m is a typical value for two generic materials in contact.

It might yet be possible to predict trends from Eq. (7.7). Persson and Tosatti [27] argue that $\mathcal{L}$ decreases quickly with increasing normal pressure with important consequences for tectonic motion, for instance that small earthquakes typically do not occur close to the earth surface. Sokoloff concluded recently [122] that even for his small value of $\mathcal{L}$, the contribution to kinetic friction due to elastic instabilities which result from a competition between surface roughness and elastic interactions would lead to rather small friction coefficients in the order of 10^{-5}, provided no contamination layer or other local friction mechanisms were present in the contacts.

B. Rubber friction

The friction force between a rubber and a rough surface is often believed to consist of an adhesive and a hysteretic component [263]. While the adhesive component is only important for very clean surfaces, the pioneering studies of Grosch [264] have shown that sliding rubber friction is in many cases related to the *internal* friction of rubber: The friction coefficient of rubber sliding on silicon carbide paper and glass surfaces give the same temperature dependence as that of the complex elastic modulus $E(\omega)$. This behavior is in contrast to most other frictional systems discussed here, for which the resistance to sliding originates from the elastic or plastic instabilities within or near the interface between the two solid bodies. The large internal friction within rubber at small frequencies is however again due to the internal instabilities rather than to "simple" phonon damping. In this sense, the relatively large rubber friction at small velocities also originates from instabilities.

In a series of recent papers, Persson and coworkers [265–267] as well as Klüppel and Gläser [268] have developed a theory which connects the friction force with the energy loss due to the deformations that a rubber experiences while sliding over a rough substrate. Depending on the sliding velocity, the rubber is able to accommodate the surface roughness profile on various length scales. In this theory, the friction coefficient can be calculated as a function of surface roughness and the frequency dependent loss- and storage modulus. Strictly speaking, the static friction force is zero in such a treatment since for infinitely low sliding speeds, $\omega = 0$ would be the main relevant frequency in

$E(\omega)$ and hence there would be no loss. However, owing to its extremely broad distribution of loss frequencies, one may argue that also the quasi-static friction forces that make our tires operate on the street are related to the above mentioned dissipation processes.

Persson and coworkers [265–267] consider a rough, rigid surface with a height profile $h(\mathbf{x})$, where $\mathbf{x}$ is a two-dimensional vector in the xy plane perpendicular to the interface. In reaction to $h(\mathbf{x})$ and its externally imposed motion, the rubber will experience a (time-dependent) normal deformation $\delta z(\mathbf{x}, t)$. If one assumes the rubber to be an elastic medium, then it is possible to relate $\delta\tilde{z}(\mathbf{q}, \omega)$, which is the Fourier transform (F.T.) of $\delta z(\mathbf{x}, t)$, with the F.T. of the stress $\tilde{\sigma}(\mathbf{q}, \omega)$. Within linear-response theory, one can express this in the rubber-fixed frame (indicated by a prime) via

$$\delta\tilde{z}'(\mathbf{q}, \omega) = G(\mathbf{q}, \omega)\tilde{\sigma}'(\mathbf{q}, \omega). \tag{7.8}$$

In the present context it will be helpful to remember that differentiating a function with respect to $\mathbf{x}$ and/or with respect to t corresponds to multiplying the F.T. of the function with $i\mathbf{q}$ and/or $-i\omega$ respectively. Baring this is mind, $i\mathbf{q}\delta\tilde{z}'(\mathbf{q}, \omega)$ can be associated with a strain and thus $-iG(\mathbf{q}, \omega)/q$ can be interpreted in the continuum limit as the inverse of a generalized frequency-dependent elastic constant $E(\omega)$. Strictly speaking $G(\mathbf{q}, \omega)$ is a tensor, for which in general $(G_{\alpha,\beta})^{-1} \neq (G^{-1})_{\alpha,\beta}$, but for the sake of a clear presentation, we omit indices here. Instead we refer to Appendix A in Ref. [266] for a more detailed discussion of the precise form of $G(\mathbf{q}, \omega)$ and $E(\omega)$ and their dependence on the Poisson ratio.

The crucial assumption is to relate the macroscopic rate of dissipation (which appears on the l.h.s. of the following equation) with the microscopic rate of dissipation (appearing on the r.h.s.):

$$\sigma_f A_0 \dot{x} = \int_{A_0} d^2x\, \delta\dot{z}'(\mathbf{x}, t)\, \sigma'(\mathbf{x}, t). \tag{7.9}$$

Here σ_f denotes the frictional shear stress occurring at the interface of area A_0. It is first assumed that during sliding the whole rubber interfacial area moves forward according to $\mathbf{r}(t)$ with $\dot{\mathbf{r}}(t) = \dot{x}(t)\mathbf{e}_x$ and that the rubber is able to deform and completely follow the substrate surface profile $h(\mathbf{x})$. The latter assumption will be replaced by assuming a velocity-dependence for the extent with which the rubber can accommodate the substrate's surface profile. For now, however, the transformation between rubber-fixed and substrate-fixed frame reads

$$\delta z'(\mathbf{x}, t) = \delta z(\mathbf{x} - \mathbf{r}(t)) \tag{7.10}$$

which with the above-made remarks is equivalent to

$$\delta z'(\vec{q}, \omega) = \tilde{h}(\vec{q}) f(\vec{q}, \omega) \tag{7.11}$$

with the definition of

$$f(\vec{q}, \omega) = \frac{1}{2\pi} \int dt\, e^{-i[\mathbf{q}\mathbf{x}(t) - \omega t]}\,. \tag{7.12}$$

Substituting Eqs. (7.8) and (7.10) through (7.12) into Eq. (7.9), one yields

$$\sigma_f(t) = \int d^2q\, d\omega\, d\omega'\, iE(-\mathbf{q}, \omega')\, \tilde{h}(\mathbf{q})\, \tilde{h}(-\mathbf{q})\, f(\mathbf{q}, \omega)\, f(-\mathbf{q}, \omega') e^{i(w+w')t}, \tag{7.13}$$

where we have made use of the comments following Eq. (7.8) and of the identity $\delta\dot{z}' = -\dot{x}\nabla\delta z$, which follows from Eq. (7.10). This equation relates the macroscopic dissipative response $\sigma_f(t)$ with the surface corrugation $h(\vec{\mathbf{q}})$, the dynamic elastic modul $E(\mathbf{q}, \omega)$ and the trajectory of the rubber, which is reflected in $f(\mathbf{q}, \omega)$. The special case of constant sliding velocity $\mathbf{r}(t) = vt\mathbf{e}_x$ corresponds to $f(\mathbf{q}, \omega) = \delta(q_x v - \omega)$ and thus for steady-state sliding

$$\sigma_f(v) = \int d^2q\, iE(-\mathbf{q}, -q_x v))\ \mid h(\mathbf{q}) \mid^2 . \tag{7.14}$$

This result was obtained by Persson [266] before the more general equation for non-steady state was obtained in Ref. [267]. An example for the connection between the loss part of the elastic modulus and the friction coefficient is shown in Fig. 20. We also want to reemphasize that $E(\mathbf{q}, \omega)$ should not be taken literally as the bulk modul or a coefficient of the tensor of elastic constants but as a more generalized expression, which is discussed in detail in Ref. [266]. For a more detailed presentation that also includes contact mechanics and that allows one to calculate the friction coefficient, we refer to the original literature [267].

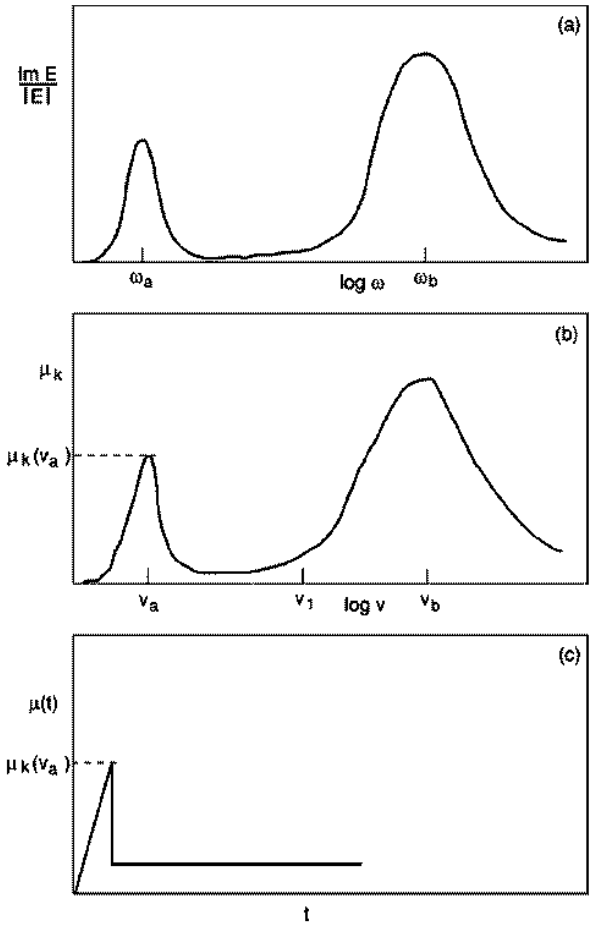

FIG. 20. (a) Loss spectrum $\mathrm{Im}[E(\omega)]/|E(\omega)|$ as a function of frequency ω. (b) Kinetic friction coefficient at constant sliding velocity v. (c) Transient behavior of the friction coefficient as a function of time t. At the smallest t, the velocity is abruptly changed from zero velocity to finite velocity.

While Eq. (7.14) gives the shear stress for an externally imposed constant sliding velocity, Eq. (7.13) provides a way to incorporate the history of the past motion into the calculation of the friction force. Persson and Volokitin suggest that also rubber friction may lead to a so-called striction peak [267], i.e. some short time after sliding is initiated, the lateral force takes a large value that it will not reach again in the following motion. This phenomenon is often observed during stick-slip motion and can easily be explained by the fact that static friction increases with the age of the contact. Here, however, the striction peak would have to be associated with relaxation processes within the rubber. Fig. 20 demonstrates the striction peak.

VIII. CONCLUDING REMARKS

Although the discussed theoretical studies constitute a significant breakthrough in our understanding of tribology, much work remains to be done. Here we would like to point out some important unresolved problems and possible directions for future studies.

The theoretical approaches which have been introduced to investigate frictional forces include large scale MD simulations, "minimalistic" models, which take into account only a few relevant interactions, and phenomenological, rate-state approaches which attempt to incorporate the basic physics ingredients and are usually convenient to apply. Each approach has its advantages and disadvantages and emphasizes different aspects, however relationships among these approaches are still missing. Even though the phenomenological and minimalistic modes have been able to reproduce most of the observations, it is unclear how to relate the parameters introduced in the models to the molecular scale properties. Mapping between 'exact' microscopic descriptions and phenomenological models presents a challenge for future theoretical studies of friction. This can allow to overcome time and length scale limitations of MD simulations (extend simulations from the nm/fs to the μm/μs) and offer a practical approach to investigate molecular systems under shear for a wide range of parameters.

In this review we would like to emphasize that the key to understanding friction lies into revealing shear induced instabilities that occur on a microscopic scale. The embedded molecular system should exhibit mechanical or also electornic instabilities in order to obtain not only static friction but also a finite kinetic friction which does not vanish in the limit of small sliding velocities. The presence of the instabilities leads to fast motion of certain degrees of freedom which becomes unavoidable even if the sliders center of mass velocity is extremely small. The important lesson to be learned is what are the microscopic mechanisms of instabilities, and how they affect the tribological behavior of sheared systems. The relative contributions of different mechanisms depend not only on the properties of the embedded system but also on the experimental configuration, and, for instance, may be different in SFA and AFM experiments. Understanding the molecular picture will allow one to control frictional forces and create desirable phases of motion.

Another important aspect of the frictional phenomena is the presence of a number of competing time scales which determine the dynamics of friction. They include intrinsic characteristic times which are associated with structural transitions, energy redistribution and various relaxation processes, and the extrinsic time that is related to the rate of the applied external force. The relationship between intrinsic and extrinsic times (the ratio is called Deborah number) is crucial for frictional processes. The elucidation of the intrinsic characteristic times, which control frictional behaviors presents one of the central and the most urgent problem. A solution of this problem will help to formulate valuable rate-sate models of friction. Unfortunately in many realistic cases there is no time-scale separation between different shear induced processes that makes the interpretation of the results more difficult.

An important direction of theoretical studies which has been overlooked is an investigation of strongly irreversible tribological processes, which include material mixing, cold welding, tribochemical and triboelectrical effects. A common feature of all these processes is the absence of steady state. So far only MD simulations have been used to study strongly irreversible phenomena. Theoretical modeling can provide deeper insight to these long sanding problems which are of high technological importance.

Acknowledgement: We are grateful to K. Binder and J. Klafter for critical comments on the manuscript. MHM and MU acknowledge support from the Israeli-German D.I.P.-Project No 352-101. MOR acknowledges support from National Science Foundation Grant DMR-DMR-0083286.

---

[1] D. Dowson. *History of Tribology*. Longman, New York, 1979.
[2] J. Krim and A. Widom. *Phys. Rev. B*, 38:12184, 1988.
[3] J. Krim, E. T. Watts, and J. Digel. *J. Vac. Sci. Technol. A*, 8:3417, 1990.
[4] J. Krim, D. H. Solina, and R. Chiarello. *Phys. Rev. Lett.*, 66:181, 1991.
[5] G. Binning, C. F. Quate, and Ch. Gerber. *Phys. Rev. Lett.*, 56:930, 1986.
[6] C. M. Mate, G. M. McClelland, R. Erlandsson, and S. Chiang. *Phys. Rev. Lett.*, 59:1942, 1987.
[7] J. N. Israelachvili, P. M. McGuiggan, and A. M. Homola. *Science*, 240:189, 1988.
[8] J. N. Israelachvili. *Surf. Sci. Rpt.*, 14:109, 1992.
[9] R. W. Carpick and M. Salmeron. *Chem. Rev.*, 97:1163, 1997.
[10] P. M. McGuiggan, J. Zhang, and S. M. Hsu. *Tribol. Lett.*, 10:217, 2001.
[11] F. Tiberg G. Bogdanovic and M. W. Rutland. *Langmuir*, 17:5911, 2001.
[12] J. A. Harrison, S. J. Stuart, and D. W. Brenner. In B. Bhushan, editor, *Handbook of Micro/Nanotribology*, page 525. CRC Press, Boca Raton, FL, 1999.
[13] M. O. Robbins and M. H. Müser. In B. Bhushan, editor, *Modern Tribology Handbook*, page 717. CRC Press, Boca Raton, FL, 2001.
[14] Amontons. *Histoire de l'Académie Royale des Sciences avec les Mémoires de Mathématique et de Physique*, page 206, 1699.
[15] J. Leslie. *An Experimental Inquiry Into The Nature and Propagation of Heat*, printed for J. Newman, No. 22 (1804).
[16] M. Brillouin. *Notice sur les Traveaux Scientifique*. Gauthiers-Vilars, Paris, 1909.
[17] G. A. Tomlinson. *Phil. Mag. Series*, 7:905, 1929.
[18] L. Prandtl. *ZS. f. angew. Math. u. Mech.*, 8:85, 1928.
[19] E. Gerde and M. Marder. *Science*, 413:285, 2001.
[20] T. Baumberger, C. Caroli, and O. Ronsin. *Phys. Rev. Lett.*, 88:075509, 2002.
[21] C. Caroli and Ph. Nozières. *Eur. Phys. J. B*, 4:233, 1998.
[22] M. Hirano and K. Shinjo. *Phys. Rev. B*, 41:11837, 1990.
[23] M. Hirano and K. Shinjo. *Wear*, 168:121, 1993.
[24] M. H. Müser and M. O. Robbins. *Phys. Rev. B*, 61:2335, 2000.
[25] M. H. Müser. *Tribol. Lett.*, 10:15, 2001.
[26] J. B. Sokoloff. *Phys. Rev. Lett.*, 86:3312, 2000.
[27] B. N. J. Persson and E. Tosatti. *Solid State Comm.*, 109:739, 1999.
[28] H. Fukuyama and P. A. Lee. *Phys. Rev B*, 17:535, 1978.
[29] D. S. Fisher. *Phys. Rev B*, 31:1396, 1985.
[30] G. He, M. H. Müser, and M. O. Robbins. *Science*, 284:1650, 1999.
[31] F. P. Bowden and D. Tabor. *The Friction and Lubrication of Solids*. Clarendon Press, Oxford, 1986.
[32] P. Berthoud and T. Baumberger. *Proc. R. Soc. A*, 454:1615, 1998.
[33] J. H. Dieterich and B. D. Kilgore. *Pure and Applied Geophysics*, 143:238, 1994.
[34] J. H. Dieterich and B. D. Kilgore. *Tectonophysics*, 256:219, 1996.
[35] I. L. Singer. Solid lubrication processes. In *Fundamentals of Friction: Macroscopic and Microscopic Processes*, pages 237–261. Elsevier, Amsterdam, 1992.
[36] B. J. Briscoe and D. Tabor. *J. Adhesion*, 9:145, 1978.
[37] B. J. Briscoe. *Phil. Mag. A*, 43:511, 1981.
[38] B. J. Briscoe and D. C. B. Evans. *Proc. Roy. Soc. A*, 380, 1982.
[39] M. L. Gee, P. M. McGuiggan, J. N. Israelachvili, and A. M. Homola. *J. Chem. Phys.*, 93:1895, 1990.
[40] A. Berman, C. Drummons, and J. N. Israelachvili. *Tribol. Lett.*, 4.
[41] J. A. Greenwood and J. B. P. Williamson. *Proc. Roy. Soc. A*, 295:300, 1966.
[42] A. Volmer and T. Natterman. *Z. Phys. B*, 104:363, 1997.
[43] B. N. J. Persson. *Phys. Rev. Lett.*, 87:116101, 2001.
[44] E. Rabinowicz. *Friction and Wear of Materials*. Wiley, New York, 1965.
[45] Sir W. B. Hardy. *Collected Works*. Cambridge University Press, Cambridge, 1936.
[46] D. M. Tolstoi. *Wear*, 10:199, 1967.
[47] J. M. Carlson and A. A. Batista. *Phys. Rev. E*, 53:4153, 1996.

[48] B. N. J. Persson. *Sliding Friction: Physical Principles and Applications*. Springer, Berlin, 1998.
[49] E. Rabonowicz. *Proc. Phys. Soc. London*, 71:668, 1958.
[50] J. H. Dieterich. *J. Geophys. Res.*, 84:2161, 1979.
[51] A. Ruina. *J. Geophys. Res.*, 88:10359, 1983.
[52] J. H. Dieterich and B. D. Kilgore. *Proc. Natl. Acad. Sci. USA*, 93:3787, 1996.
[53] F. Heslot, T. Baumberger, B. Perrin, B. Caroli, and C. Caroli. *Phys. Rev. E*, 49:4973, 1994.
[54] T. Baumberger and C. Caroli. *Comments Cond. Mat. Phys.*, 17:306, 1995.
[55] P. Hänggi, P. Talkner, and M. Borkovec. *Rev. Mod. Phys.*, 62:251, 1990.
[56] P. Berthoud and T. Baumberger. *Europhys. Lett.*, 41:617, 1998.
[57] Y. Estrin and Y. Bréchet. *Pageoph*, 147:745, 1996.
[58] P. Le Doussal P. Chauve, T. Giamarchi. *Europhys. Lett.*, 44:110, 1998.
[59] P. Le Doussal P. Chauve, T. Giamarchi. *Phys. Rev. B*, 62:6241, 2000.
[60] S. Panyukov and Y. Rabin. *Phys. Rev. E*, 56:7053, 1997.
[61] M. H. Müser, L. Wenning, and M. O. Robbins. *Phys. Rev. Lett.*, 86:1295, 2001.
[62] P. A. Lee and T. M. Rice. *Phys. Rev. B*, 19:3970, 1979.
[63] M. R. Sørensen, K. W. Jacobsen, and P. Stoltze. *Phys Rev. B*, 53:2101, 1996.
[64] H. Risken. *The Fokker Planck equation*. Springer, Heidelberg, 1984.
[65] G. E. Uhlenbeck and L. S. Ornstein. *Phys. Rev.*, 36:823, 1930.
[66] H. Risken and H. D. Vollmer. *Z. Phys. B*, 33:297, 1979.
[67] M. R. Falvo et. al. *Nature*, 397:236, 1999.
[68] M. R. Falvo, J. Steele, R. M. Taylor II, and R. Superfine. *Phys. Rev B*, 62:10665, 2000.
[69] M. F. Yu, B. I. Yakobson, and R. S. Ruoff. *J. Phys. Chem. B*, 104:8764, 2000.
[70] J. Liu et al. *Science*, 280:1253, 1998.
[71] A. Buldum and S. Ciraci. *Phys. Rev. Lett.*, 83:5050, 1999.
[72] M. Damnjanovic, I. Milosevic, T. Vukovic, and Sredanovic R R. *J. Phys. A*, 32:4097, 1999.
[73] A. N. Kolmogorov and V. H. Crespi. *Phys. Rev. Lett.*, 85:4727, 2000.
[74] L. Wenning and M. H. Müser. *Europhys. Lett.*, 54:693, 2001.
[75] C. A. J. Putman, M. Igarashi, and R. Kaneko. *Appl. Phys. Lett.*, 66:3221, 1995.
[76] P. Schwarz, O. Zwörner, P. Köster, and R. Wiesendanger. *Phys. Rev. B*, 56:6987, 1997.
[77] H. Klein, D. Pailharey, and Y. Mathey. *Surf. Sci.*, 387:227, 1997.
[78] M. Weiss and F.-J. Elmer. *Phys. Rev. B*, 53:7539, 1996.
[79] T. Gyalog and H. Thomas. *Z. Phys. B*, 104:669, 1997.
[80] E. Gnecco, R. Bennewitz, T. Gyalog, C. Loppacher, M Bammerlin, E. Meyer, and H. J. Güntherodt. *Phys. Rev. Lett.*, 84:1172, 2000.
[81] M. Porto, V. Zaloj, M. Urbakh, and J. Klafter. *Tribol. Lett.*, 9:45, 2000.
[82] E. Gnecco, R. Bennewitz, T. Gyalog, and E. Meyer. *J. Phys.: Condens. Mat.*, 13:R619, 2001.
[83] D. S. Fisher. *Phys. Rev. Lett.*, 50:1486, 1983.
[84] T. Baumberger and C. Caroli. *Eur. Phys. J. B*, 4:13, 1998.
[85] A. A. Middleton. *Phys. Rev. Lett.*, 68:670, 1992.
[86] E. Evans. *Annu. Rev. Biophys. Biomol. Struct.*, 30:105, 2001.
[87] Y. Sang, M. Dubé, and M. Grant. *Phys. Rev. Lett.*, 87:174301, 2001.
[88] O. K. Dudko, A. E. Filippov, J. Klafter, and M. Urbakh. *Chem. Phys. Lett.*, 352:499, 2002.
[89] E. Evans and K. Ritchie. *Biophys. J.*, 72:1541, 1997.
[90] J. N. Glosli and G. McClelland. *Phys. Rev. Lett.*, 70:1960, 1993.
[91] T. Ohzono, J. N. Glosli, and M. Fujihara. *Jpn. J. Appl. Physics*, 37:6535, 1998.
[92] T. Bouhacina, S. Gauthier J. P. Aimé, D. Michel, and V. Heroguez. *Phys. Rev. B*, 56:7694, 1997.
[93] E. L. Florin, V. T. Moy, and H. E. Gaub. *Science*, 264:415, 1994.
[94] M. Rief, F. Oesterhelt, B. Heymann, and H. E. Gaub. *Science*, 275:1295, 1997.
[95] A. F. Oberhauser, P. E. Marszalek, H. P. Erickson, and J. M. Fernandez. *Nature*, 393:181, 1998.
[96] G. U. Lee and L. A. Chrisey AMD R. J. Colton. *Science*, 266:771, 1994.
[97] Th. Charitat and J.-F. Joanny. *Eur. Phys. J. E*, 3:369, 2000.
[98] Y. I. Frenkel and T. Kontorova. *Zh. Eksp. Teor. Fiz.*, 8:1340, 1938.
[99] U. Dehlinger. *Ann. der Phys.*, 5:749, 1929.
[100] O. M. Braun and Yu. S. Kishvar. *Phys. Rep.*, 306:1, 1998.
[101] D. S. Fisher. *Phys. Rep.*, 301:113, 1998.
[102] S. Aubry. *J. Phys. (Paris) 44*, 44:147, 1983.
[103] M. Peyrard and S. Aubry. *J. Phys. C*, 16:1593, 1983.
[104] R. S. MacKay. *Physica D*, 50:71, 1991.
[105] P. M. Chaikin and T. C. Lubensky. chapter 10. Cambridge University Press, Cambridge, 1995.
[106] F. C. Frank and J. H. Van der Merwe. *Proc. Roy. Soc.*, 198:205, 1949.

[107] A. Kochendörfer and A. Seeger. *Z. Physik*, 127:533, 1950.
[108] M. J. Rice, A. R. Bishop, J. A. Krumhansl, and S. E. Trullinger. *Phys. Rev. Lett.*, 36:432, 1976.
[109] D. J. Bergman, E. Ben-Jacob, Y. Imry, and K. Maki. *Phys. Rev. A*, 27:3345, 1983.
[110] R. Peierls. *Proc. Roy. Soc. (London)*, 52:34, 1940.
[111] F. R. N. Nabarro. *Proc. Roy. Soc. (London)*, 59:256, 1947.
[112] V. G. Bar'yakhtar, B. A. Ivanov, A. L. sukstanskii, and E. V. Tartakovskaya. *Teor. Mat. Fiz.*, 74:46, 1988.
[113] P. Bak. *Rep. Progr. Phys.*, 45:587, 1982.
[114] P. Bak and Fukuyama. *Phys. Rev. B*, 21:3287, 1980.
[115] B. Hu, B. Li, and H. Zhao. *Europhys. Lett.*, 53:342, 2001.
[116] H. Miyake and H. Matsukawa. *J. Phys. Soc. Jpn.*, 67:3891, 1998.
[117] V. L. Popov. *Phys. Rev. Lett.*, 83:1632, 1999.
[118] C.-I. Chou, C.-I. Ho, and B. Hu. *Phys. Rev. E*, 55:5092, 1997.
[119] S. F. Mingaleev, Y. B. Gaididei, E. Majernikova, and S. Shpyrko. *Phys. Rev. E*, 61:4454, 2000.
[120] A. Vanossi, J. Röder, A. R. Bishop, and V. Bortolani. *Phys. Rev. E*, 63:017203, 2001.
[121] T. Kawaguchi and H. Matsukawa. *Phys. Rev. B*, 56:13932, 1997.
[122] J. B. Sokoloff. *Phys. Rev. B*, 65:115415, 2002.
[123] M. Weiss and F.-J. Elmer. *Z. Phys. B*, 104:55, 1997.
[124] F. Lancon, J. M. Penisson, and U. Dahmen. *Eur. Phys. Lett.*, 57:74, 2002.
[125] F. Lancon. *Eur. Phys. Lett.*, 57:74, 2002.
[126] M. Hirano, K. Shinjo, R. Kaneko, and Y. Murata. *Phys. Rev. Lett.*, 67:2642, 1991.
[127] J. M. Martin, C. Donnet, and Th. Le Mogne. *Phys. Rev. B*, 48:10583, 1993.
[128]
[129] M. Hirano, K. Shinjo, R. Kaneko, and Y. Murata. *Phys. Rev. Lett.*, 78:1448, 1997.
[130] J. Krim. *Scientific American*, 275(4):74, 1996.
[131] A. Dayo, W. Alnasrallay, and J. Krim. *Phys. Rev. Lett.*, 80:1690, 1998.
[132] M. O. Robbins and J. Krim. *MRS Bull.*, 23(6):23, 1998.
[133] M. S. Tomassone, J. B. Sokoloff, A. Widom, and J. Krim. *Phys. Rev. Lett.*, 79:4798, 1997.
[134] M. Cieplak, E. D. Smith, and M. O. Robbins. *Science*, 265:1209, 1994.
[135] E. D. Smith, M. Cieplak, and M. O. Robbins. *Phys. Rev. B.*, 54:8252, 1996.
[136] B. N. J. Persson. *Phys. Rev. B*, 44:3277, 1991.
[137] L. W. Bruch. *Phys. Rev. B*, 61:16201, 2000.
[138] B. L. Mason, S. M. Winder, and J. Krim. *Tribol. Lett.*, 10:59, 2001.
[139] T. Novotný and B. Velický. *Phys. Rev. Lett.*, 83:4112, 1999.
[140] V. L. Popov. *JETP Lett.*, 69:558, 1999.
[141] R. L. Renner, J. E. Rutledge, and P. Taborek. *Phys. Rev. Lett.*, 83:1261, 1999.
[142] J. Krim. *Phys. Rev. Lett.*, 83:1262, 1999.
[143] M. S. Tomassone and J. B. Sokoloff. *Phys. Rev. B*, 60:4005, 1999.
[144] C. Mak and J. Krim. *Faraday Discuss.*, 107:389, 1997.
[145] A. Brass, H. J. Jensen, and A. J. Berlinsky. *Phys. Rev. B*, 39:102, 1989.
[146] M. J. Williams. *J. Appl. Mech.*, 19:526, 2001.
[147] M. C. Kuo and D. B. Bogy. *J. Appl. Mech.*, 41:197, 1974.
[148] Jr. E. D. Reedy. *Engineering Fracture Mech.*, 36:575, 1990.
[149] O. Vafek and M. O. Robbins. *Phys. Rev. B*, 60:12002, 1999.
[150] J. A. Hurtado and K. S. Kim. *Proc. Royal Soc. Ser. A*, 455:3363, 1999.
[151] J. A. Hurtado and K. S. Kim. *Proc. Royal Soc. Ser. A*, 455:3385, 1999.
[152] J. A. Nieminen, A. P. Sutton, and J. B. Pethica. *Acta Metall. Mater.*, 40:2503, 1992.
[153] U. Landman, W. D. Luedtke, N. A. Burnham, and R. J. Colton. *Science*, 248:454, 1990.
[154] U. Landman, W. D. Luedtke, and E. M. Ringer. *Wear*, 153:3, 1992.
[155] U. Landman and W. D. Luedtke. *Surf. Sci. Lett.*, 210:L117, 1989.
[156] U. Landman and W. D. Luedtke. *J. Vac. Sci. Technol. B*, 9:414, 1991.
[157] H. Raffi-Tabar, J. B. Pethica, and A. P. Sutton. *Mater. Res. Soc. Symp. Proc.*, 239:313, 1992.
[158] O. Tomagnini, F. Ercolessi, and E. Tosatti. *Surf. Sci.*, 287/288:1041, 1993.
[159] U. Landman, W. D. Luedtke, and J. Gao. *Langmuir*, 12:4514, 1996.
[160] J. A. Harrison, C. T. White, R. J. Colton, and D. W. Brenner. *Surf. Sci.*, 271:57, 1992a.
[161] J. A. Harrison, D. W. Brenner, C. T. White, and R. J. Colton. *Thin Solid Films*, 206:213, 1991.
[162] J. Belak and I. F. Stowers. In I. L. Singer and H. M. Pollock, editors, *Fundamentals of Friction: Macroscopic and Microscopic Processes*, page 511. Kluwer Academic Publishers, Dordrecht, 1992.
[163] T. Moriwaki and K. Okuda. *Annals of CIRP*, 38:115, 1989.
[164] N. P. Suh. *Tribophysics*. Prentice-Hall, Englewood Cliffs, 1986.
[165] L. Zhang and Hiroaki Tanaka. *Wear*, 211:44, 1997.

[166] L. Zhang and Hiroaki Tanaka. *Tribol. Int*, 31:425, 1998.
[167] D. A. Rigney and J. E. Hammerberg. *MRS Bull.*, 23(6):32, 1998.
[168] J. E. Hammerberg, B. L. Holian, J. Röder, A. R. Bishop, and J. J. Zhou. *Physica D*, 123:330, 1998.
[169] F. F. Abraham. *J. Chem. Phys.*, 68:3713, 1978.
[170] S. Toxvaerd. *J. Chem. Phys.*, 74:1998, 1981.
[171] I. K. Snook and W. van Megen. *J. Chem. Phys.*, 72:2907, 1980.
[172] S. Nordholm and A. D. J. Haymet. *Aust. J. Chem.*, 33:2013, 1980.
[173] M. Plischke and D. Henderson. *J. Chem. Phys.*, 84:2846, 1986.
[174] P. A. Thompson and M. O. Robbins. *Phys. Rev. A*, 41:6830, 1990.
[175] J. Magda, M. Tirrell, and H. T. Davis. *J. Chem. Phys.*, 83:1888, 1985.
[176] M. Schoen, C. L. Rhykerd, D. J. Diestler, and J. H. Cushman. *J. Chem. Phys.*, 87:5464, 1987.
[177] I. Bitsanis and G. Hadziioannou. *J. Chem. Phys.*, 92:3827, 1990.
[178] P. A. Thompson, M. O. Robbins, and G. S. Grest. *Israel J. of Chem.*, 35:93, 1995.
[179] J. Gao, W. D. Luedtke, and U. Landman. *J. Phys. Chem. B*, 101:4013, 1997a.
[180] J. Gao, W. D. Luedtke, and U. Landman. *J. Chem. Phys.*, 106:4309, 1997b.
[181] P. A. Thompson and M. O. Robbins. *Science*, 250:792, 1990.
[182] U. Landman, W. D. Luedtke, and M. W. Ribarsky. *J. Vac. Sci. Technol. A*, 7:2829, 1989.
[183] M. Schoen, J. H. Cushman, D. J. Diestler, and C. L. Rhykerd. *J. Chem. Phys.*, 88:1394, 1988.
[184] M. Schoen, C. L. Rhykerd, D. J. Diestler, and J. H. Cushman. *Science*, 245:1223, 1989.
[185] J.-L. Barrat and L. Bocquet. *Faraday Discuss.*, 112:1, 1999.
[186] L. Bocquet and J.-L. Barrat. *Phys. Rev. E*, 49:3079, 1994.
[187] J.-L. Barrat and L. Bocquet. *Phys. Rev. Lett.*, 82:4671, 1999.
[188] P. A. Thompson and S. M. Troian. *Nature*, 389:360, 1997.
[189] R. G. Horn and J. N. Israelachvili. *J. Chem. Phys.*, 75:1400, 1981.
[190] J. E. Curry, F. Zhang, J. H. Cushman, M. Schoen, and D. J. Diestler. *J. Chem. Phys.*, 101:10824, 1994.
[191] P. A. Thompson, G. S. Grest, and M. O. Robbins. *Phys. Rev. Lett.*, 68:3448, 1992.
[192] G. S. Grest and M. H. Cohen. In *Advances in Chemical Physics*, pages 455–. Wiley, New York, 1981.
[193] A. J. Liu and S. R. Nagel. *Jamming and Rheology: Constrained dynamics on microscopic and macroscopic scales*. Taylor and Francis, London, 2000.
[194] G. He and M. O. Robbins. *Phys. Rev. B*, 64:035413, 2001.
[195] G. He and M. O. Robbins. *Tribol. Lett.*, 10:7, 2001.
[196] J. P. Gao, W. D. Luedtke, and U. Landman. *Tribol. Lett.*, 9:3, 2000.
[197] A. L. Demirel and S. Granick. *Phys. Rev. Lett.*, 77:2261, 1996a.
[198] J. Van Alsten and S. Granick. *Phys. Rev. Lett.*, 61:2570, 1988.
[199] S. Granick. *MRS Bull.*, 16:33, 1991.
[200] J. Klein and E. Kumacheva. *Science*, 269:816, 1995.
[201] D. Y. C. Chan and R. G. Horn. *J. Chem. Phys.*, 83:5311, 1985.
[202] J. N. Israelachvili. *J. Colloid Interface Sci.*, 110:263, 1986.
[203] J. Baudry, E. Charlaix, A. Tonck, and D. Mazuyer. *Langmuir*, page 5232, 2001.
[204] Y. Zhu and S. Granick. *Phys. Rev. Lett.*, 87:096105, 2001.
[205] J. Klein and E. Kumacheva. *J. Chem. Phys.*, 108:6996, 1998.
[206] J. N. Israelachvili, P. M. McGuiggan, M. Gee, A. M. Homola, M. O. Robbins, and P. A. Thompson. *J. Phys.: Condens. Matter*, 2:SA89, 1990.
[207] Y. Zhu and S. Granick. *Phys. Rev. Lett.*, 87:096104, 2001.
[208] Uri Raviv, Pierre Laurat, and Jacob Klein. *Nature*, 413:51, 2001.
[209] M. J. Stevens, M. Mondello, G. S. Grest, S. T. Cui, H. D. Cochran, and P. T. Cummings. *J. Chem. Phys.*, 106:7303, 1997.
[210] J. D. Ferry. *Viscoelastic Properties of Polymers, 3rd Ed.* Wiley, New York, 1980.
[211] W. Götze and L. Sjögren. *Rep. Prog. Phys.*, 55:241, 1992.
[212] M. O. Robbins and A. R. C. Baljon. In V. V. Tsukruk and K. J. Wahl, editors, *Microstructure and Microtribology of Polymer Surfaces*, page 91. American Chemical Society, Washington DC, 2000.
[213] A. R. C. Baljon and M. O. Robbins. In B. Bhushan, editor, *Micro/Nanotribology and Its Applications*, page 533. Kluwer, Dordrecht, 1997.
[214] A. R. C. Baljon and M. O. Robbins. *Science*, 271:482, 1996.
[215] M. O. Robbins and E. D. Smith. *Langmuir*, 12:4543, 1996.
[216] M. H. Müser. cond-mat/0204395.
[217] H. Czichos, S. Becker, and J. Lexow. *Wear*, 135:171, 1989.
[218] G. T. Gao, X. C. Zeng, and D. J. Diestler. *J. Chem. Phys.*, 113:11293, 2000.
[219] S. Nasuno, A. Kudrolli, and J. P. Gollub. *Phys. Rev. Lett.*, 79:949, 1997.
[220] C. T. Veje, D. W. Howell, and R. P. Behringer. *Phys. Rev. E*, 59:739, 1999.

[221] A. D. Gopal and D. J. Durian. *Phys. Rev. Lett.*, 75:2610, 1995.
[222] H. Yoshizawa and J. N. Israelachvili. *J. Phys. Chem.*, 97:11300, 1993.
[223] D. E. McCumber. *J. App. Phys.*, 39:3113, 1968.
[224] A. A. Batista and J. M. Carlson. *Phys. Rev. E*, 57:4986, 1998.
[225] A. Dhinojwala and S. Granick. unpublished.
[226] P. A. Thompson and G. S. Grest. *Phys. Rev. Lett.*, 67:1751, 1991.
[227] H. M. Jaeger, S. R. Nagel, and R. P. Behringer. *Rev. Mod. Phys.*, 68:1259, 1996.
[228] M. J. Stevens and M. O. Robbins. *Phys. Rev. E*, 48:3778, 1993.
[229] B. J. Ackerson, J. B. Hayter, N. A. Clark, and L. Cotter. *J. Chem. Phys.*, 84:2344, 1986.
[230] M. Lupowski and F. van Swol. *J. Chem. Phys.*, 95:1995, 1991.
[231] A. L. Demirel and S. Granick. *Phys. Rev. Lett.*, 77:4330, 1996b.
[232] A. Buldum and S. Ciraci. *Phys. Rev. B*, 55:12892, 1997.
[233] M. O. Robbins and P. A. Thompson. *Science*, 253:916, 1991.
[234] P. A. Thompson, M. O. Robbins, and G. S. Grest. In D. Dowson, C. M. Taylor, T. H. C. Childs, M. Godet, and G. Dalmaz, editors, *Thin Films in Tribology*, page 347. Elsevier, Amsterdam, 1993.
[235] J. Peachey, J. V. Alste, and S. Granick. *Rev. Sci. Instrum.*, 62:462, 1991.
[236] V. Zaloj, M. Urbakh, and J. Klafter. *J. Chem. Phys.*, 110:1263, 1999.
[237] V. Zaloj, M. Urbakh, and J. Klafter. *Phys. Rev. Lett.*, 81:1227, 1998.
[238] A. L. Demirel and S. Granick. *J. Chem. Phys.*, 109:6889, 1998.
[239] H.-W. Hu, G. A. Carson, and S. Granick. *Phys. Rev. Lett.*, 66:2758, 1991.
[240] Y.-K. Cho and S. Granick. *Wear*, 200:346, 1996.
[241] G. Luengo, F. J. Schmitt, R. Hill, and Israelachvili J. *Macromolecules*, 30:2482, 1997.
[242] G. Luengo, J. Israelachvili, and S. Granick. *Wear*, 200:1263, 1999.
[243] A. L. Demirel and S. Granick. *J. Chem. Phys.*, 115:1498, 2001.
[244] M. G. Rozman, M. Urbakh, and J. Klafter. *Phys. Rev. E*, 57:7340, 1998.
[245] V. Zaloj, M. Urbakh, and J. Klafter. *Phys. Rev. Lett.*, 82:4823, 1999.
[246] J.-C. Géminard, W. Losert, and J. P. Gollub. *Phys. Rev. E*, 59:5881, 1999.
[247] L. Bureau, T. Baumberger, and C. Caroli. *Phys. Rev. E*, 62:6810, 2000.
[248] F.-J. Elmer. *Phys. Rev. E*, 57:R4903, 1998.
[249] J. P. Gao, W. D. Luedtke, and U. Landman. *J. Phys. Chem. B*, 102:5033, 1998.
[250] M. Heuberger, C. Drummond, and J. N. Israelachvili. *J. Phys. Chem. B*, 102:5038, 1998.
[251] A. Cochard, L. Bureau, and T. Baumberger. cond-mat/0111369.
[252] F. Lacombe, S. Zapperoi, and H. J. Herrman. *Eur. Phys. J. E*, 2:181, 2000.
[253] M. Linker and J. H. Dieterich. *J. Geophys. Res.*, 97:4923, 1992.
[254] E. Richardson and C. Marone. *J. Geophys. Res.*, 104:28859, 1999.
[255] C. M. Mate and A. M. Homola. In B. Bhushan, editor, *Micro/Nanotribology and Its Applications, Vol. 330 of NATO Advanced Sciences Institutes Series E: Applied Sciences*, page 647. Kluwer Academic Publishers, Dordtrecht, 1997.
[256] E. Ott, C. Grebogi, and J. A. York. *Phys. Rev. Lett.*, 64:1196, 1990.
[257] E. Barreto, E. J. Kostelich, C. Grebogi, E. Ott, and J. A. York. *Phys. Rev. E*, 51:4169, 1995.
[258] H. D. I. Abarbanel, R. Brown, J. L. Sidorowich, and L. S. Tsimring. *Rev. Mod. Phys.*, 65:1331, 1993.
[259] B. Bhushan. In B. Bhushan, editor, *Modern Tribology Handbook*, page 49. CRC Press, Boca Raton, FL, 2001.
[260] R. Burridge and L. Knopoff. *Bull. Seismol. Soc. Am.*, 57:341, 1967.
[261] J. M. Carlson, J. S. Langer, and B. E. Shaw. *Rev. Mod. Phys.*, 66:657, 1994.
[262] A. I. Larkin and Yu. N. Ovchinnikov. *J. Low Temp. Phys.*, 34:409, 1979.
[263] A. D. Roberts. *Rubber Chem. Technol.*, 65:3, 1992.
[264] K. A. Grosch. *Proc. Roy. Soc, (London)*, A274:21, 1963.
[265] B. N. J. Persson and E. Tosatti. *J. Chem. Phys.*, 112:2021, 2000.
[266] B. N. J. Persson. *J. Chem. Phys.*, 115:3840, 2001.
[267] B. N. J. Persson and A. I. Volokitin. *Phys. Rev. B*, 65:134106, 2002.
[268] M. Klüppel and G. Heinrich. *Rubber Chem. Technol.*, 73:578, 2000.